Physik Department

Technische Universität München

Characterization, phase behavior and processing of silk proteins for controlled drug delivery

Andreas Stephan Lammel

Dissertation an der Technische Universität München

April 2010

TECHNISCHE UNIVERSITÄT MÜNCHEN

Physik Department

Lehrstuhl für Zellbiophysik E27

Characterization, phase behavior and processing of silk proteins for controlled drug delivery

Andreas Stephan Lammel

Vollständiger Abdruck der von der Fakultät für Physik der Technischen Universität München zur Erlangung des akademischen Grades eines Doktors der Naturwissenschaften genehmigten Dissertation.

Vorsitzender: Univ.-Prof. Dr. Roland Netz

Prüfer der Dissertation: 1. Univ.-Prof. Dr. Andreas Bausch

2. Univ.-Prof. Dr. Thomas Scheibel, Universität Bayreuth

Die Dissertation wurde am 29.04.2010. bei der Technischen Universität München eingereicht und durch die Fakultät für Physik am 09.06.2010 angenommen.

Technische Universität München

Physik-Department

E27-Zellbiophysik

Dissertation

Characterization, phase behavior and processing of silk proteins for controlled drug delivery

Andreas Stephan Lammel

April 2010

„ Look not at what you see but at what it took to produce what you see.“

Benoît B. Mandelbrot

Summary

Due to their extraordinary mechanical and biochemical properties, silks have long been a focus of research. The versatility of silk proteins, along with their biocompatibility and biodegradability, make silk-based materials good candidates for biomedical applications such as drug delivery systems and scaffolds for tissue engineering.

Here, we report on the processing, production and characterization of silk based drug carriers and films for coatings or scaffolds. We compare carriers produced from regenerated *Bombyx mori* cocoon silk fibroin and recombinantly produced engineered spider silk (mimicking the known amino acid sequence of the natural spider silk protein from the European garden spider *Araneus diadematus*) with respect to their features. We present an all-aqueous process at ambient conditions for the production and loading of silk carriers for small molecule drugs. The particles were produced by salting out a silk protein solution with potassium phosphate. For silk fibroin particles, the effect of ionic strength and pH of potassium phosphate solution on the yield and morphology of the particles was determined. Secondary structure and zeta potential of the silk particles could be controlled by pH. Particles produced by salting out with 1.25 M potassium phosphate pH 6 showed a dominating silk II (crystalline) structure whereas particles produced at pH 9 were mainly composed of silk I (less crystalline). The results show that silk I rich particles possess chemical and physical stability and secondary structure which remained unchanged during post treatments even upon exposure to 100% ethanol or methanol. A model is presented to explain the process of particle formation based on intra- and intermolecular interactions of the silk domains, influenced by pH and kosmotropic salts. The reported silk fibroin particles can be loaded with small molecule model drugs, such as alcian blue, rhodamine B, and crystal violet, by simple absorption based on electrostatic interactions. In vitro release of these compounds from the silk particles depends on charge-charge interactions between the compounds and the silk. With crystal violet we demonstrated that the release kinetics is dependent on the secondary structure of the particles.

Investigation of the influence of physicochemical factors on the assembly process of engineered spider silk protein (eADF4(C16)) into particles revealed that particle size (250 nm to 3 µm) and size distribution can be controlled by mixing intensity and concentration of potassium phosphate and concentration of eADF4(C16). Particle characterization revealed that particles made of the engineered spider silk protein eADF4(C16) are colloidally stable in solution, which is crucial for parenteral applications. On the basis of eADF4(C16) particles we systematically studied the loading process for small molecule drugs in more detail. Therefore we employed twelve different model drugs differing in physicochemical properties like molecular weight, dissociation constants (*pKa*) and partition coefficients (*logP*). We show that the loading efficiencies correlate with the distribution coefficient (*logD*) of small molecules of weak alkaline nature. Our results show that constant release rates can be realized for a period of two weeks at physiological conditions *in vitro*, with accelerated release rates within acidic environments. Enzymatic degradation studies of eADF4(C16) particles indicated that the silk proteins degrade slowly and the particles decrease in size. The release study upon degradation revealed that during the first day the total release is apparently independent of amount of enzyme added, whereas after one day accelerated release with increasing enzyme concentration is observed.

Further, this work reports on the control of eADF4(C16) film features useful for the design of coatings or scaffolds. We show that the secondary structure can be influenced by post casting treatments and macroscopic properties like porosity and mechanical stability can be controlled by additives like poly(ethylene oxide) (PEO) and glycerol. In vitro release of crystal violet loaded eADF4(C16) films showed that the release is sensitive to pH and ionic strength.

In summary, this work indicates that due to the processability into various morphologies, control of properties on the molecular and macroscopic level along with their biocompatibility and biodegradability silk proteins may play an important role for future applications in novel biomaterials.

1 Introduction

1.1 Controlled drug delivery systems

1.1.1 The concept of controlled drug delivery

Conventional drug administration by means of tablets or intravenous injections usually does not provide rate-controlled release and therefore exhibits the disadvantage that the entire dose is released in one portion. Thereby, very high plasma concentrations of drug are reached for a short period of time, potentially close to toxic levels leading to undesirable side effects. In the following, a therapeutic level is maintained for a relatively short period of time before the drug concentration drops below the effective level and re-administration is required yielding strong fluctuating drug levels (Figure 1a). To achieve the optimal therapeutic effect a long term appropriate drug concentration is needed. Therefore, in order to improve the effectiveness of pharmaceutical therapies a lot of effort has been put into the research and development of controlled drug delivery systems (DDS) during the last decades (Allen and Cullis, 2004; Bartus et al., 1998; Couvreur and Puisieux, 1993; Langer, 1990). The idea behind a controlled DDS is to deliver drug molecules to a specific site in the body with a sustained, controlled and constant release rate. Therefore toxic side effects are reduced and the number of drug administration is decreased, while cellular uptake and bioavailability are improved (Jung et al., 2000; Roser et al., 1998; Uhrich et al., 1999; Vasir et al., 2003; Yasutomo et al., 2002) . To achieve this goal two main concepts have been realized: mobile drug carrier systems and depot systems (Langer and Peppas, 2003). Carrier systems are usually employed to target specific tissues or cells whereas therapeutic depot systems are local systems typically implanted at the site of interest. Local depot systems are especially envisioned in form of implant coatings in which drug molecules are embedded to improve the body-implant interface (e.g. incorporation of growth factors to promote cell growth) (Thierry et al., 2003; Wang et al., 2007a) (Figure 1b). Furthermore one can distinguish between: Matrix, membrane and conjugated systems (Cheema et al., 2007; Crampton and Simanek, 2007; Riley et al., 1999).

a)

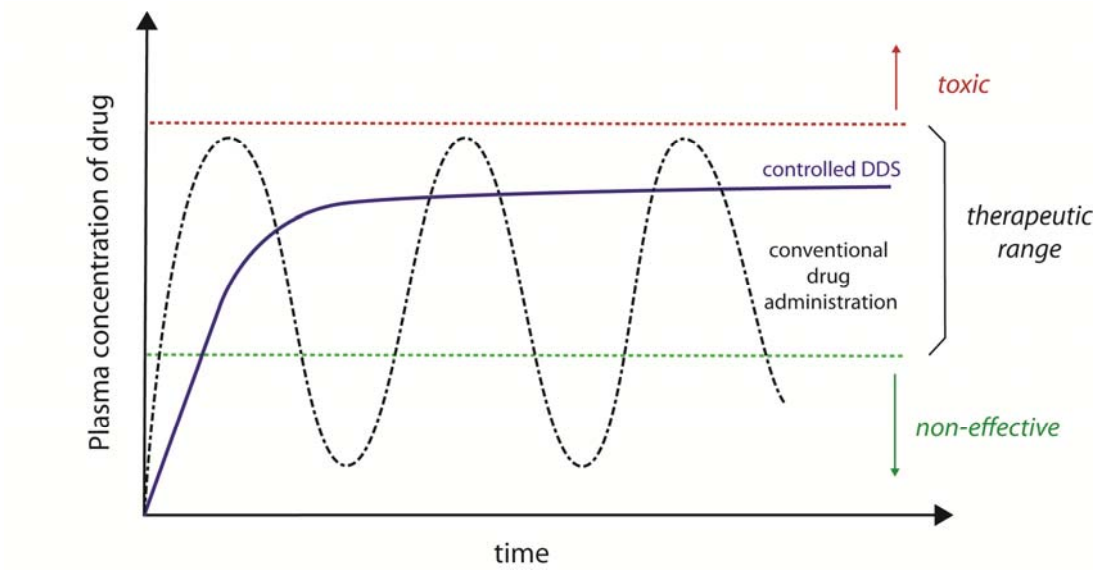

b)

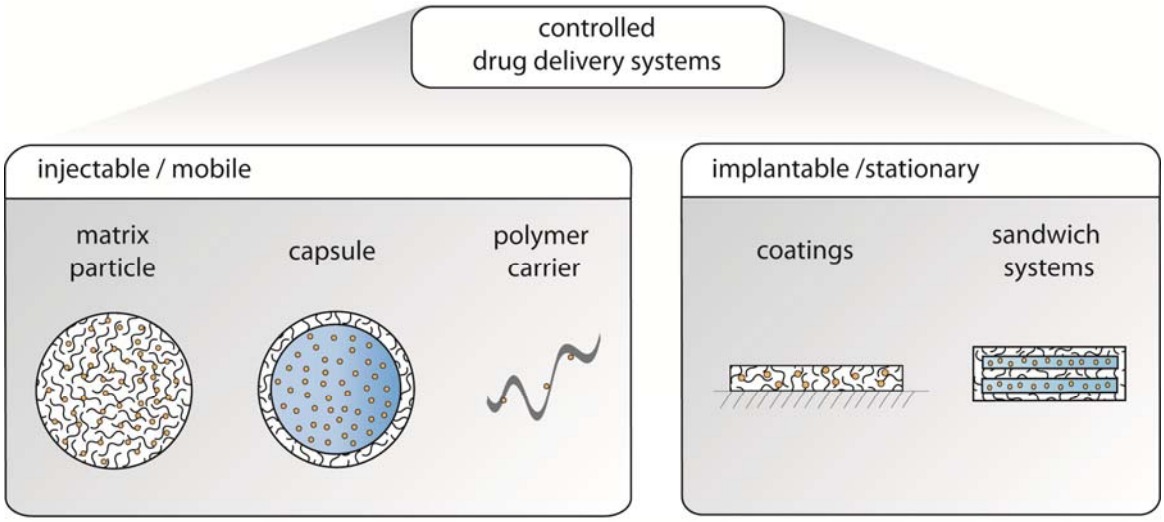

Figure 1: The concept of controlled drug delivery. **a)** Plasma concentration of drug as a function of time in case of conventional drug administration and in case of administration employing a controlled drug delivery device. **b)** Classification of controlled drug delivery systems. Generally, controlled DDS can be classified into injectable mobile systems (e.g. matrix particles, capsules and conjugated systems like polymer carriers) and implantable stationary DDS in the form of self supporting therapeutic systems (e.g. sandwich systems) or functional coatings.

In a matrix system the compound is dispersed in a polymer matrix. The density of the polymer network determines the diffusion and release of the compound (Tongwen and Binglin, 1998). In membrane systems the compound is surrounded by a membrane

which functions as a diffusion barrier (McHugh, 2005; Santos et al., 2008). Conjugated systems are characterized by chemical coupling of the compound to a polymer chain (Liso et al., 1995; Sakuma et al., 2007). All of these approaches are based on the principle of protection of the active compound from early degradation by masking the compound in such a way that it is invisible to the immune system (Sheng et al., 2009). Therefore, the active compound remains longer in circulation before enzymatic degradation processes take place and transport to the desired site of action is possible (Chickering et al., 1997; Coombes et al., 1997; Esmaeili et al., 2008; Gobin et al., 2006; Ruxandra et al., 1999)

1.1.2 Colloidal drug carriers

Especially colloidal micro- and nanoparticulate carriers have extensively been investigated as a platform for controlled drug delivery (Couvreur et al., 1990; Edlund and Albertsson, 2002; Pilar et al., 1996; Sokolsky-Papkov et al., 2007). One of their most useful features is that they are easy to inject either into tissue or intravenously and that their size facilitates specific targeting and cellular uptake via phagocytosis (Kohane, 2007; Kreuter, 2001; Panyam and Labhasetwar, 2003). The production of suitable particles remains challenging since in terms of biocompatibility appropriate materials and processing must be considered, including avoiding organic solvents, surfactants, initiators or crosslinking agents (Arshady, 1990; George et al., 1994; Vandelli et al., 2001). In principle two main concepts are utilized to produce small particles for pharmaceutical applications: template assisted techniques or phase separation (Quintanar-Guerrero et al., 1996; Zambaux et al., 1998) . In the first case usually emulsion droplets are used to define shape and size (Edwin et al., 1998; Hermanson et al., 2007b; Wang et al., 2007b; Wenk et al., 2008). These preparation techniques usually have the disadvantage of being relatively complicated and typically emulsion stabilizers and/or crosslinkers are involved which have negative effects on the biocompatibility (MacAdam et al., 1997; Rubino et al., 1993). The obtainable colloidal particles may have a solid, hollow or core shell structure. In contrast, the bottom up approach of particle formation by desolvation or solvent shifting by addition of salts or miscible non-solvents

is relatively simple (Aubry et al., 2009; Ibrahim et al., 1992; Ribeiro et al., 2008). This technique offers less control on particle ensemble characteristics like monodispersity. However, it is very well suited to produce matrix particles which have the major advantage that they are not subjected to dose dumping compared to membrane systems in case of membrane rupture. The loading of carriers with compounds is typically performed by mixing the compound with the polymer containing phase (Reza, 1990a; Reza, 1990b). Upon particle formation the drug molecules are incorporated and entrapped in the polymer matrix. In order to prevent the loss of expensive medication the loading efficiency (defined as the ratio of the amount of compound in the carrier to the total amount of compound initially employed) is intended to be very high (ideally 100 %) (Bilati et al., 2005a; Bilati et al., 2005b). Another important parameter is the achievable loading (defined as the ratio of mass of compound to mass of carrier) which influences the applicable dosage as well as the duration of release (Govender et al., 2000; Govender et al., 1999). Loading and loading efficiency are mainly influenced by the method of particle production as well as the intermolecular interactions between the matrix constituting polymer and the compound (Jain, 2000). The release behavior of compounds from the carrier depends on the structure of the particle matrix and the chemical properties associated with both the polymer and the drug. In vivo, drug release is typically controlled by a combination of polymer matrix degradation and diffusion due to concentration gradients (Washington, 1990). Besides physicochemical parameters like intermolecular interactions, additional factors associated with the release involve the polymer molecular weight and composition, crystallinity and drug distribution (Freiberg and Zhu, 2004; Soppimath et al., 2001; Vila et al., 2002).

1.1.3 Therapeutic depot systems

In contrast to colloidal carriers implantable therapeutic systems have macroscopic dimensions and function as a local depot (Wang et al., 2005). Typically those systems are implantable degradable devices which are placed directly at the site of interest. Compared to particulate drug delivery systems, their main advantage is that due to their size usually prolonged release can be realized for a longer period of time and therefore they are better suited for long term local treatments. Additionally, there is no necessity

for surgical removal of the implant after the therapy is completed. Furthermore, due to their macroscopic dimensions implantable devices are easier to prepare and allow for variation in geometries like size, shape and porosity, which can be tailored to specific needs (Cbreve et al., 1996; Mingzhong et al., 2002; Yang et al., 2002). Especially drug depot systems as implant coatings are of interest for example to promote cell growth at the tissue material interface of orthopedic implants or to avoid blood clotting and restenosis after implantation of stents with anticoagualting agents containing coatings (Thierry et al., 2003).

1.1.4 The complexity of a drug delivery system

The successful development of a controlled drug delivery system involves aspects from various disciplines like medical science, biology, chemistry, physics and engineering. Biomedical knowledge is required in order to evaluate the biocompatibility and effectiveness as well as using the appropriate targeting strategies for specific therapies. Engineering aspects are important in terms of material processing and production of particles or membranes with designable properties considering that the techniques employed have to be scalable for industrial production. During reiterative optimization processes of the drug delivery system, physicochemical aspects have to be considered and analyzed in terms of interfacial properties, transport and release mechanisms. Figure 2 illustrates the complexity of a drug delivery system by considering different levels of abstraction with increasing degree of detail. On the first level the technological system of a DDS (e.g. in form of a particle) is brought in contact with the biological system. Depending on the route of administration (parenteral or oral) the tissue or body fluid with first contact depends on the site of application. At this level particle size, material and surface properties will be responsible if the particles are recognized by the immunosystem and also influence their body distribution (Assender et al., 2002; Desai et al., 1996; Park et al., 2001). On the next level, looking at the interface of the particle material and the surrounding media (e.g. extracellular matrix (ECM) or body fluid), particle matrix properties (e.g. cross-linking degree, density, etc) and physicochemical properties of the media (pH, ionic strength, viscosity etc.) determine the release and transport properties of compounds from the DDS (Chorny et al., 2002; Lee et al., 2004;

Pitt et al., 1979; Somnath and Jagdish, 2007; Zolnik and Burgess, 2007). Finally, on the molecular level, inter- and intramolecular interactions determine on the one hand the conformation of the polymer matrix (e.g. amorphous, helical or crystalline) and on the other hand the binding strength of compounds. Eventually, all these properties and factors along with their interdependency on different length scales finally influence the overall stability, biocompatibility, release and degradation behavior of the drug delivery system employed.

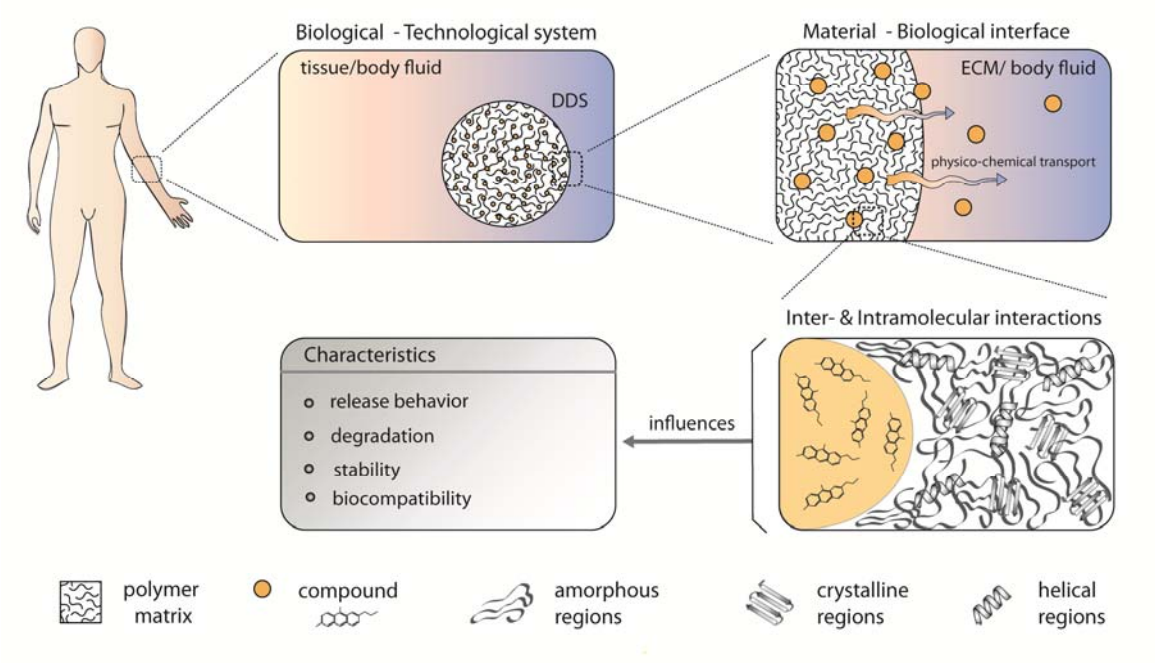

Figure 2: The complexity of drug delivery systems considering different levels of abstraction. On the first level particle size, material and surface properties of the DDS influence the body distribution and the immunogenicity. On the next level, looking at the material-media interface particle matrix properties (e.g. cross-linking degree, density, etc.) and physicochemical properties of the media (pH, ionic strength, viscosity etc.) have to be considered in terms of release and transport properties of compounds from the DDS. Finally, on the molecular level, inter- and intramolecular interactions determine on the one hand the conformation of the polymer matrix (e.g. amorphous, helical or crystalline) and on the other hand the binding strength of compounds. Eventually, all these factors prominent on different length scales influence the overall characteristics like stability, biocompatibility, release and degradation of the DDS.

1.2 Polymeric biomaterials

In general, the material employed for biomedical applications should be non immunogenic and offer control of structure, morphology and function, while also exhibiting good mechanical stability (Altman et al., 2003). Therefore, biodegradable and biocompatible polymers are preferred since they retain their properties for a limited period of time before they gradually decompose into soluble nontoxic degradation products that can be excreted from the body (Mathiowitz et al., 1997; Tamber et al., 2005). Many synthetic (aliphatic polyesters, poly(glycolic acid) (PGA), poly (lactid acid) (PLA), etc. (Lück et al., 1998; Sokolsky-Papkov et al., 2007)) and natural (alginate(George and Abraham, 2006), chitin (Mi et al., 2003), chitosan (Berthold et al., 1996; Calvo et al., 1997a; Calvo et al., 1997b), proteins (Latha et al., 1995; Liebmann et al., 2008; Liu et al., 2005; Megeed et al., 2002; Numata et al., 2009; Sahin et al., 2002) etc.) polymers have been employed to produce degradable vehicles for encapsulation, incorporation or binding of active compounds. While synthetic polymers offer the potential of sustaining the release of the encapsulated therapeutic agent over a period of days up to several months, they typically demand organic solvents or relatively harsh formulation conditions during processing with potentially limited biocompatibility, due to remaining toxic solvents and acidic degradation products (Morlock et al., 1997). Natural polymers in contrast can be processed at ambient mild conditions. In spite of the possible advantages of natural polymers concerning biocompatibility and processability, most biopolymers present a main drawback of rapid resolubilization in aqueous environments since they are often hydrophilic, thus resulting in fast drug release profiles (Soppimath et al., 2001). In order to resolve this problem, chemical cross-linking procedures (e.g. using glutaraldehyde and formaldehyde treatment) have been considered (Latha et al., 1995; Sahin et al., 2002; Vandelli et al., 2001). Unfortunately, the presence of residual crosslinking agents could lead to toxic side effects. In addition, unwanted reactions between the drug and the cross-linker could result in the formation of toxic or even inactivated derivatives (Digenis et al., 1994; Speer et al., 1980). The disadvantages of a system based on a hydrophilic biopolymer can be diminished upon using a hydrophobic biopolymer capable for sustained drug release (Liu et al., 2005). Silk proteins are amphiphilic biopolymers and unify all aforementioned properties necessary for an

optimized drug delivery system (Hofmann et al., 2006; Numata and Kaplan, 2010). They are particularly promising for biomaterial applications due to their unique combination of biocompatibility (Allmeling et al., 2008; Meinel et al., 2005; Vollrath F, 2002), biodegradability (Horan et al., 2005; Wang et al.), mechanical stability, controllable structure and morphology (Altman et al., 2003; Hardy et al., 2008; Huang et al., 2008; Lammel et al., 2010).

1.3 Silk materials

Silk from the mulberry silkworm *Bombyx mori* (*B. mori*) has been used to produce textiles for thousands of years due to its attractive luster along with light weight and tear resistance. However during the last decades silk arouse increasing interest as a novel biomaterial due to some extraordinary material properties. Silks, especially spider silks combine impressive mechanical stability (Table 1) with biocompatibility (Mei et al., 2006; Panilaitis et al., 2003; Yang et al., 2007), biodegradability (Gellynck et al., 2008; Wang et al.), and the ability for amino acid side chain modification for functionalization (e.g. growth factors) (Huemmerich et al., 2006; Uebersax et al., 2007; Vollrath and Porter, 2006).

Generally, silks are produced by several worms of the order *Lipedoptera* (including mites, butterflies and moths) and by members of the class *Arachnida* (over 30,000 species of spiders) employed for building structures outside the body of the animals (Yonemura et al., 2009). During 400 million years of evolution, silks have been optimized in respect to their material properties to fulfill a great variety of functions (Vollrath, 1999). Typically, silks are used as filaments or threads with diameters ranging from a few hundred nanometers to 50 µm (Kaplan et al., 1997). While spiders are able to produce up to seven different kinds of silk for different purposes (nests, webs, safety lines and egg protection etc.), silkworms produce only one kind of silk for its cocoon (Vollrath, 2000; Zhao et al., 2007). Among all these silks, the cocoon silk of *B. mori* and the major ampullate silk (MA silk) (composing the frame and radii of the web) of the orb weaving spiders *Nephila clavipes* and *Araneus diadematus*, are the most extensively studied and

characterized (Heim et al., 2009; Holland et al., 2007; Kaplan, 1998; Scheibel, 2004; Scheibel, 2005; Vendrely and Scheibel, 2007; Vepari and Kaplan, 2007; Yang et al., 2009).

Table 1. Mechanical properties of silk fibers (*Araneus diadematus* drag line silk and *B. mori* cocoon silk) in comparison to other synthetic high performance materials (Kevlar, Nylon and steel). The data shown are taken from (Gosline et al., 1999).

Material	Density [gcm^{-3}]	Tensile strength [GPa]	E-modulus [GPa]	Elasticity [%]	Toughness [MJm^{-3}]
Araneus diadematus silk (Drag line)	1.3	1.1	10	27	180
B. mori silk (cocoon)	1.3	0.6	7	18	70
Kevlar 49	1.4	3.6	130	2.7	50
Nylon 6.6	1.1	0.95	5	18	80
Steel	7.8	1.5	200	0.8	6

1.3.1 Structure of silk

Generally silk fibers have a core shell type structure. In the case of *B. mori* silk, the fiber consists of two filaments coated and glued together with sericine forming a twin filament. Finally, the fiber is coated with a variety of other proteins postulated to protect the cocoon against microbes and predators (Figure 3a).

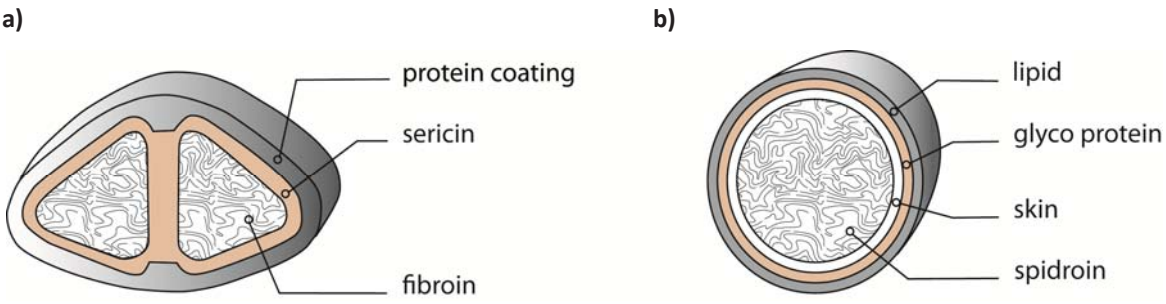

Figure 3. Schematic cross section views of silk fibers showing the core shell structure. **a)** *B. mori* cocoon silk. **b)** Major ampulate silk.

The fibroin filaments are composed of a complex of two protein chains and a glycoprotein. The heavy-chain (H-chain: 392 kDa) and light-chain (L-chain: 26 kDa) are linked by a disulfide bond whereas the glycoprotein (P25: 30 kDa) is associated via

hydrophobic interactions (Inoue et al., 2000; Tanaka et al., 1999; Wang et al., 2009). MA silks have only one core filament embedded in a protein skin, a glycoprotein coat and a final lipid layer. The core is a composite of two major spider silk proteins which differ in their hydrophobicity (Gatesy et al., 2001). In the case of silk from the spider *Araneus diadematus* these proteins are called ADF-3 (hydrophilic) and ADF-4 (hydrophobic) (Exler et al., 2007). Despite the different macroscopic architecture of silk fibers, the main silk protein components share some common features. First of all, silk proteins appear to have extremely large molecular weights, probably the largest for any class of proteins. The size of full length native dragline silk proteins have been identified to have molecular weights between 175 kDa and 400 kDa (Zbilut et al., 2006), which is at the same order of magnitude as the *B. mori* H-chain. Despite the variability in primary structure, silk proteins possess a common well-defined organization. A large repetitive hydrophobic core with complex, non-repetitive, more hydrophilic N- and C-terminal blocks (Mita et al., 1994; Sponner et al., 2004; Sponner et al., 2005; Vendrely et al., 2008) (Figure 4).

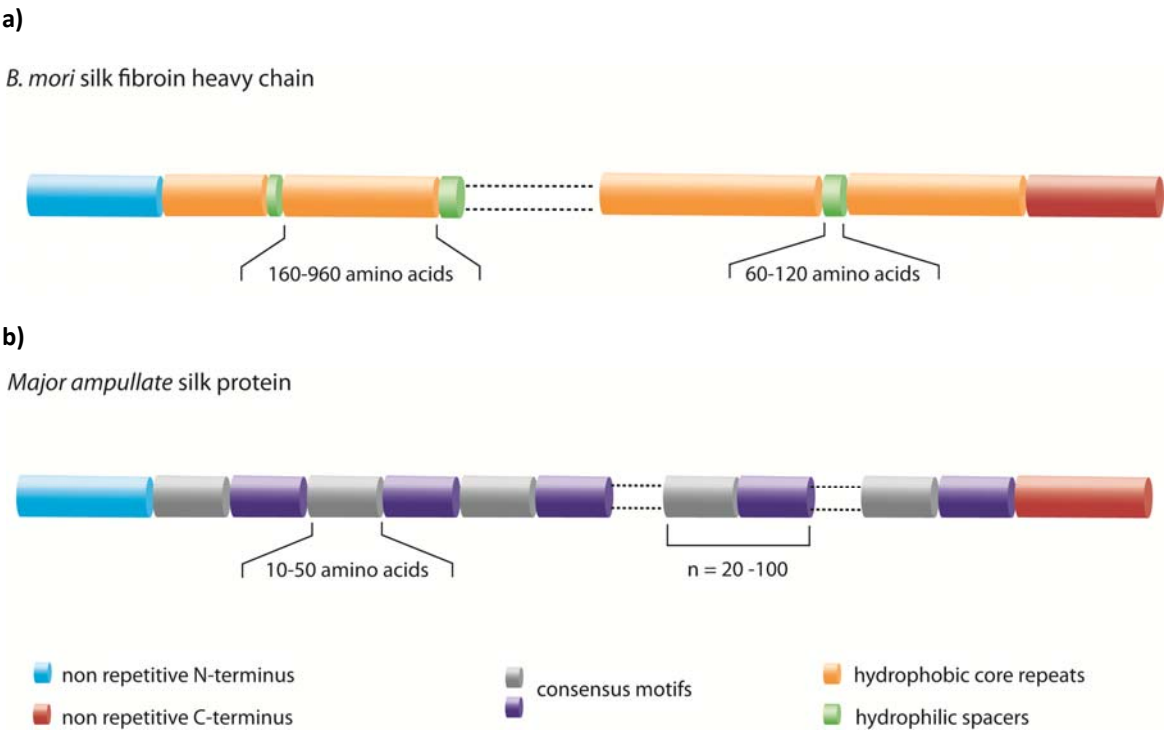

Figure 4. Model of silk protein primary structures. Silk proteins possess a common well-defined organization. A large repetitive hydrophobic core with complex, non-repetitive, more hydrophilic N- and C-terminal blocks **a)** The core central repeats of *B. mori* silk fibroin heavy chain are separated by regularly

interspersed more complex non-repetitive hydrophilic spacers of variable size **b)** In MA silk protein the hydrophilic component is included within the low complexity repetitive unit.

The central part is composed of repeating units, containing combinations of reiterated motifs with predominant contents of hydrophobic amino acids such as alanine and glycine (Bini et al., 2004). In contrast to spider silk, *B. mori* silk also contains high levels of serine (Zhao et al., 2007). Spider silk, on the other hand, has higher contents of charge-carrying residues, such as glutamic acid and arginine. In contrast to major ampullate silk protein, where the hydrophilic component is included within the low complexity repetitive unit, the core central repeats of *B. mori* silk are separated by regularly interspersed more complex non-repetitive hydrophilic spacers of variable size (approximately one tenth the size of the hydrophobic regions) (Figure 4).

In *B. mori* silk the repetitive oligopeptide motife is GAGAGX (where X = A, S, V or T). The repeating motife GAGAGS, dominating the repetitive core, is widely accepted as the building block for β-sheet crystallites. Tyrosine containing segments, are supposed to form β-sheet crystals with different unit cell structure from the one formed by GAGAGS segments. The non-repetitive regions that intervene between the repetitive domains are quite hydrophilic and may adopt a loop structure changing the direction of preceding backbone by 180° and thus facilitating an anti-parallel β-sheet formation (Bini et al., 2004; Guerette et al., 1996; Inoue et al., 2000; Jin and Kaplan, 2003; McGrath and Kaplan, 2004; Vepari and Kaplan, 2007).

In MA silk proteins the repetitive motifs are usually grouped into four categories $(GA)_n/A_n$, GGX, GPGXX, and spacers (Römer and Scheibel, 2008; Vendrely et al., 2008). The $(GA)_n/A_n$ module, like GAGAGS hexapeptide in *B. mori* fibroin H-chain, functions as β-sheet former in (Holland et al., 2008a; Holland et al., 2008b; Parkhe et al., 1997). In comparison, the GGX motif probably adopts a 3_{10} helical secondary structure and is partially incorporated into β-sheet crystal (Lefèvre et al., 2007; van Beek et al., 2002). The GPGXX motif (in many cases, X = Q) is thought to be involved in a β-turn spiral, based on structures of comparable proteins like elastin, and be responsible for the extensibility of spider major ampullate silk (Brooks et al., 2008). Figure 5 provides an

overview over typical motifs identified in *B. mori* and MA silk correlated with their putative structure and their impact on silk fiber properties after assembly.

protein origin	motif	putative structure	property
B. mori cocoon silk	GAGAGS GAGAGY		crystalline
	spacer		amorphous
	GAAS		elastic
Major ampullate spider silk	(GA)n / An		crystalline
	GGX		amorphous
	GPGQQ		elastic
	NR_C-domain NR_N-domain		

Figure 5. Typical amino acid motifs of *B. mori* cocoon silk fibroin and MA silk spidroin. The different amino acid motifs present in *B. mori* and MA silk are correlated with their putative structure and their impact on the fiber properties. The function of the non repetitive parts in MA silk is not fully understood, presumably these parts play a role in triggering the assembly of spider silks (Hagn et al., 2010; Ittah et al., 2007) .

The outstanding strength of silkworm and spider silks arises from the hierarchical and sophisticated composition of structural elements in which crystalline regions of different dimensions are embedded in an amorphous or pre-oriented matrix (Heim et al., 2010; Porter and Vollrath, 2009; Smith and Scheibel, 2010). The hierarchical structure of silk is exemplarily shown for dragline silk from *Araneus Diadematus* in Figure 6.

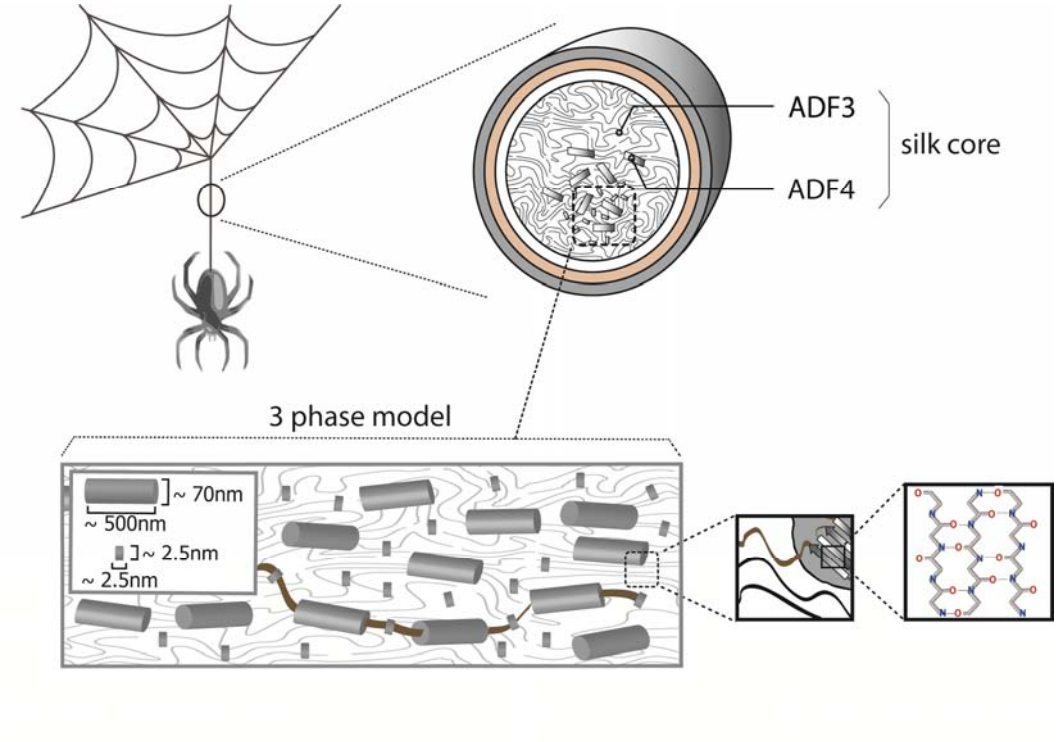

Figure 6. Structure of spider silk. *Araneus Diademtus* spider dragline silk mainly consists of two proteins, ADF3 and ADF4. On the molecular level spider silk exhibits crystalline regions of different dimensions embedded in an amorphous matrix. (Figure adopted from (Smith and Scheibel, 2010))

Upon shear deformation, the large number of hydrogen bonds in the intermolecular β-sheet nanocrystals leads to dissipative stick slip deformation responsible for the exceptional mechanical properties exceeding that of steel or Kevlar (Keten et al., 2010; Semmrich and Bausch, 2010). Additional features controlling the mechanical behavior of the material are the ratios of the ordered and disordered fractions as well as the degree of hydration (Dicko et al., 2007). It is widely accepted that highly ordered, crystalline regions play a major role in determining the strength and stiffness of silks, while non-crystalline regions contribute to the elasticity of the material (Gosline et al., 1984; Hu et al., 2006b; Jelinski, 1998; Krasnov et al., 2008; Kummerlen et al., 1996; Papadopoulos et al., 2007; Simmons et al., 1994; Sponner et al., 2007; Zax et al., 2004).

1.3.2 Natural assembly of silk proteins

To exploit and control silk material properties for applications it is essential to understand the processing mechanisms of silk proteins. Especially, *in vivo* and *in vitro* studies of the fiber formation process has shed light into the silk protein assembly (Jin and Kaplan, 2003; Lefèvre et al., 2008; Rammensee et al., 2008). In nature, silk proteins are synthesized and excreted by specialized cells lining the epithelium in the silk glands of insects and spiders (Winkler and Kaplan, 2000). A schematic representation of the silk fiber assembly process is exemplarily shown for spider silk proteins in Figure 7. The spinning dope, a protein solution of high concentration (up to 50 %) is stored in the glands' lumen without aggregation. The silk fibers are formed on demand upon passage of the spinning dope through the spinning duct where the proteins assemble by a liquid-solid phase transition accompanied by structural changes to form a stable fiber which is released to the exterior (Heim et al., 2009; Jin and Kaplan, 2003; Lammel et al., 2008a; Römer and Scheibel, 2008). The phase transition is triggered by several tightly controlled biochemical and physical factors involving a slight acidification of the spinning dope, most likely leading to a neutralization of (the more abundant) acidic side chains, allowing tighter interactions of the molecules (Foo et al., 2006a; Matsumoto et al., 2008). Hydrophobic intermolecular interactions are further enhanced by a change in the ionic composition inside the duct: the more chaotropic ("salting-in") ions sodium and chloride are exchanged by the more kosmotropic ("salting-out") ions phosphate and potassium. In a next step at the distal part of the duct, water is resorbed from the solution, thus increasing the protein concentration, which will additionally favor intermolecular interactions (Mukhopadhyay and Sakthivel, 2005). Finally, the viscous solution is subjected to increasing elongational flow and shear forces, which are thought to further align the molecules (Braun and Viney, 2003). A detailed review on the fiber assembly process is given by (Heim et al., 2009).

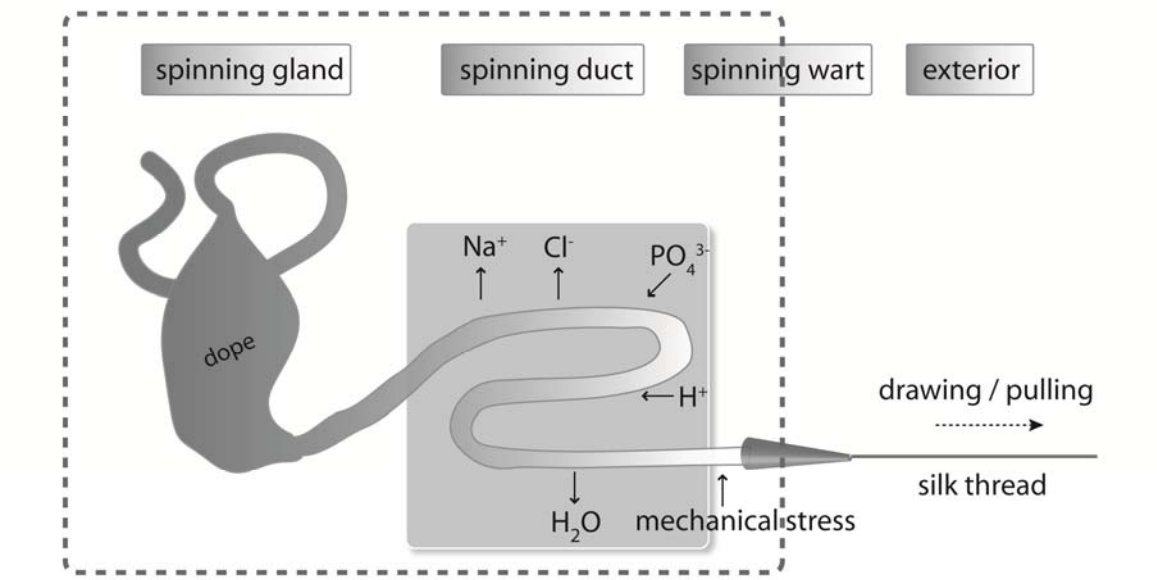

Figure 7. Natural assembly of silk proteins into fibers. Dragline silk proteins are stored in the spinning gland. Upon passage of the spinning dope through the spinning duct, the proteins are subjected to a change of physicochemical parameters leading to a liquid-solid phase transition necessary for fiber formation. Shortly before the exit at the spinning wart, the viscous protein solution is subjected to increasing elongational flow and shear forces, which are thought to further align the molecules into the final state in the fiber (Figure adopted from (Heim et al., 2009)).

1.3.3 Processing of silk proteins

In order to exploit silk as a material for technical applications it is necessary to gain the raw material of silk proteins for further processing into new products. Due to its extensive use in textile industry silkworm silk from *B. mori* is readily available. The caterpillars are kept in farms and fed by mulberry leaves. After one month they are mature enough for metamorphosis into a moth for which they build a protective cocoon of silk (Adachi et al., 2006; Zhao et al., 2005). The silk is harvested from the cocoon after killing the caterpillars via exposure to hot steam. In the following the silk is reeled off the cocoon and the crude silk is purified from other constituents and degummed (removal of the glue-like sericin) before processing and selling (Freddi et al., 2003; R. Mossotti, 2006). In contrast to silkworm silk, breeding spiders and harvesting their silk has been limited due to their cannibalistic nature. Due to advances in biotechnology it is now possible to produce recombinant spider silk as well as tailoring silk genes enabling protein engineering and to design properties tailored to specific requirements (Bogush et al., 2009; Lazaris et al., 2002; Teule et al., 2009; Winkler et al., 1999; Wong Po Foo and

Kaplan, 2002). The approach for recombinant production of engineered spider silk proteins used in this work is reviewed in (Vendrely and Scheibel, 2007). It is based on multimerization of consensus amino acid motifs derived from the repetitive part of natural proteins ADF-3 and ADF-4 yielding engineered spider silk proteins called eADF3 and eADF4 (Huemmerich et al., 2004a; Vendrely et al., 2008).

As outlined in 1.3.2 , processing of silk proteins into a fiber is a sophisticated process which involves a chain of tightly controlled parameters (Heim et al., 2009). The fundamental principal crucial for the production, of materials from silk solution is the induction of a phase separation. The two key parameters involved in the phase separation are the silk concentration in solution and the trigger factor decreasing the solvent quality by which phase separation is initiated. The trigger factor involves chemical parameters like the amount and type of additives (salts, non-solvents, polymers, etc.) along with its properties (ionic strength (Vladimir, 2002), pH (Foo et al., 2006a; Terry et al., 2004), miscibility (Liu et al., 2004; Panya et al., 2007; Zhang et al., 2007) etc.) and physical parameters like viscosity (Matsumoto et al., 2008), mechanical shear (Rammensee et al., 2008) and temperature (Glišović and Salditt, 2007; Jin and Young Hwan, 2001; Tanaka et al., 2002) etc.. To visualize the influence of those two key parameters Figure 8 shows a qualitative ternary phase diagram at constant temperature and pressure. Each corner of the triangle represents 100% of the respective component: silk protein, solvent and non-solvent. Any point along the side of the triangle represents the composition of the binary mixtures constituted by the two components at the corresponding corners. Therefore a state inside the phase diagram can be expressed by the silk concentration and the solvent quality expressed by the ratio of solvent to non-solvent. Commonly used solvents for silk proteins are formic acid (Um et al., 2001), hexafluoroisopropanol (Chenhua et al., 2003), ionic liquids (Phillips et al., 2004) and water (Lawrence et al., 2008; Scheibel, 2004). To obtain aqueous silk solutions, the proteins are dissolved in chaotropic slats like guanidiniumthiocyanat and subsequently dialyzed against water to remove the salt (Foo et al., 2006b). The *spinodal* represents the set of conditions denoting the boundary of absolute instability of a solution where small fluctuations in composition lead to a spontaneous phase separation via spinodal decomposition. The region between the *spinodal* and *binodal* is the metastable region

where the *binodal* denotes the boundary condition at which two distinct phases may coexist.

Changes in the composition of the silk protein-solvent-nonsolvent system can be schematically represented in the ternary phase diagram by a composition path. The arrows numbered from 1 to 4 represent some distinguishing changes in composition of the liquid ternary system. The corresponding structures formed by different composition paths are schematically shown below the phase diagram. Grey hatched areas represent the solid silk protein whereas blue areas represent the miscible solvent/nonsolvent constituent. The composition path 1 means that the silk protein concentration increases accompanied by an increase in viscosity. Depending on end concentration and kinetic issues the protein molecules entangle and solidify by gelation or crystallization into a dense, compact structure. In case of complete desolvation a protein film can be obtained. Addition of porogens into the silk protein and following this path porous structures or foams can be produced upon leaching out the porogens after solidification. Path 2 denotes that the ternary silk protein solution becomes metastable. Concentration fluctuations enable the formation of protein lean phase nuclei which induce phase inversion upon growth. The nuclei grow until the surrounding polymer-rich phase solidifies and a more or less developed cellular structure is formed. In case of composition path 3 the ternary protein solution becomes unstable and even small concentration fluctuations induce the phase inversion process by spinodal demixing into a protein rich and a protein lean phase. The fundamental characteristic of spinodal demixing is the continuous and gradual change of composition accompanied by a slow growth of the quantity of both phases which are interconnected within themselves forming a three-dimensional bicontinuous network. The composition path 4 indicates the formation of protein rich nuclei in the matrix of a polymer-lean phase which form solid beads upon growth. This state can be in form of a gel or particles. A gel is formed if the concentration is high enough to build a continuous network by which the liquid component is immobilized (Matsumoto et al., 2006). If the concentration is below a certain threshold particles are formed by nucleation and growth.

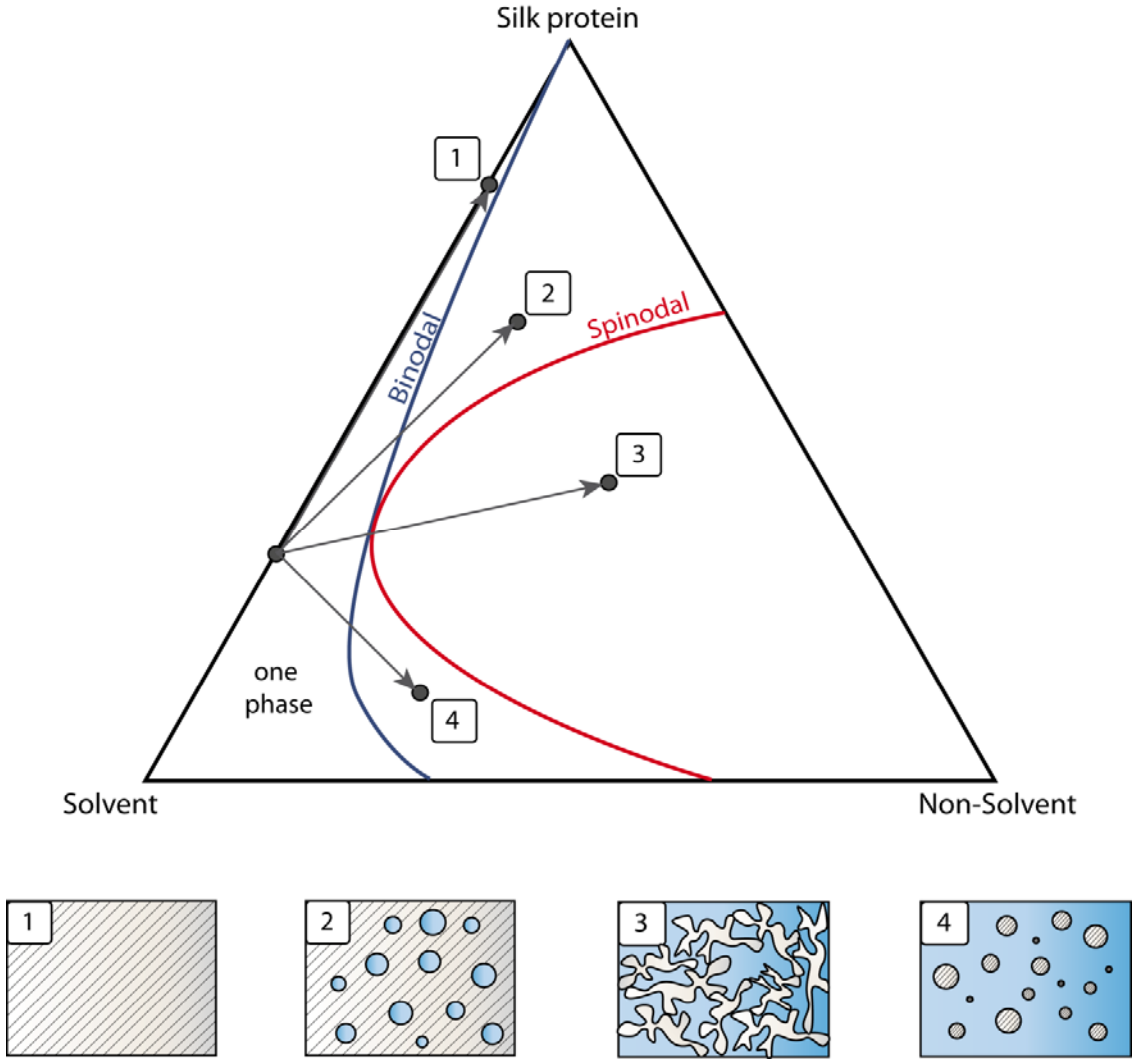

Figure 8. Ternary phase diagram of the silk protein/solvent/non-solvent system with various composition paths and modes of phase separation indicated by arrows and numbers. **1:** solidification, **2:** nucleation and growth of a polymer-lean phase, **3:** spinodal demixing, **4:** nucleation and growth of a silk protein-rich phase.

For fiber formation phase separation has to take place in combination with mechanical shearing and elongation (Rammensee et al., 2008). In nature silk is mainly employed in form of one-dimensional threads for various tasks, but silk proteins contain a much higher potential. As outlined, depending on the path taken in a phase diagram to initiate phase transition diverse morphologies for biomaterial applications in tissue engineering and drug delivery can be obtained (Figure 9). For instance, silk films by casting or layer by layer deposition employed as scaffolds or surface coatings (Huemmerich et al., 2006; Lawrence et al., 2008; Lawrence et al., 2009; Slotta et al., 2006). Nonwovens prepared

by electrospinning (Jin et al., 2002; Stephens et al., 2005). Porous foam like structures prepared by salt leaching, gas foaming or freeze drying (Lun et al., 2007; Nazarov et al., 2004; Wang et al., 2006). Hydrogel scaffolds formed upon sol gel transition induced by sonication or incubation in presence of ions and/or acids (Rammensee et al., 2006; Wang et al., 2008). Microspheres as carriers for controlled drug delivery formed by phase separation initiated by kosmotropic salts (Huemmerich et al., 2004b; Lammel et al., 2008b; Slotta et al., 2008; Wenk et al., 2008) and microcapsular carriers prepared by self assembly of silk proteins at an emulsion interface (Hermanson et al., 2007a; Hermanson et al., 2007b).

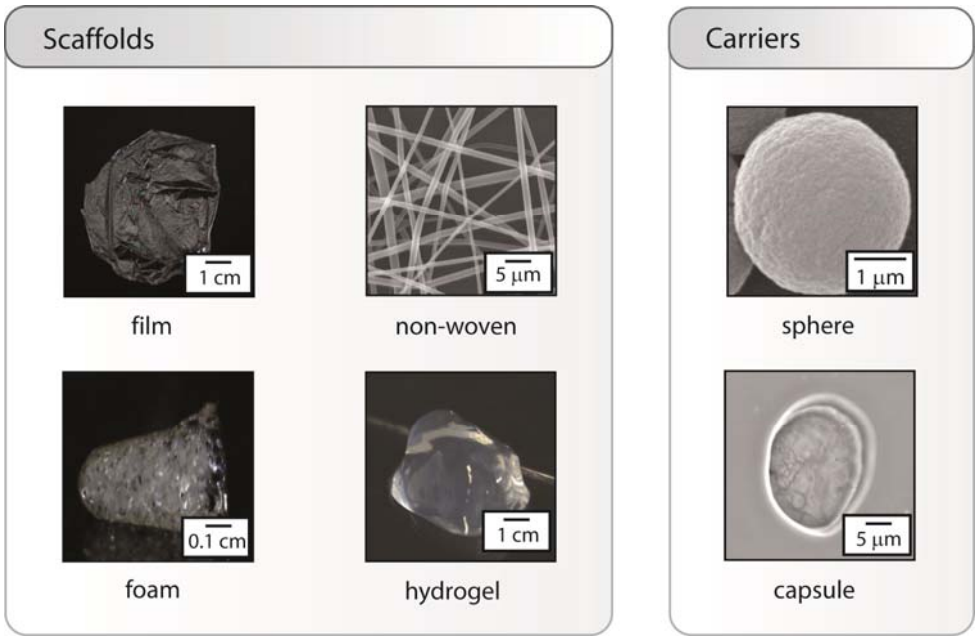

Figure 9. Assembly forms of silk proteins categorized according to potential applications as scaffolds in tissue engineering and drug carriers for drug delivery.

1.4 Motivation and aims of the thesis

Due to their mechanical stability along with its features of biocompatibility and biodegradability silk materials have a high potential for biomedical applications such as drug delivery systems. The motivation of the thesis was to develop a simple method to produce silk protein based drug carriers which can be produced and loaded within an all-aqueous process. Therefore, two different silk proteins (regenerated *B. mori* silk fibroin and recombinantly produced spider silk eADF4(C16)) were characterized with respect to their phase behavior and processing. The particle production process was characterized with respect to the adjustability of particles size, size distribution and the influence of process parameters on particle morphology and secondary structure. The applicability of silk based drug carriers was studied by detailed investigation of the loading process and release behavior employing various model drugs with different physicochemical properties. Additionally, the degradability and the release upon degradation was exemplarily studied using eADF4(C16) particles employing a mixture of elastase and trypsin, two naturally occurring proteases in vertebrates. Among the various morphologies (films, gels, fibers, nonwovens, foams, capsules and particles) into which silk proteins can be processed, films are the most interesting in terms of biomedical application for implant coatings or scaffolds in tissue engineering. Therefore, the processing of eADF4(C16) into films was studied in detail employing different solvents and additives in order to investigate how film features like secondary structure, surface morphology, mechanical stability and porosity can be controlled.

2 Materials and Methods

2.1 Materials and Instruments

2.1.1 Chemicals

Name	Company
Acetaminophen	Sigma-Aldrich (Deisenhofen, Germany).
Biperiden*HCl	Sigma-Aldrich (Deisenhofen, Germany).
Calciumchloride	Merck (Darmstadt, Germany)
Chlorthalidone	Sigma-Aldrich (Deisenhofen, Germany).
Ephedrine*HCl	Sigma-Aldrich (Deisenhofen, Germany).
Ethacridine lactate	Sigma-Aldrich (Deisenhofen, Germany).
Ethanol	VWR (Leuven, Netherlands)
Dipotassiumhydrogenphosphate	Merck (Darmstadt, Germany)
Glycerol p.a.	Sigma-Aldrich (Deisenhofen, Germany).
Guanidiniumhydrochlorid, > 99 %	Merck (Darmstadt, Germany)
Guanidiniumthiocyanat, zur Synthese	Merck (Darmstadt, Germany)
1,1,1,3,3,3 Hexafluor-2-Propanol	Merck (Darmstadt, Germany)
Magnesiumchloride	Merck (Darmstadt, Germany)
Methanol	Merck (Darmstadt, Germany)
Methyl violet	Sigma-Aldrich (Deisenhofen, Germany).
Nipagin	Sigma-Aldrich (Deisenhofen, Germany).
Papaverine*HCl	Sigma-Aldrich (Deisenhofen, Germany).
Phenol red	Sigma-Aldrich (Deisenhofen, Germany).
poly(ethylene oxide) (900 kDa)	Sigma-Aldrich (Deisenhofen, Germany).
Potassiumchloride	Merck (Darmstadt, Germany)
Potassiumdihydrogenphosphate	Merck (Darmstadt, Germany)
Procaine*HCl	Sigma-Aldrich (Deisenhofen, Germany).
Propranolol*HCl	Sigma-Aldrich (Deisenhofen, Germany).
Urea	Merck (Darmstadt, Germany)
PLGA RG502H	Boehringer Ingelheim (Ingelheim, Germany)
PLGA RG503H	Boehringer Ingelheim (Ingelheim, Germany)
PLGA RG504H	Boehringer Ingelheim (Ingelheim, Germany)
PLGA RG755S	Boehringer Ingelheim (Ingelheim, Germany)
Sodiumhydrogenphosphate	Merck (Darmstadt, Germany)
Sodiumchloride	Merck (Darmstadt, Germany)

Tetracaine*HCl	Sigma-Aldrich (Deisenhofen, Germany).
Tris-(hydroxymethyl)-aminomethan (Tris)	Roth (Karlsruhe, Germany)

All other inorganic salts, acids and bases as well as organic solvents were purchased from Merck (Darmstadt, Germany) or Roth (Karlsruhe, Germany). All buffers were made with bidistilled or ultra purified water from the Milli-Q-system of Millipore (Billerica, MA, USA).

2.1.2 Consumables

Name	Company
AFM plates, 15 mm	Ted Pella (Redding, USA)
Conducting silver	Plano W Planet GmbH (Wetzlar, Germany)
Disposable kuvettes, PMMA	Brand (Wertheim, Germany)
Glas suparasil kuvettes (different types)	Hellma (Mühlheim, Germany)
Pointprobe NCH-50 (Siliciumnitrid, radius ~ 7 nm)	Nanosensors(Neuchatel, Schweiz)
Spectrapore Dialysis membrane (MWCO 6-8 kDa)	Spectrum Laboratories Inc. (Rancho Dominggues, CA, USA)
Spectrapore Dialysis membrane (MWCO 3.5 kDa)	Spectrum Laboratories Inc. (Rancho Dominggues, CA, USA)
Slide-a-Lyzer dialysis cassettes (MWCO 3.5 kDa)	Thermo Scientific (Waltham, MA, USA)
Thermanox® plastic cover slips	Nalge Nunc Int. (Rochester, NY, USA)

All other consumables like tubes, pipettes, syringes and gloves etc. were purchased from Roth (Karlsruhe, Germany), Sarstedt (Nürnbrecht, Germany), Eppendorf (Hamburg, Germany) or VWR (Leuven, Netherlands).

2.1.3 Instruments

Name	Model	Company
Absorption spectrophotometer (UV-Vis)	Cary 100	Varian Medical Systems (Palo Alto, USA).
	Genesys6 (USA)	Thermo Fisher Scientific Inc. (Waltham, MA,USA)
Atomic force microscope (AFM)	MultiMode™ Scanning Probe Microscope	Veeco Instruments Inc. (Woodbury, NY, USA)

Centrifuges	Optima MAX-E, Rotor: TLA-45	Beckmann Coulter Inc.
	Optima MAX-XP, Rotor: TLA-55	(Fullterton, CA, USA)
	Avanti J-25, Rotors: JA10 &, JA25.50	
	Sigma 1-5	Sigma (Osterode, Germany)
Climate incubator	Certomat® IS	B. Braun Biotech (Melsungen, Germany)
Confocal microscope	DMIRE2	Leica (Wezlar, Germany)
Dynamic light scattering (DLS)	BI200-SM	Brookhaven (Holtsville, NY, USA)
Force transducer	FORT 25	WPI (Sarosota, USA)
Fourier transform infrared spectrometer (FTIR)	Equinox 55/ Tesnor 27 –Hyperion	Bruker (Ettlingen, Germany)
	IMV-4000 multi-channel FTIR-6200	Jasco (Japan)
Infrared microscope	IRscope	Bruker (Ettlingen, Germany)
Laser diffraction spectrometer	Partica LA-950	Horiba (Japan)
Light microscopy	Axio Scope	Carl Zeiss(Jena, Germany)
	Nikon-Laboshot	Nikon (Tokyo, Japan)
Linear motor	PS01-23x80 + B1100 controller	Linmot AG (Switzerland)
Micromixing device	100DX syringe pump + Series D pump controller	ISCO (Göttingen, Germany)
pH-meter	MP 220	Mettler Toledo (Greifensee, Switzerland)
Scanning electron microscope (SEM)	Zeiss Supra 55 VP SEM	Carl Zeiss (Jena, Germany) (Peabody, MA, USA)
	JSM 5900 LV	JEOL Ltd. (Japan)
Sonicator	Sonifier®ultrasonic cell disruptor	Branson (Danbury, CT, USA)
T-shape mixing element	Peek Tee, P-728 Threads 10-32	Upchurch Scientific (Oak Harbor, WA, USA)
Ultra fine scale	UMX-2	Mettler Toledo
Zetasizer	Nano ZS	Malvern (Worcestershire, UK)

2.2 Experimental Approaches

2.2.1 Aqueous silk protein solutions

2.2.1.1 Regenerated silk fibroin from *Bombyx mori*

Silk fibroin aqueous stock solutions were prepared as previously described by (Sofia et al., 2001). Briefly, cocoons of *B. mori* silkworm silk obtained from Tsukuba (Japan) were boiled for 30 min in an aqueous solution of 20 mM sodium carbonate (Na_2CO_3), and then rinsed thoroughly with distilled water to extract the glue-like sericin (Vepari and Kaplan, 2007). After air drying, the extracted silk fibroin was dissolved in 9.3 M LiBr solution at 60°C for 4 h, yielding a 20% (w/v) solution. The solution was dialyzed against distilled water using Slide-a-Lyzer dialysis cassettes (MWCO 3.5 kDa, Pierce) for 3 days to remove the salt. The solution was centrifuged 2 times at 10,000 rpm for 20 min to remove silk aggregates as well as debris from original cocoons. The final concentration of silk fibroin aqueous solution was approximately 8% (w/v), based on weighing the residual solid of a known volume of solution after drying at 60°C. The 8% silk stock solution was stored at 4°C and diluted with ultrapure water before use.

2.2.1.2 Recombinantly produced engineered spider silk eADF4(C16)

The amino acid sequence of eADF4(C16) was adapted from the natural sequence of ADF4 from *Araneus diadematus* (Huemmerich et al., 2004a). The repetitive part of ADF4 is generally composed of a single conserved repeat unit displaying only slight variations. Repetitive elements in the sequence of ADF4 display a polyalanine-rich motif with high glycine content, which was named C. Our previously established engineering approach allowed the combination and multimerization of single motifs, resulting in the eADF4(C16) protein comprising 16 repeats of the sequence GSSAAAAAAAASGPGGYGPENQGPSGPGGYGPGGP resulting in a molecular mass of 47.7 kDa (Huemmerich et al., 2004a). The protein was purified with purity higher than 98% as described previously by Huemmerich et al. (Huemmerich et al., 2004a). Lyophilized protein eADF4(C16) was dissolved in 6 M guanidinium thiocyanate. Dialysis was performed against 10 mM tris(hydroxymethyl)aminomethane(Tris)/HCl, pH 8, at 4°C

using membranes having a molecular weight cut-off at 6-8 kDa (Spectrum Laboratories, Rancho Dominguez, USA). The concentration of eADF4(C16) solution was determined by UV-Vis-spectrometry at 20°C using a Cary100 spectrophotometer (Varian Medical Systems, Palo Alto, USA) and the molar extinction coefficient of eADF4(C16) at 276 nm (ε = 46400 $M^{-1}cm^{-1}$).

2.2.1.3 Computation of physicochemical parameters based on amino acid sequence

To compute the values of physicochemical properties (charge distribution, isoelectric point (pI) an hydropathicity according to Kyte and Doolittle (Kyte and Doolittle, 1982)) of protein domains the ProtParam tool (ExPASy: Expert Protein Analysis System) was used (Bioinformatics). The amino acid sequences for H-fibroin and L-fibroin have been employed based on the Swiss-Prot/TrEMBL accession numbers P05790 and P21828 (Appendix A1 and A2). The amino acid sequence of eADF4(C16) is shown in Appendix A3. The amino acids were classified as positively charged (R and K), negatively charged (D and E), hydrophobic (A, G, L, V, W, C, I, M, F, P), and hydrophilic (N, Q, S, T, Y, R, D, E, H, K).

2.2.2 Silk fibroin particles

2.2.2.1 Particle preparation

Silk fibroin particles were prepared by an aqueous phase separation method. Briefly, the silk solution was mixed with potassium phosphate in volumetric ratios of 1:5 using a pipette. The influence of process parameters (ionic strength, pH and protein concentration) on salting out efficiency and particle formation were studied systematically. The resulting particles were stored in the refrigerator for 2 h before centrifugation at 2000 *g* for 15 min. Subsequently, particles were re-dispersed in purified water and washed three times.

2.2.2.2 Post treatments

In order to investigate the influence of different post treatments on the secondary structure of silk fibroin particles, FTIR spectra were collected after the various treatments. Particles were incubated in 5, 10, 20, 40, 70 and 100% ethanol or methanol for 24h. Changes in secondary structure were investigated upon sonication of a particle dispersion in a 2 ml Eppendorf tube by using a Branson ultrasonic cell disruptor with an energy output of 20% maximum amplitude for increasing exposure times (5, 10, 20, 30, 40, 60 s).

2.2.2.3 Stability in denaturating agents

Silk particles were exposed to aqueous solutions of 4, 6, and 8 M urea, 2, 4 and 6 M guanidinium hydrochloride (GdmCl) and 6 M guanidinium thiocyanate (GdmSCN). After particle incubation for three days at room temperature, all samples were assessed by phase contrast microscopy and compared to the control sample (incubation in water). If no difference regarding the presence and integrity of the particles was detected the particles were regarded chemically stable.

2.2.2.4 Drug loading

For experiments related to drug delivery a stock dispersion of protein particle concentration (10 mg/ml) was used. Particle concentrations (particles in mg/ml) were determined gravimetrically. Particles were produced by salting out a silk fibroin solution (c=5 mg/ml) with potassium phosphate (1.25 M, pH 8). Drug loading of the silk particles was conducted as follows: 100 µl of a silk particle suspension containing 2.4 nmol of silk protein was mixed with 900 µl of a model drug solution containing different molar ratios (silk fibroin (SF):model drug (MD) = 5, 10, 20, 30, 40, 60, 100). After 10 min of incubation at room temperature samples were centrifuged for 15 min at 2000 *g*, and the supernatant was analyzed for residual drug concentration using UV-Vis spectrometry. Standard calibration curves for model drugs were used for drug quantification. A control group of samples containing 100 µl water mixed with 1.0 ml of model drug solution was prepared for each experiment. Drug concentrations of control and sample supernatants

were used to calculate the amount of drug incorporated in the silk particles. All experiments were performed in triplicate. Encapsulation efficiency and loading were determined using equation (1) and (2), respectively:

$$encapsulation\ efficiency\ (w/w\,\%) = \frac{amount\ of\ model\ drug\ in\ particles}{model\ drug\ initially\ added} \times 100 \quad (1)$$

$$loading\ (w/w\,\%) = \frac{amount\ of\ model\ drug\ in\ particlese}{amount\ of\ particles} \times 100 \quad (2)$$

2.2.2.5 In vitro release

Drug loaded silk particles were washed with distilled water and suspended in 1 ml PBS (pH 7.4) before incubation at 37°C with constant shaking. Each vial contained 2 mg of drug loaded particles comprising 4.8 nmol silk protein. The solvent was periodically removed from each sample and replaced with fresh PBS (pH 7.4). The drug content in the medium was analyzed using UV-Vis-spectrometry. The percentage of cumulative model drug release (% w/w) was investigated as a function of incubation time. Each experiment was performed in triplicate. To study the effect of secondary structure of silk particles on release behavior, 2 mg drug loaded silk particles produced at pH 7, pH 8 and pH 9 were incubated in 1.0 ml PBS at pH 7.4 for 7 days. The solvent was withdrawn daily and the particles were redispersed in fresh media. Supernatants of drawn samples were analyzed for drug content with UV-Vis-spectrometry.

2.2.3 eADF4(C16) particles

2.2.3.1 Preparation of eADF4(C16) solution

Lyophilized protein eADF4(C16) was dissolved in 6 M guanidinium thiocyanate. Dialysis was performed against 10 mM tris(hydroxymethyl)aminomethane(Tris)/HCl, pH 8, at 4°C using membranes having a molecular weight cut-off at 6-8 kDa (Spectrum Laboratories, Rancho Dominguez, USA). The concentration of eADF4(C16) solution was determined by UV-Vis-spectrometry at 20°C using a Cary100 spectrophotometer (Varian Medical Systems, Palo Alto, USA) and the molar extinction coefficient of eADF4(C16) at 276 nm (ε = 46400 $M^{-1}cm^{-1}$).

2.2.3.2 Particle Preparation

Four aqueous preparation methods with different mixing intensities of an eADF4(C16) solution with potassium phosphate (2 M , pH 8) were employed for inducing phase separation via salting out: 1) simple mixing (pipette) 2) mixing in a micromixing device under laminar flow conditions (2 ml/min, Reynolds number (Re) *Re* = 85). 3) mixing in a micromixing device under turbulent flow conditions (50 ml/min, *Re* = 2122). 4) Dialysis of eADF4(C16) solution against 1 M potassium phosphate (pH8).

Micromixing Device: Constant volume flows of educt solutions (potassium phosphate and eADF4(C16) solution) were generated by two identical syringe pumps (Model 100DX, Teldyne Isco, Inc., USA). Pumps were operated by a digital controler (ISCO Series D, Teldyne Isco, Inc., USA). Mixing and precipitation was performed in a T-shaped mixing element with a circular mixing zone with a diameter of 500 µm (Peek Tee, P-728 Threads 10-32, Upchurch Scientific). The feed tubes were 500 µm in diameter located opposite to each other. In order to characterize the flow through the mixing element, a mixing Reynolds number is defined according to equation (3)

$$Re = \frac{u \cdot d}{\nu} = \frac{4 \cdot Q}{\pi \cdot d \cdot \nu} \qquad (3)$$

where u is the average fluid velocity, d is the diameter of the mixing zone, ν is the dynamic viscosity of water and Q is the volumetric flow rate. In the discussed experiments mixing was conducted at flow rates of 2 ml/min and 50 ml/min which correspond to Reynolds numbers of *Re* = 85 and *Re* = 2122. The flow inside the mixing zone can be considered turbulent due to the impinging of the two solutions. The generated suspensions were collected in 1.5 ml Eppendorf tubes.

2.2.3.3 Colloidal stability

The colloidal stability of eADF4(C16) particles in suspension was studied by adding 1.0 mg of particles to 1.0 ml of $(NH_4)_2SO_4$ solutions of varying concentration (0 - 2.0 M) and measuring the intensity of scattered light at a wavelength of 400 nm after 15 min. Based on Mie theory the intensity of scattered light in forward direction increases with

increasing particle size (Morrison and Ross, 2002). Therefore, the onset of electrolyte induced flocculation in dilute dispersions can be detected by an increase in intensity of scattered light in forward direction (Riley et al., 1999).

2.2.3.4 Drug loading

For experiments related to drug delivery a stock dispersion of known protein particle concentration (10 mg/ml) was used for all experiments. eADF4(C16) particles were prepared using a phase separation procedure as described above. Briefly, an aqueous eADF4(C16) (c = 1.0 mg/ml) solution was mixed with potassium phosphate (2 M, pH 8) in volumetric ratios of 1:10 using a pipette. The resulting particles were centrifuged for 10 min at 10,000 *g* and washed three times with purified water. Particles were redispersed in water, and particle concentrations (particles in mg/ml) were determined gravimetrically. Drug loading of spider silk particles was conducted as follows: 100 µl of spider silk particle suspension containing 21 nmol silk protein were mixed with 1.0 ml of model drug solution containing 210 nmol model drug. After 10 min of incubation at room temperature samples were centrifuged for 10 min at 10000 g, and the supernatant was analyzed for residual drug concentration using UV-Vis spectrometry. Standard calibration curves for model drugs were used for drug quantification. A control group of samples containing only 100 µl water mixed with 1.0 ml of model drug solution was prepared for each experiment. Drug concentrations of control and sample supernatants were used to calculate the amount of drug incorporated in the spider silk particles. All experiments were performed in triplicate. Encapsulation efficiency and loading were determined using equation (1) and (2), respectively.

2.2.3.5 In vitro release

Drug loaded eADF4(C16) particles were washed with distilled water and suspended in 1 ml PBS (pH 7.4) before incubation at 37°C with constant shaking. Each vial contained 2 mg of drug loaded particles comprising 42 nmol spider silk protein. The solvent was periodically removed from each sample and replaced with fresh PBS (pH 7.4). Then, the drug content in the medium was analyzed using UV-Vis-spectrometry. The percentage of cumulative model drug release (% w/w) was investigated as a function of incubation

time. Each experiment was performed in triplicate. To study the effect of different pH values on the release behavior of drug loaded eADF4(C16) particles, 1 mg drug loaded silk particles were incubated in 1.0 ml PBS at 5 different pH values (pH 2, 4, 6, 7.4 and 8.8) for 5 days. The solvent was withdrawn daily and the particles were redispersed in fresh media. Supernatants of drawn samples were analyzed for drug content with UV-Vis-spectrometry.

2.2.3.6 In vitro degradation

In order to analyze the degradability of eADF4(C16) silk particles, we employed a mixture of elastase and trypsin, two naturally occurring proteases in vertebrates. Elastase is a single polypeptide chain of 240 amino acid residues and contains four disulfide bridges. Elastase is synthesized as an inactive zymogen, which requires limited proteolysis at its N-terminal by trypsin in order to produce the active enzyme (Boyer, 1971). Elastase is a serine protease with a broad specifity, as it will cleave proteins at the carboxyl side of small hydrophobic amino acids such as Ile, Gly, Ala, Ser, Val and Leu. Due to the relatively high content of glycin and alanin in eADF4(C16) (≈ 50% of the total amino acid composition), such proteases were chosen to study the degradability of eADF4(C16) particles. Furthermore, degradation studies employing elastase are of special interest since it is mainly secreted by neutrophils and macrophages which are important components of the innate human immune system (Jones et al., 1990; Sonawane et al., 2006). Elastase and trypsin have an optimum activity at 25°C. To assess the degradability, 1.0 mg of silk particles with an average diameter of 700 nm were incubated at 25°C in 1.0 ml PBS in the presence of 0.8 µg elastase and 12.5 µg trypsin. Over two weeks, samples were drawn on a daily basis and centrifuged. The pellets, containing eADF4(C16) particles, were redispersed in distilled water and washed three times for further analysis of size and morphology using laser diffraction spectrometry and scanning electron microscopy. Elastase and trypsin from hog pancreas were supplied by Sigma Aldrich (St. Louis, USA).

2.2.3.7 In vitro release upon degradation

The release upon degradation was exemplarily studied with methyl violet loaded eADF4(C16) particles. Therefore, 2 mg of loaded particles were suspended in 1 ml PBS (pH 7.4) in presence of a mixture of elastase and tryppsin at five different concentrations [*control:* no enzymes; *C1:* (0.8 µg elastase + 12.5 µg trypsin)/ 1mg eADF4(C16); *C2:* (1.6 µg elastase + 25 µg trypsin)/ 1mg eADF4(C16); *C3:* (2.4 µg elastase + 37.5 µg trypsin)/ 1mg eADF4(C16); *C4:* (4.0 µg elastase + 62.5 µg trypsin)/ 1mg eADF4(C16); *C5:* (8.0 µg elastase + 125 µg trypsin)/ 1mg eADF4(C16)]. The release upon degradation was conducted by incubation in different release media at 25°C with constant shaking for 7 days. The solvent was periodically removed from each sample and replaced with fresh release media. Then, the drug content in the medium was analyzed using UV-Vis-spectrometry. The percentage of cumulative methyl violet release (% w/w) was investigated as a function of incubation time. Each experiment was performed in triplicate.

2.2.4 eADF4(C16) films

2.2.4.1 Preparation of samples for mechanical analysis

Engineered spider silk protein eADF4(C16) was dissolved in hexafluoroisopropanol (HFIP) at a concentration of c=50 mg/ml and casted onto a PDMS substrates (30 x 30 mm). For films blended with 10%, 20%, 30% and 40% glycerol the corresponding amount was added to the eADF4(C16)/HFIP solution prior to casting and incubated over night to ensure homogeneous mixing. Films without glycerol were air dried at room temperature for 48 h whereas films containing glycerol were dried for 7 days. Subsequently, the films were treated with 50% Methanol for stabilization. After 24 h drying the samples used for mechanical testing (2 x 15 mm) were cut with a scalpel.

2.2.4.2 Preparation of samples for analysis of secondary structure

To study the influence of different solvents (HFIP and water), additives (glycerol and poly(ethylene oxide) (PEO)), and different posttreatments (water, 10 – 100 % Methanol)

on eADF4(C16) film secondary structure, films were directly casted onto CaF_2 discs and analyzed using fourier transform infrared spectroscopy (FTIR).

2.2.4.3 Microstructuring by blending with PEO

Blending of eADF4(C16) with polyethylene oxide (PEO) can be used to create porous structures since PEO can be dissolved by water after stabilization (e.g. with methanol) of eADF4(C16) films. Therefore, different amounts of PEO were blended with aqueous eADF4(C16) solutions and eADF4(C16)/HFIP solutions (PEO: eADF(C16)= 1-333% (w/w)). The influence of PEO content on pore formation and pore size was studied using scanning electron microscopy (SEM).

2.2.5 Preparation of PLGA Films

Different grades of poly(lactic-*co*-glycolic acid) (PLGA) called RG502H, RG503H, RG504H, and RG755S (purchased from Boehringer Ingelheim) were dissolved in aceton at a concentration of c = 100 mg/ml and casted onto a 50 x 50 mm Teflon substrate. The Films were air dried at room temperature for two weeks and subsequently cut into rectangular (2 x 20 mm) samples. The different PLGAs varied in respect to their composition, free endgroup, and inherent viscosity which is a measure for the degree of polymerization. The higher the inherent viscosity of a polymer in a solvent the higher is the molecular mass of the polymers. The characteristics of the employed PLGAs are summarized in Table 2.

Table 2. Overview of different PLGA grades specifications (composition, chain length controller, and group and inherent viscosity). PLGA Resomers® were purchased from Boehringer-Ingelheim.

PLGA grade	Composition	Chain length controller	End group	Inherent viscosity [dl/g]
RG502H	Poly(D,L-lactide-co-glycolide) 50:50	hydroxycarboxylic acid	free carboxylic acid	0.16-024
RG503H	Poly(D,L-lactide-co-glycolide) 50:50	hydroxycarboxylic acid	free carboxylic acid	0.32-0.44
RG504H	Poly(D,L-lactide-co-glycolide) 50:50	hydroxycarboxylic acid	free carboxylic acid	0.45-0.60
RG755S	Poly(D,L-lactide-co-glycolide) 75:25	alcohol	alkyl	0.71-1.0

2.3 Analytical methods

2.3.1 Light microscopy

Phase contrast light microscopy was used to analyze the presence of particles after phase separation. Therefore, 20 µl silk particle suspensions were placed under an inverted light microscope (Axio Scope, Carl Zeiss, Jena, Germany or Nikon-Laboshot, Nikon, Tokyo, Japan) and Images were taken with the installed software.

2.3.2 Confocal microscopy

B. mori silk fibroin particles: The RhB-loaded silk particles were prepared and resuspended in purified water. A small portion of the suspension was imaged using a 63×, 1.4 N.A. water 14 immersion lens on a Leica DMIRE2 microscope (Wezlar, Germany) at an excitation wavelength of 555 nm and an emission wavelength of 580 nm. Several *xy* scans with an optical slice of 100 nm were stacked along the z-direction to obtain a 3-*D* image and visualize the crossections of silk particles and the distribution of encapsulated RhB.

Porous eADF4(C16) films: The presence of transmembrane pores was assessed by performing *xy* scans with an optical slice thickness of 100 nm along the z direction. From the obtained 3-D image crossections were drawn to visualize the paths and dimensions of pores in the membrane.

2.3.3 Scanning electron microscopy (SEM)

B. mori silk fibroin particles: Twenty microliters of the silk particle suspension in water were added directly on top of a conductive tape mounted on a SEM sample stub. The samples were dried overnight in air and then sputtered with platinum. The morphologies of silk spheres were imaged using a Zeiss Supra 55 VP SEM (Carl Zeiss SMT, Peabody, MA. Images were taken with the installed software.

eADF4(C16) particles: The eADF4(C16) particles were immobilized on Thermanox plastic cover slips (Nagle Nunc, USA), dried at room temperature, gold sputtered under vacuum, and analyzed with a JSM 5900 LV scanning electron microscope (JEOL Ltd., Japan, at 20 kV).

eADF4(C16) and PLGA films: For determination of film thickness air dried films prepared as described in 2.2.4.1 and 2.2.5 were vertically immobilized on Thermanox plastic cover slips (Nagle Nunc, USA), gold sputtered under vacuum, and analyzed with a JSM 5900 LV scanning electron microscope (JEOL Ltd., Japan, at 20 kV).

2.3.4 Atomic force microscopy (AFM)

Atomic force microscopic images of porous eADF4(C16) films were taken in order to analyze the surface topography. Porous films were placed on freshly cleaved mica AFM plates. Tapping mode imaging was carried out on a multimode scanning probe microscope (Veeco, Santa Barbara, CA, USA) using a siliconnitrid cantilever *(*NCH-50, Nanosensors; tip ~7 nm) and data recording was performed at 1.5 Hz. For determination of surface topography the installed Software Nanoscope (Veeco) was employed.

2.3.5 UV-Vis-spectrometry

Protein concentration: Determination of protein concentration: The concentration of eADF4(C16) solutions was determined by UV measurements at 20°C using a Cary100 spectrophotometer (Varian Medical Systems, Palo Alto, USA). The molar extinction coefficient of eADF4(C16) (40974 $M^{-1}cm^{-1}$) at 276 nm and 20°C was employed.

Drug loading and release: Ultraviolet–visible spectrometry, using a Genesys6 (Thermo Fisher Scientific Inc., Waltham, MA, USA), was employed for determination of drug concentration in supernatants as a basis for the calculation of loading efficiency and release behavior. Calibration curves for all model drugs were obtained by using five different concentrations of all stock solutions.

2.3.6 Laser diffraction spectrometry

Particles sizes and their distributions were determined in triplicate using Laser diffraction spectrometry (Horiba, Partica LA-950, Japan). Refractive indices of 1.33 for water and 1.60 for protein were taken for computation of particle sizes. In order to eliminate concentration effects, all samples were measured at equal concentrations resulting in a transmittance of 82%. In addition, a dry specimen of each preparation was analyzed by SEM to confirm sphere formation and sphere sizes.

2.3.7 Dynamic light scattering

DLS experiments were performed using a Brookhaven Instrument BI200-SM goniometer (Holtsville, NY) equipped with a diode laser operated at a wavelength, λ = 532 nm. The temperature was kept at 25°C with 0.05°C accuracy with a temperature-controlled re-circulating bath. Refractive indices of 1.33 for water and 1.60 for protein were taken for computation of particle sizes. In addition, a dry specimen of each preparation was analyzed by scanning electron microscopy (SEM) to confirm spherical shape and sphere size.

2.3.8 Fourier transform infrared spectroscopy (FTIR)

B. mori silk fibroin and eADF4(C16) particles: Washed silk particle samples were first cast on CaF_2 IR transparent discs and then placed under a Bruker Equinox 55 FTIR spectrometer or a IMV-4000 multi-channel FTIR microscopic spectrometer (Jasco, Japan, interfaced to a FTIR-6200 Spectrometer) or, with a liquid nitrogen cooled MCT (mercury cadmium telluride) detector. Analysis was performed in transmission mode using the microscope. The position and focus of the samples were adjusted microscopically through an aperture in the IR optical system. For each measurement, 128 scans were co-added and Fourier transformed employing a Genzel-Happ apodization function to yield spectra with a nominal resolution of 4 cm^{-1}. The measurements were carried out at 25°C and 30% relative humidity. The wave number ranged from 400 to 4000 cm^{-1}. To identify secondary structures of protein samples from the absorption spectra, the amide I region

(1595 - 1705 cm^{-1}) was investigated by Fourier self-deconvolution (Hu et al., 2006a) using the Opus 5.0 software from Bruker Optics Corp. (Billerica MA), as described previously. Using a high pass filter, the broad and indistinct amide I bands (C=O stretching bonds in protein backbones) were narrowed synthetically to provide a deconvoluted spectrum with better peak resolution (Hu et al., 2006a). The deconvoluted spectra were curve-fitted by subsequent Gaussian peaks (Hu et al., 2006a). Finally, the deconvoluted amide I spectra were area-normalized, and the relative areas of the single bands were used to determine the fraction of the secondary structural elements. Secondary structure elements were assigned to their corresponding absorption bands at frequencies as listed in Table 3.

Table 3. Vibrational band assignments in the Amide I region (1595 - 1705 cm-1) for silk proteins (Hu et al., 2006a).

Wavenumber range [cm^{-1}]	Assignement
1616-1637	β-sheets
1638-1655	random coil
1656-1663	alpha-helices
1663-1695	β-turns
1695–1705	β-sheets

2.3.9 Zetapotential Analysis

eADF4(C16) particles: In order to elucidate and characterize the loading mechanism of eADF4(C16) particles with model drugs, zeta potential measurements have been conducted as a function of amount of model drug added. The zeta potential was determined using a Nanoseries Malvern Zetasizer (Malvern, Worcestershire, UK). Automatic titration was conducted with a Malvern Multipurpose Titrator MPT-2. Experiments have been performed in distilled water (pH 7) at 25°C. Each measurement was performed in triplicate.

B. mori silk fibroin particles: Zeta potential measurements were determined using a Nanoseries Malvern Zetasizer (Malvern, Worcestershire, UK). In order to investigate the influence of particle loading, zeta potential measurements were conducted as a function of model drug content.

2.3.10 Mechanical analysis

The mechanical characteristics (tensile strength, elongation, E-modulus and toughness) of eADF4(C16) films were assessed in a custom built vertical tensile test setup. Briefly, the top end of the samples was fixed to a force sensor and the bottom end to a linear motor. Therefore, a Linmot PS01-23x80 motor (Linmot AG, Switzerland) controlled by a Linmot B1100 controller which was connected to the control computer via RS-232 was used. The force transducer (FORT25, WPI, Sarosota, USA) used in this setup works by measuring small deflections of a cantilever by optical methods. In detail, this means that the measurement cantilever is illuminated by an LED light source, and the total intensity that is collected in the photosensor is measured. For small cantilever deflections, a linear relation between the deflection of the cantilever and the signal in the photosensor is reported by the manufacturer. The force sensor was calibrated by pipetting known volumes of water into a vial hanging from the sensor. The calibration showed that the sensor is perfectly linear in the used measurement range. The tensile test apparatus is controlled by the software provided by the manufacturer of the linear motor and by a custom-built LabView program which triggers the motor and records force sensor data to the hard disk of the computer. The pulling velocity for each measurement was 1 mm/s and the data was recorded at a rate of 500 datapoints/s.

3 RESULTS

3.1 Silk fibroin particles for drug delivery

3.1.1 Characterization of *Bombyx mori* silk fibroin

Regenerated silkworm cocoon silk from *B. mori* contains two structural proteins, the fibroin heavy chain (H-chain ≈ 392 kDa) and light chain (L-chain ≈25 kDa). The H- and L-chains are linked by a single disulfide bond at the twentieth residue from the carboxyl terminus of H-chain (Cys-c20) and Cys-172 of L-chain (Tanaka et al., 1999). In order to characterize the silk fibroins unfolded state, the hydophobicty plots of H- and L-chain were computed based on their amino acid composition (Appendix A1 and A2) using the model of Kyte and Doolittle (Kyte and Doolittle, 1982). The position at the x axis reflects the corresponding amino acid of the protein, starting at the amino terminus and ending at the carboxy terminus (Figure 10 a,b). The hydrophobicity index relates the relative hydrophobicity among amino acids in which more positive values indicate stronger hydrophobicity.

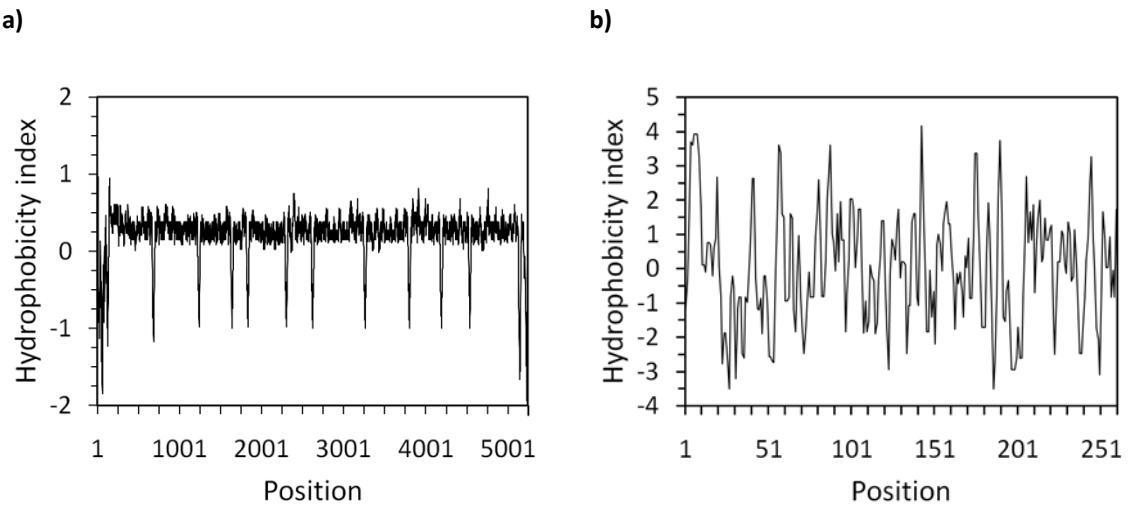

Figure 10. Hydrophobicity plot of *B. mori* silk fibroin. The position at the x axis reflects the corresponding amino acid of the protein, starting at the amino terminus and ending at the carboxy terminus. The hydrophobicity index relates the relative hydrophobicity among amino acids; more positive values indicates stronger hydrophobicity. **a)** Heavy chain: Hydrophilic N- and C-terminal domains with a repetitive

central part with predominant contents of hydrophobic amino acids separated by regularly interspersed hydrophilic spacers. **b)** Light chain: Irregular counterbalanced amphilicity.

Furthermore, to model the primary structure the protein has been (virtually) subdivided into four domains: N-Terminus, repetitive part, C-Terminus and L-chain for each of which physicochemical properties (charge, isoelectric point (pI), hydropathicity and size) were determined based on the amino acid sequences (Table 4).

Table 4: Computed physicochemical parameters (charge ratio, isoelectric point (pI), hydropathicity and size) of N-terminus, repetitive part and C-Terminus of silk fibroin heavy chain as well as the C-terminal linked light chain.

	N-terminus	repetitive part	C-terminus	light chain
charge ratio (-/+)	(20/12)	(34/5)	(1/9)	(22/15)
pI	4.6	3.8	10.5	5.1
hydropathicity	-0.35	0.24	-0.48	0.05
size (aa)	151	5062	50	262

The derived model of the unfolded silk fibroin is shown in Figure 11. The N- and C-termini are hydrophilic domains (Figure 10a) with the N-terminus being negatively charged (pI = 4.6) and the C-terminus (pI = 10.5) being positively charged at a physiological pH of 7.4 (Table 4). The repetitive part (pI = 3.8) consists of long hydrophobic domains with short intervening hydrophilic blocks (spacers) with negative charges (Figure 10a, Table 4). The L-chain has a counterbalanced amphiphilicity and a slightly dominant average negative charge (Figure 10b, Table 4).

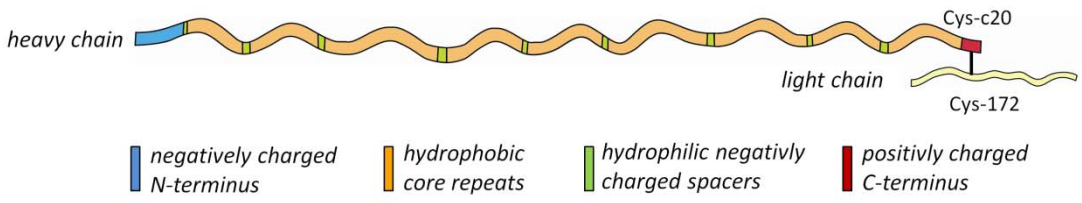

Figure 11. Model of unfolded silk fibroin from *B. mori* based on amino acid sequence and computed parameters (charge ratio, isoelectric point (pI), hydropathicity and size) as listed in Table 4.

3.1.2 Phase behavior of silk fibroin upon salting out

In an aqueous solution, dissolved proteins are covered with a hydration layer. The quality of the hydration layer depends on the interaction of the protein with water as well as on the presence of other solutes (ions, polymers etc.) or surfactants in solution.
As outlined in the introduction, depending on the initial protein concentration as well as on the extent of solvent quality reduction phase transition into protein particles or gelation occurs. In this work, our interest was to produce particles within an all-aqueous biocompatible (without surfactants or stabilizers) process. Therefore we investigated the phase behavior of *B. mori* silk fibroin upon addition of different salts. According to the Hofmeister series ions can be classified with respect o their influence on water structure. Kosmotropic ions, increase the structure of water stabilizing the protein structure which gives rise to salting-out whereas chaotropic ions have the adverse effect (Figure 12).

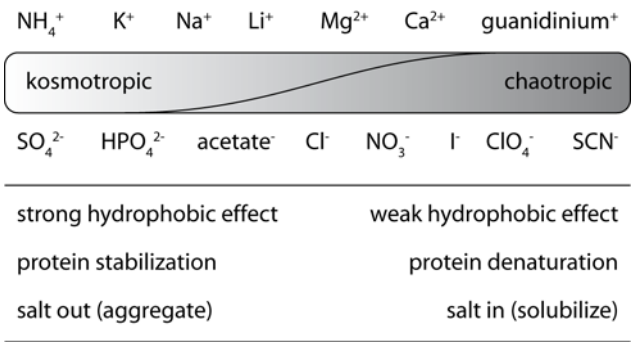

Figure 12. Hofmeister series: Salts have consistent effects on the solubility of proteins and on the stability of their secondary and tertiary structure. Importantly, anions have a larger effect than cations.(Figure adopted from (Lammel et al., 2008a))

To assess the effect of different kosmotropic salts on the phase separation, salt solutions (ionic strength = 1.5 M) were mixed with an aqueous silk fibroin solution (c = 5 mg/ml) at a volumetric ratio of 2:1. After incubation for 10 min and subsequent centrifugation at 2000 *g* for 15 min the protein concentration in the supernatant was determined with UV-Vis-spectrometry and the salting out efficiency was calculated using equation (4) (Figure 13a).

$$salting\ out\ efficiency\ (\%) = \left(1 - \frac{silk\ concentration\ in\ supernatant}{initial\ silk\ concentration}\right) \times 100 \quad (4)$$

The presence of particles, examined by light microscopy was observed for salting out with Na_2SO_4, K_2HPO_4 and $NaPO_4$ whereas for NH_4Cl and NaCl no particles could be detected. Furthermore, the influence of ionic strength on particle formation was studied by addition of potassium phosphate (pH8) of different ionic strengths (Figure 13b). The lower threshold of ionic strength necessary for particle formation was determined to be approximately 0.75 M. To investigate the influence of pH at constant ionic strength (1.25 M) we employed potassium phosphate, since the pH can be adjusted by mixing mono- and dibasic potassium phosphate solutions (KH_2PO_4 solution = pH 4; K_2HPO_4 solution = pH 9) without adding other ions (which would be the case for typical pH adjustment using HCl and NaOH).

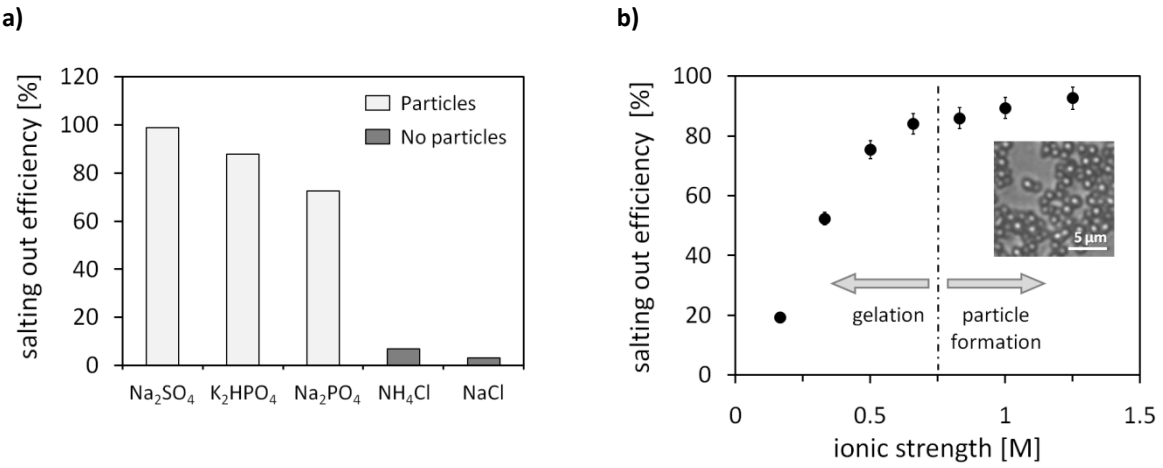

Figure 13. Influence of salts on phase separation determined by investigation of salting out efficiencies. **a)** Salting out efficiency of different salts as indicated. The presence of particles, examined by light microscopy was observed for salting out with Na_2SO_4, K_2HPO_4 and $NaPO_4$. **b)** Influence of ionic strength on phase separation by salting out with potassium phosphate (pH 8). The threshold of ionic strengths for particle formation was determined to be 0.75 M.

Figure 14a shows the salting out efficiency as a function of pH and phase contrast micrographs taken of particles produced at pH 4, 6 and 9. Below pH 5 the particles aggregated into non-dispersible clusters due to dominating intermolecular hydrogen bonding, which correlates with the theoretical isoelectric point of silk fibroin, pI = 4.53 [47]. Figure 14b-15d show scanning electron micrographs of the particles formed at pH 4, 5 and 6. No difference of particle morphology produced at pH > 6 was evident.

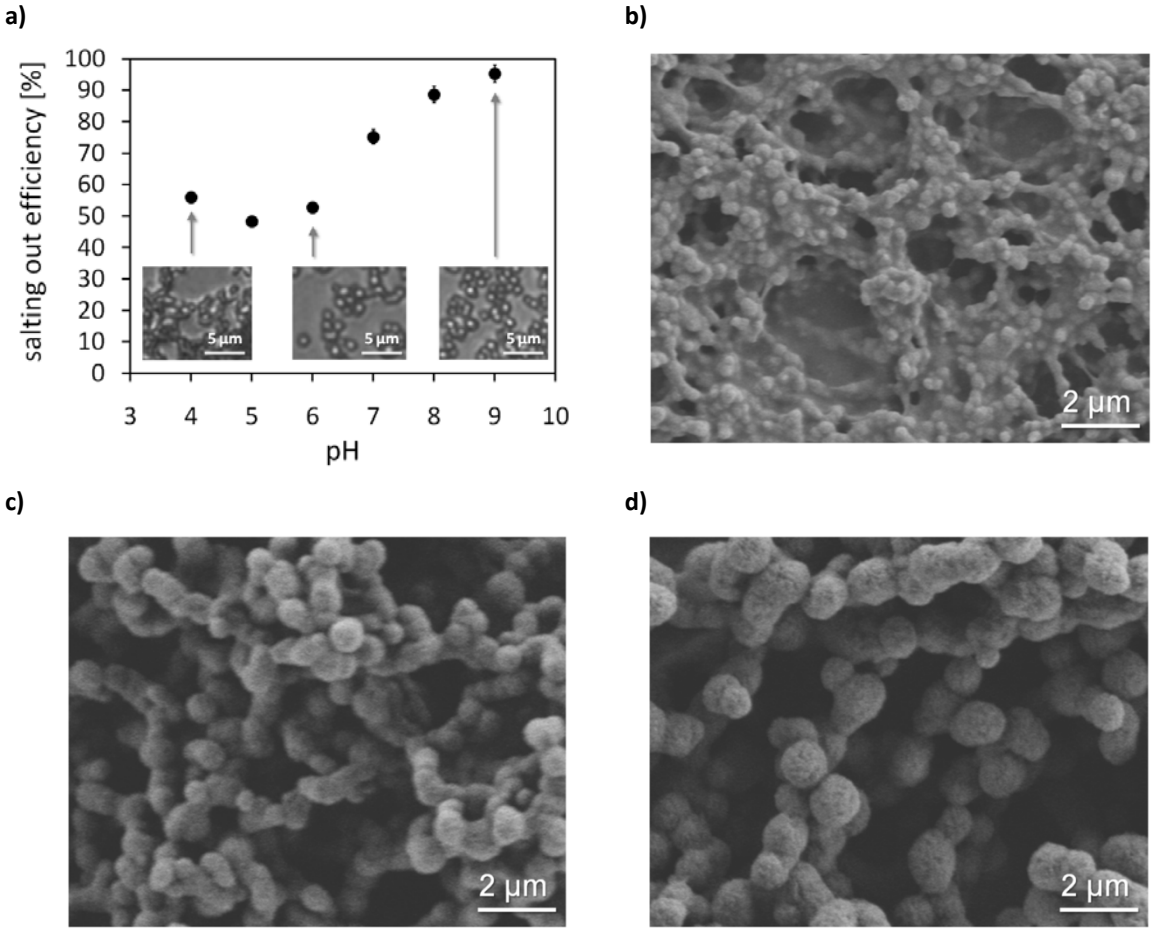

Figure 14. Influence of pH on silk particle formation by salting out with 1.25 M potassium phosphate. **a)** Salting out efficiency as a function of pH as indicated. **b-d)** Scanning electron micrographs of particles produced by salting out with 1.25M potassium phosphate at **b)** pH 4, **c)** pH 5 and d**)** pH 6.

3.1.3 Phase separation of silk fibroin solution into particles of varying size

As mentioned before, the initial protein concentration is mainly responsible if particle formation or gelation takes place upon addition of kosmotropic salts. Therefore we studied the effect of protein concentration on particle formation by salting out silk fibroin with 1.25 M potassium phosphate (pH 8). Dynamic light scattering showed that in the concentration range between 0.25 mg/ml and 2 mg/ml particle size increased linearly from an average diameter of 486 nm to 1.2 µm with a narrow size distribution (Figure 15 a,b). From 4 mg/ml to 8 mg/ml the average size increased slightly from 1.4 to 2.0 µm with a broader size distribution (Figure 15 a,b). Above a concentration of 10 mg/l the size distribution increased, caused by the formation of clusters and amorphous

aggregates (Figure 15 a,b,e). The averages sizes were confirmed qualitatively by SEM (Figure 15 c-d).

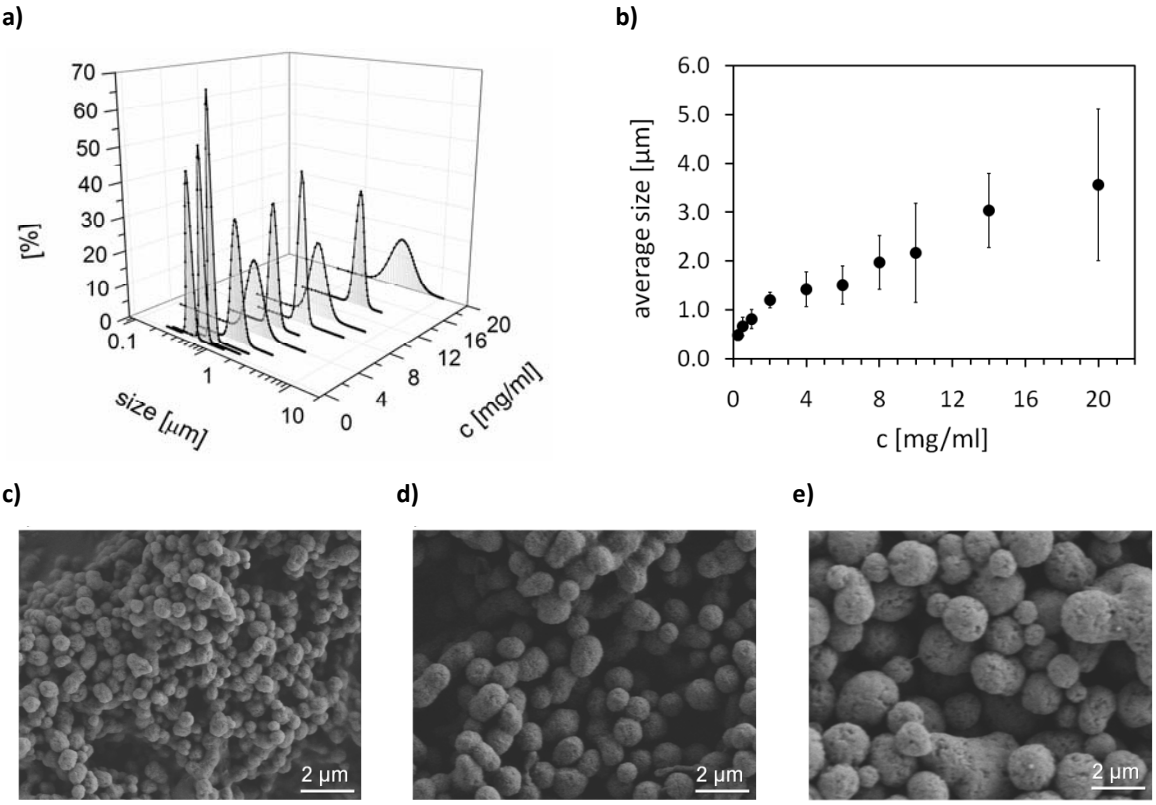

Figure 15. Size analysis of silk particles produced from different concentrations of protein by salting out with potassium phosphate (1.25 M, pH 8). **a)** Size distributions of silk particles as a function of protein concentration. **b)** Average size of silk particles as a function of protein concentration. Error bars indicate the width of the size distribution. **c)-e)** Scanning electron micrographs of silk particles produced by salting out with potassium phosphate (1.25 M, pH 8) from silk fibroin solution of **c)** 0.25 mg/ml, **d)** 2 mg/ml **e)** 20 mg/ml.

3.1.3 Characterization of silk fibroin particles

The following section summarizes the results regarding the characterization of secondary structure, zetapotential and stability in denaturating agents for different production conditions.

3.1.3.1 Secondary structure

FTIR analysis of silk fibroin particles produced at different pH values showed that the secondary structure changed from a silk II-rich structure at pH 4 to a silk I-rich structure at pH 9 (Figure 16a). The secondary structure composition of particles produced at different pHs was determined by Fourier self deconvolution (FSD). Example FSD spectra for pH 6, pH 7 and pH 8 are shown in Figure 16 b-16 d. Table 5 provides the quantitative analysis of secondary structures of different particles produced.

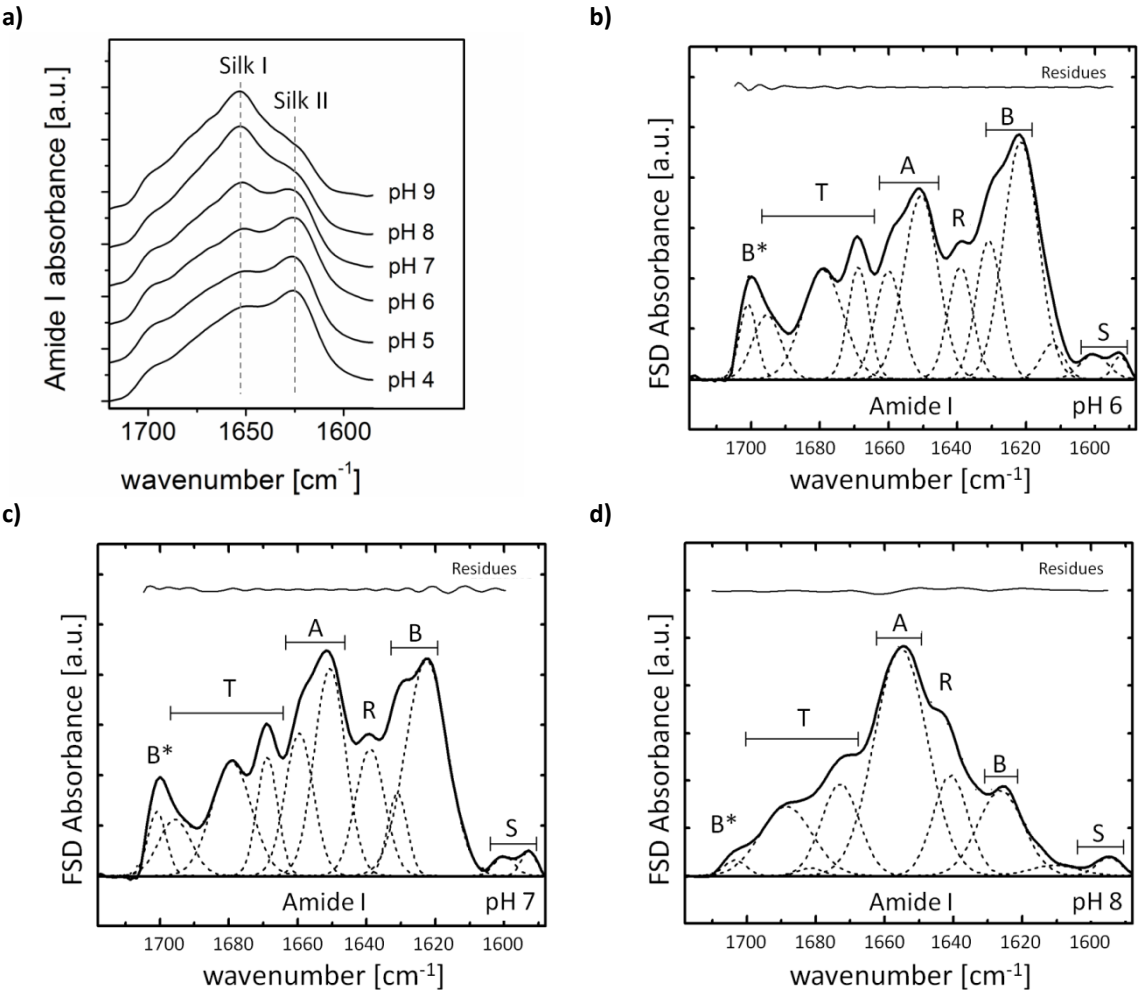

Figure 16. Influence of pH on secondary structure of silk fibroin particles. **a)** FTIR spectra of particles produced by salting out with 1.25 M potassium phosphate at different pH values as indicated. **c-d)** Fourier self deconvolution of FTIR spectra for particles produced by salting out with 1.25 M potassium phosphate at **b)** pH 6 **c)** pH 7 and **d)** pH 8. The peaks are marked with abbreviations that stand for: turns (T), alpha helix (A), random coil (R), inter- and intramolecular beta sheets (B), intramolecular beta sheets (B*) and side chains (S).

Table 5. Secondary structure content of silk fibroin particles produced by salting out with 1.25 M potassium phosphate at different pH values.

Secondary structure	Particles produced at					
	pH 4	pH 5	pH 6	pH 7	pH 8	pH 9
Beta-sheets [%] (±2%) (1610–1635 cm^{-1}, 1695–1700 cm^{-1})	39.4	37.4	37.4	31.1	15.1	21.5
Alpha-Helix [%] (±2%) (1647–1664 cm^{-1})	24.1	25	26.1	29.9	44.1	38.4
Random-coil [%] (±1%) (1635–1645 cm^{-1})	9.2	8.6	10.3	10.6	12.5	10.2
Beta-turns [%] (±2%) (1666–1695 cm^{-1})	25.7	26.8	24.3	27.3	26.7	28.7
others [%] (±1%) (1590–1605 cm^{-1})	1.6	1.2	1.9	1.1	1.6	1.2
(1699-1703cm^{-1})	5.5	3.1	3.7	1.1	1.2	2

3.1.3.2 Zetapotential

Zeta potential measurements of particles produced at different pH values indicate that the zeta potential increased from -26.3 mV (pH 4) to -46.0 mV (pH 9) when measured after washing three times with ultrapure water (Figure 17).

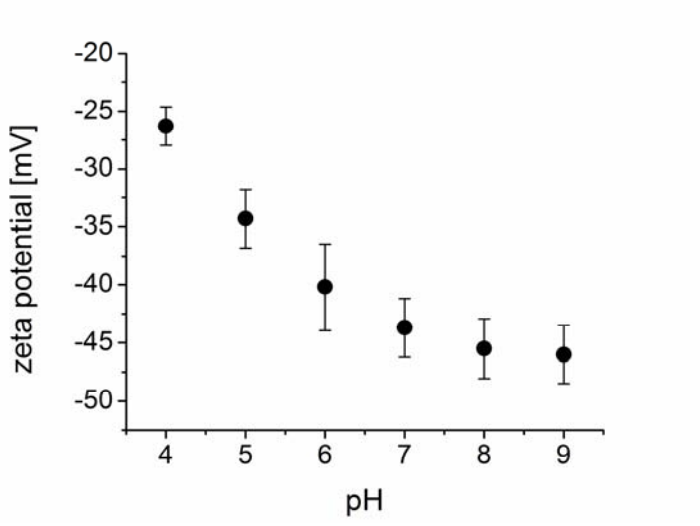

Figure 17. Zeta potential of particles produced by salting out with 1.25 M potassium phosphate at different pH values. Error bars indicate the width of the zeta potential distribution of the particles.

3.1.3.3 Stability in denaturating agents

The chemical stability of particles produced at pH 7, pH 8 and pH 9 was assessed by incubation of particles in urea and chaotropic salts like GdmHCl and GdmSCN at different concentrations. After particle incubation for three days at room temperature, all samples were assessed by phase contrast microscopy and compared to the control sample (incubation in water). If no difference regarding the presence and integrity of the particles was detected the particles were regarded chemically stable. All particles were stable in water and dissolved in 6M GdmSCN (Table 6). Within the studied pH range the chemical stability of the particles decreased when the particles were produced at lower pH values (with higher silk II structural content) (Table 5 and Table 6).

Table 6. Solubility of silk fibroin particles produced at different pH values in water; 4, 6, 8M Urea; 2, 4, 6 M GdmHCl and 6 M GdmSCN. After particle incubation for three days at room temperature, all samples were assessed by phase contrast microscopy and compared to the control sample (incubation in water). If no difference regarding the presence and integrity of the particles was detected the particles were regarded chemically stable.. + fully resolved particles, - non-soluble/ stable intact particles, +/- morphology change of particles into a gel like structure.

Resolved in	Water	Urea 6 M	Urea 8 M	GdmHCl 2 M	GdmHCl 4 M	GdmHCl 6 M	GdmSCN 6 M
Particles produced at							
pH 9	-	-	-	-	-	-	+
pH 8	-	-	-	-	-	+/-	+
pH 7	-	-	+/-	-	+/-	+	+

3.1.4 Post treatment

In order to investigate the influence of post processing treatment with alcohols or sonication on the secondary structure of silk fibroin particles, FTIR spectra were recorded. Figure 2a shows only minor changes in secondary structure upon treatments with increasing ethanol concentration. Therefore the particles can be sterilized with ethanol without affecting their secondary structure. Interestingly methanol treatments

showed a similar result (Figure 2b) indicating that the silk I - conformation in *B. mori* silk fibroin particles produced by salting out is very stable. Sonication is often used for making particle suspensions. Since silk hydrogels with silk II conformation are formed upon sonication of a silk solution for exposure times < 30s (Wang et al., 2008), FTIR spectra were recorded of particles after sonication at 20% maximum amplitude for increasing exposure times (5, 10, 20, 30, 40, 60 s). Figure 2c shows that only with an exposure time >40s the silk I particles undergo a change in conformation to silk II. Microscopy analysis showed that particle integrity did not change.

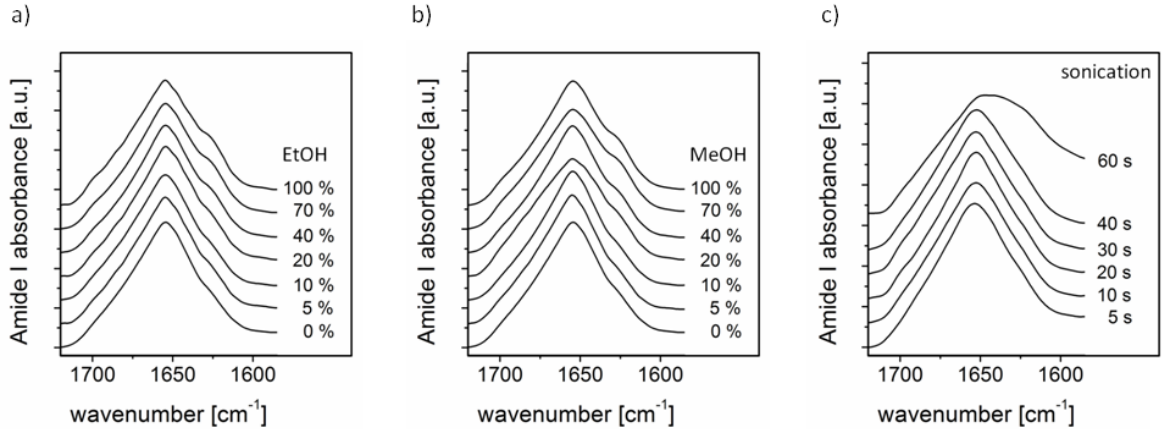

Figure 18. FTIR spectra of silk particles produced by salting out with potassium phosphate (1.25 M, pH 8) followed by treatment with ethanol, methanol or sonication. **a)** EtOH (incubated for 24 h), **b)** MeOH (incubated for 24 h), **c)** Sonication with 20% maximum amplitude for exposure times indicated.

3.1.5 Loading with small molecular model drugs

In order to investigate the applicability of silk fibroin particles as a drug delivery systems, three positively charged low molecular model drugs (alcian blue (6 positive charges, MW=1,299 Da), rhodamine B (hybrid ion, MW=479 Da), and crystal violet (1 positive charge, MW=408)) were loaded on negatively charged silk fibroin particles by charge-charge interaction. Upon incubation of particles in drug solution, drug molecules adhere to the surface followed by diffusion into the protein matrix. The loading was studied with respect to the molar ratio of the model drug (MD) to silk fibroin (SF) (Figure 19 a,b). Confocal images of RhB loaded silk fibroin particles illustrate that small molecular drugs diffuse into the matrix (Figure 19d). Zeta potential measurements of extracted particles

showed that the zeta potential decreases with increasing loading and in the case of alcian blue the potential becomes positive for loadings >7% (Figure 19c) accompanying the decreasing loading efficiency of alcian blue (Figure 19a,b).

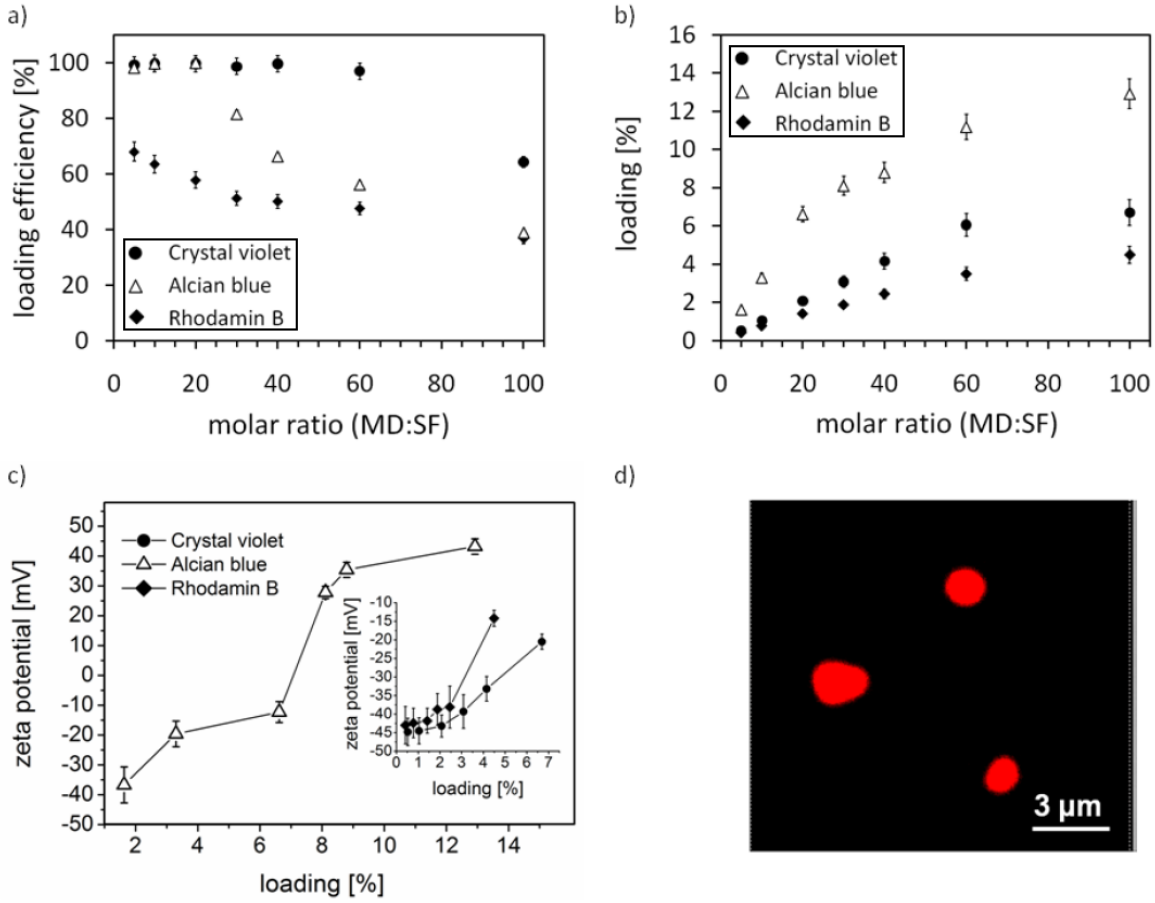

Figure 19. Loading of silk fibroin particles. **a)** Loading efficiencies of silk fibroin particles incubated in aqueous solutions containing the model drugs (MD) crystal violet, alcian blue and rhodamin B of different concentrations yielding molar ratios of model drug (MD): silk fibroin (SF) as indicated. **b)** Loading of particles (i.e. model drug content). **c)** Zeta potential of crystal violet, alcian blue and rhodamine B loaded particles as a function of loading. **d)** Confocal microscopy of RhB loaded particles.

3.1.6 In vitro release

The *in vitro* release behavior of the model drugs from the particles showed that positively charged molecules were released in a more prolonged or sustained fashion. The initial burst (cumulative release within the first 3 hours) was 83% for rhodamine B, 17% for crystal violet, and 3% for alcian blue (Figure 20a). The influence of the secondary

structure of the particles on their release behavior was studied with crystal violet (CV). Particles with a higher content of silk II structure showed an increased initial burst with release of 29% CV for particles produced at pH 7, 17% CV for particles produced at pH 8, and 11% CV for particles produced at pH 9 (Figure 20b). Particles produced at pH 7 show an increased release rate over the whole period of time compared to particles produced at pH 8 and pH 9 (Figure 20b).

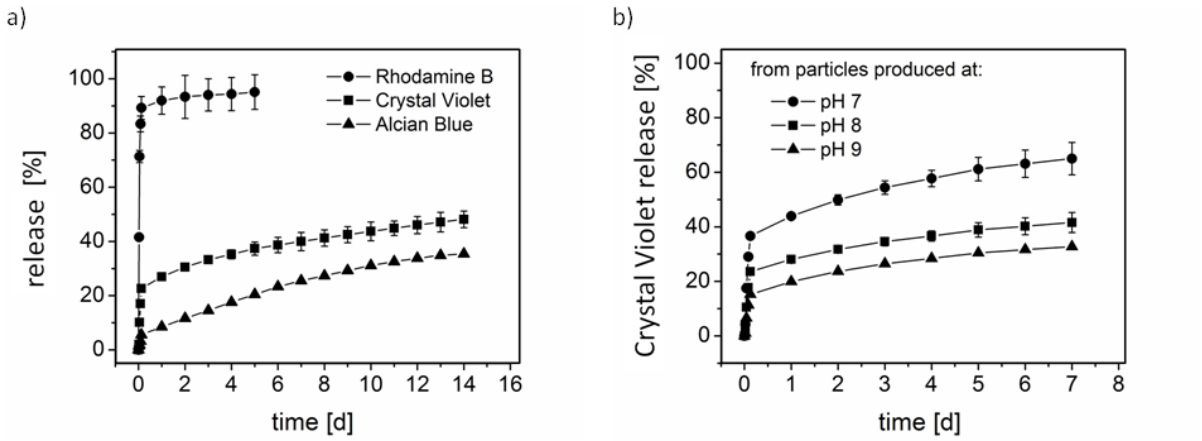

Figure 20. Release from silk fibroin particles. **a)** Release of rhodamine B, crystal violet and alcian blue from particles produced by salting with potassium phosphate (1.25 M, pH 8) **b)** Crystal violet release from particles produced at different pH values.

3.2 Spider silk particles for drug delivery

3.2.1 Characterization of engineered spider silk protein eADF4(C16)

Similar to *B. mori* silk fibroin (section 3.1), the unfolded state of eADF4(C16) was characterized by computation of the hydophobicty plot according to Kyte and Doolittle [50] (Figure 21) and physicochemical properties (charge, isoelectric point (pI), hydropathicity and size: Table 7) based on the amino its acid sequence (Appendix A3). Engineered spider silk eADF4(C16) is an amphiphil protein and comprised of 16 C modules and a C-terminal T7 tag (used for determination of protein purity). The C-module has a theoretical isoelectric point (pI) of 3.13 indicating a net negative charge at a physiological pH of 7.4, whereas the T7-Tag with a pI of 9.5 is positively charged.

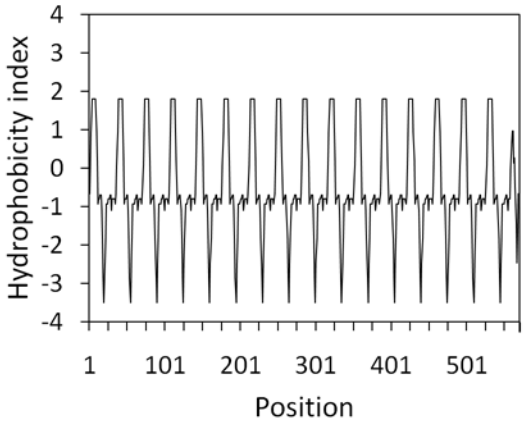

Figure 21. Hydrophobicity plot of eADF4(C16). The hydrophobicity index relates the relative hydrophobicity among amino acids; more positive values indicate stronger hydrophobicity. The position at the x axis reflects the corresponding amino acid of the protein, starting at the amino terminus and ending at the carboxy terminus The repetitive sequence of eADF4(C16) results in a very regular amphiphilic pattern.

Table 7. Computed physicochemical parameters (charge ratio, isoelectric point (pI), hydropathicity and size) of eADF4(C16) and C-terminal T7-Tag.

	repetitive part	T7-Tag
charge ratio (-/+)	(16/0)	(0/1)
pI	3.13	9.50
hydropathicity	-0.466	-0.558
size (aa)	560	12

The derived model of the unfolded eADF(C16) is shown in Figure 22. eADF4(C16) is an amphiphilic molecule with dominating hydrophobic character with 16 regularly spaced negative charges and one positive charge on the C-terminal T7-Tag.

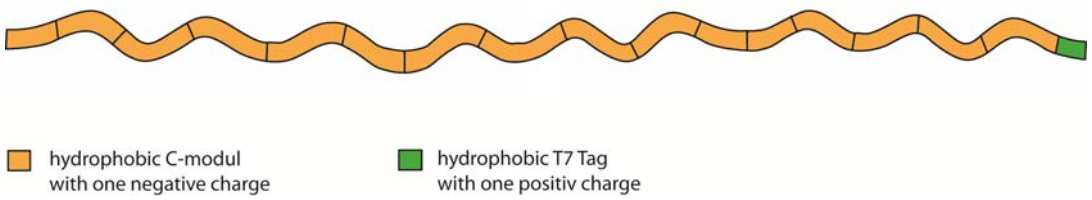

Figure 22. Model of unfolded eADF4(C16) based on amino acid sequence and computed parameters (charge ratio, isoelectric point (pI), hydropathicity and size) as listed in Table 7

3.2.2 Phase behavior of eADF4(C16) upon salting out

Similar to the experiments regarding the *B. mori* silk fibroin phase behavior (section 3.1.2), the phase behavior of eADF4(C16) upon addition of potassium phosphate was investigated. An aqueous eADF4(C16) solution (10 mM Tris, pH 8) of 0.5 mg/ml or 1 mg/ml was salted out in presence of 500 mM or 1 M potassium phosphate (pH 8). Using stopped flow, it was determined that the required time for salting out of 50% of eADF4(C16) (t_{50}) was t_{50} = 50 s in the presence of 500 mM potassium phosphate (pH 8) and t_{50} = 30 s in the presence of 1 M potassium phosphate (pH 8) (Figure 23a). Independent of the starting protein concentration the equilibrium between soluble and aggregated eADF4(C16) is only dependent on potassium phosphate concentration. Interestingly, a constant amount of protein per volume of 1 ml remained soluble in each sample: 333 µg calculated in presence of 500 mM potassium phosphate and 250 µg calculated in presence of 1 M potassium phosphate (Figure 23a). Furthermore, we investigated the aggregation of eADF4(C16) as a function of potassium phosphate concentration after 1 hour of incubation at three different constant temperatures (10°C, 30°C and 60°C). In each experiment the eADF4(C16) concentration was 1 mg/ml and volume was kept constant at 1 ml. Figure 23b shows that at lower salt concentrations the aggregation is accelerated with increasing temperature 50% of the protein is

aggregated at 381 ± 4.2 mM and 10 °C, at 205.5 ± 4.3 mM and 30°C and at 85.2 ± 1.7 mM and 60°C, respectively.

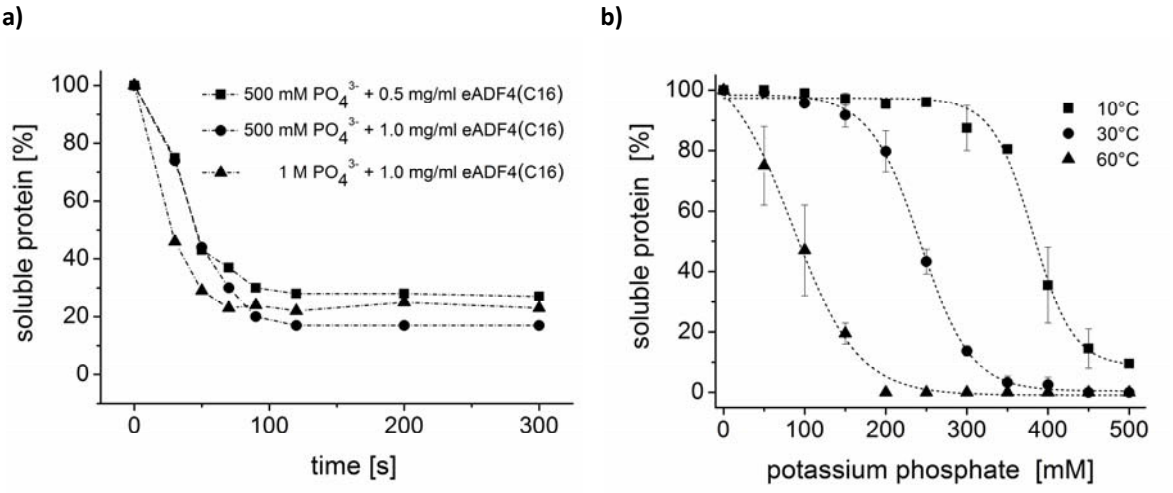

Figure 23. Aggregation assay of eADF4(C16) protein. **a)** Aggregation behavior of eADF4(C16) as a function of time at 25°C and at protein and potassium phosphate concentrations as indicated. **b)** eADF4(C16) aggregation as a function of potassium phosphate concentration and temperature after 1 hour of incubation. At lower salt concentrations the aggregation is accelerated with increasing temperature. 50% of the protein is aggregated at 381 ± 4.2 mM and 10 °C, at 205.5 ± 4.3 mM and 30°C and at 85.2 ± 1.7 mM and 60°C, respectively.). In each experiment the eADF4(C16) concentration was 1 mg/ ml and volume was kept constant at 1 ml.

SEM investigation of the aggregates morphology showed that approximately above a potassium phosphate concentration of 500 mM quantitative formation of microspheres occurs (Figure 24).

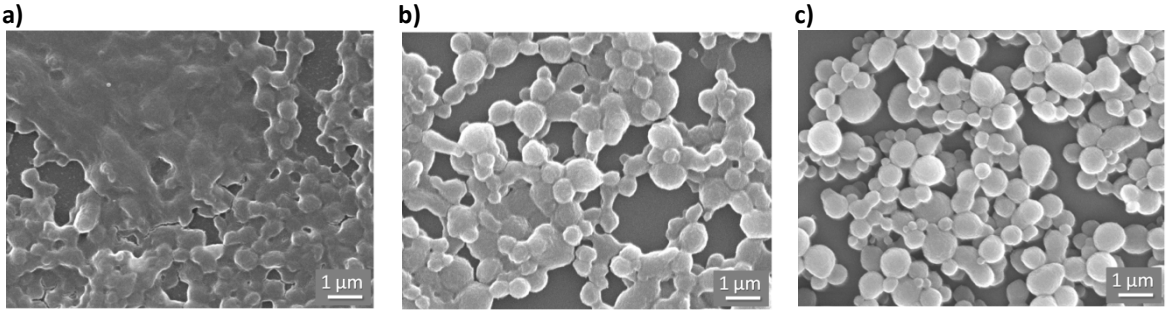

Figure 24. Scanning electron micrographs of eADF4(C16) aggregates upon salting out with potassium phosphate at pH 8 and different ionic strength. **a)** 330 mM **b)** 500 mM **c)** 1 M.

3.2.3 Mixing conditions influence particle sizes and size distributions

In order to analyze the influence of mixing on particle formation, several different methods were employed for mixing including dialysis, simple mixing with pipette and micromixing within a T-mixing element. Upon mixing, the samples were analyzed with laser diffraction spectrometry and scanning electron microscopy (SEM). Accordingly, different sphere characteristics with respect to sphere sizes, size distributions and formation of sphere clusters could be detected depending on the method of preparation. At 500 mM potassium phosphate (pH 8) silk spheres formed clusters at all examined preparation methods (dialysis, pipette, micromixing at 2 ml/min (Reynolds number: *Re* = 85, see 2.2.3.2) and 50 ml/min (*Re* = 2122)). Figure 25 a shows a typical SEM picture of silk spheres produced by salting out with 500 mM potassium phosphate (pH 8). The picture illustrates that spheres with a diameter of approximately 500 nm build larger clusters of aggregates. In contrast, in salting out experiments performed with 1 M potassium phosphate (pH 8) mainly fully developed microspheres could be observed (Figure 25 b, c, d). Micromixing with higher mixing intensities led to the formation of smaller spheres than salting out with dialysis or simple mixing with pipette. Figure 25c depicts spheres produced by micromixing with 2 ml/min and Figure 25d spheres produced by mixing with a flow rate of 50 ml/min. Strikingly, sphere production by dialysis which reflects the slowest mixing conditions resulted in the largest observed spheres of diameters greater than 1 µm (Figure 25b).

a) **b)**

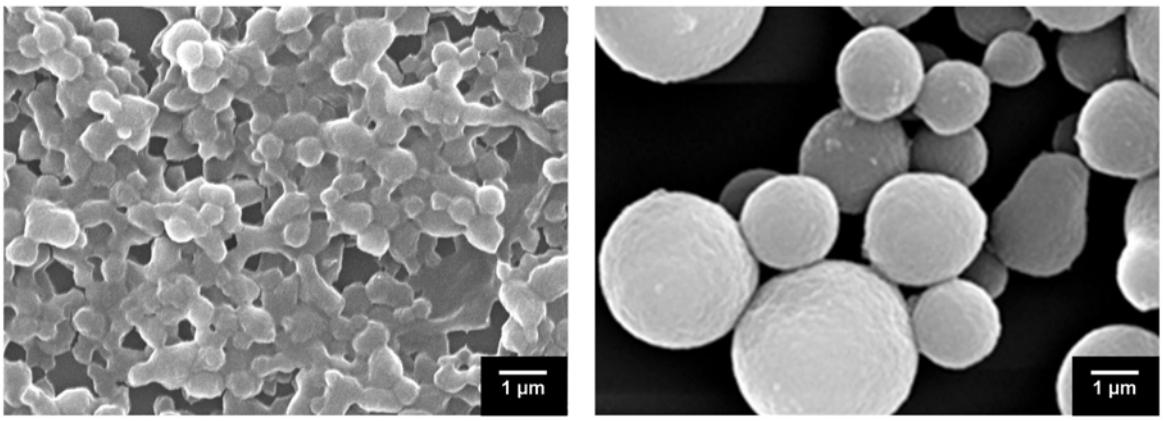

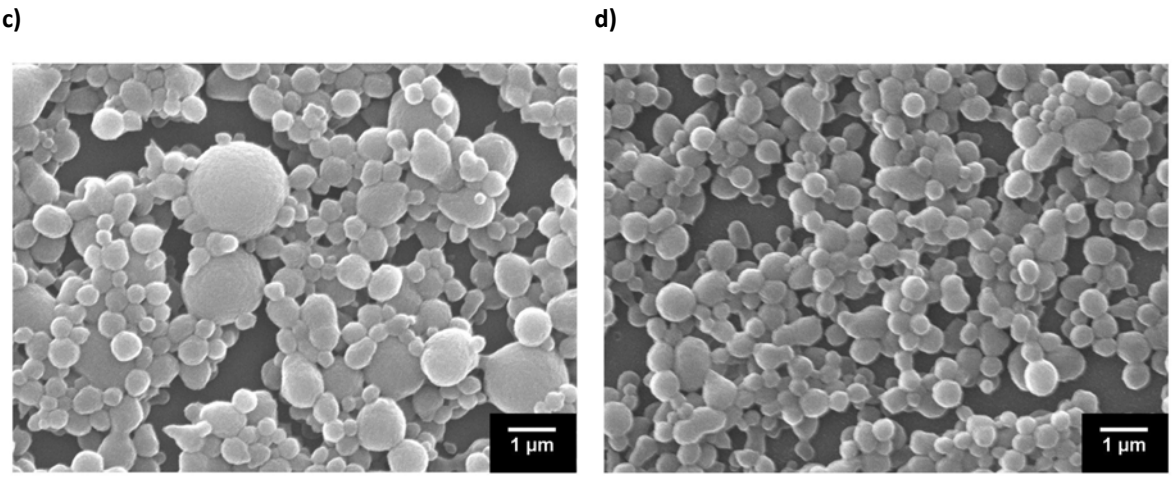

Figure 25. Scanning electron micrographs of microspheres produced by different methods. **a)** Micromixing of 500 mM potassium phosphate (pH8) with 0.5 mg/ml eADF4(C16) solution at a flow rate of 50 ml/min. **b)** Dialysis of a eADF4(C16) solution with a protein concentration of 1 mg/ml against 1 M potassium phosphate (pH 8). **c)** Micromixing of 1 M potassium phosphate (pH8) with a 1 mg/ml eADF4(C16) solution at a flow rate of 2 ml/min. **d)** Micromixing of 1 M potassium phosphate (pH8) with a 1 mg/ml eADF4(C16) solution at a flow rate of 50 ml/min.

For quantification of size distributions, as qualitatively observed by SEM, all samples were analyzed by laser diffraction spectrometry. To investigate the stability of particles and clusters thereof, sphere size distributions were measured with laser spectrometry over a time period of ten minutes with constant mixing to prevent sedimentation of microspheres. Figure 24b, Figure 25 a and Figure 26a exemplarily show that particles produced at low potassium phosphate concentration (500 mM, pH 8) formed clusters which disassembled into fragments of ca. 350 nm upon incubation in water and induced shear stress provided by stirring (Figure 26a). With 1 M potassium phosphate (pH 8), stable microspheres could be produced independent of protein concentration or mixing condition (Figure 25 b, c, d and Figure 26). Figure 26b shows the size distribution of spheres produced by mixing of 1 M potassium phosphate (pH 8) with 1 mg/ml eADF4(C16) solutions with pipette as well as with micromixing at a rate of 2 ml/min and 50 ml/min. Figure 26c illustrates the size distribution of spheres salted out by dialysis of 0.5 mg/ml and 1 mg/ml eADF4(C16) solutions against 1 M potassium phosphate (pH 8). As seen by sharp peaks, controlled mixing with a micromixing device leads to a smaller size distribution compared to mixing with pipette or salting out by dialysis. Simple

mixing with pipette at eADF4(C16) concentrations of 0.5 mg/ml and 1 mg/ml led to stable microspheres with average diameters of 350 nm and 510 nm, respectively (Figure 26d). By controlled mixing at a flow rate of 2 ml/min, microspheres with an average size of 290 nm (0.5 mg/ml) and 370 nm (1 mg/ml) were formed, whereas at a flow rate of 50 ml/min smaller microspheres with an average diameter of 250 nm and 320 nm could be detected (Figure 26d). Dialysis yielded stable spheres with average sizes of 1.6 µm and 2.1 µm, respectively, with a rather broad size distribution (Figure 26c, d).

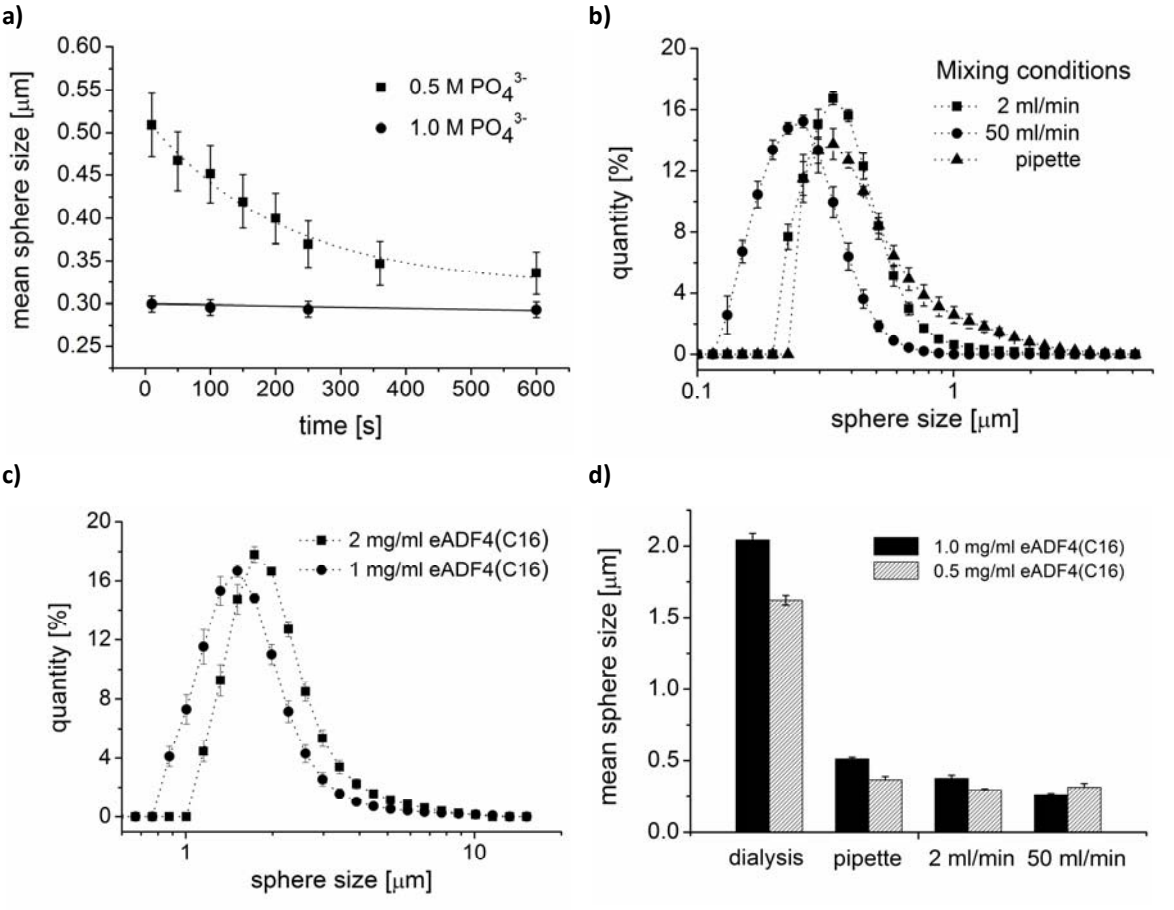

Figure 26. Size analysis of microspheres salted out with 1M potassium phosphate (pH 8). **a)** Conformational stability of particles produced by micromixing of 0.5 mg/ml eADF4(C16) with potassium phosphate (pH 8) at a flow rate of 2 ml/min. Upon protein salting out with 1 M potassium phosphate (pH 8) stable spheres are formed. After 10 min of stirring no decrease or increase in particle size could be detected. In case of micromixing of 500 mM potassium phosphate (pH 8) with 0.5 mg/ ml eADF4(C16), clusters were formed which slowly disassembled upon stirring. **b)** Size distribution of eADF4(C16) microspheres prepared by different methods: simple mixing with pipette and controlled mixing with a

micromixing device at flow rates of 2 ml/min and 50 ml/min **c)** Size distribution of eADF4(C16) particles prepared by dialysis. **d)** Calculated mean sphere size of eADF4(C16) microspheres prepared by different methods as indicated.

3.2.4 Characterization of eADF4(C16) particles

3.2.4.1 Secondary structure

FTIR analysis of eADF4(C16) particles produced by salting out with potassium phosphate at pH 8 showed that the particles are β-sheet rich (Figure 27 and Table 8). The secondary structure was determined by Fourier self deconvolution (FSD) as shown in Figure 27b. Table 5 provides the quantitative analysis of secondary structure elements.

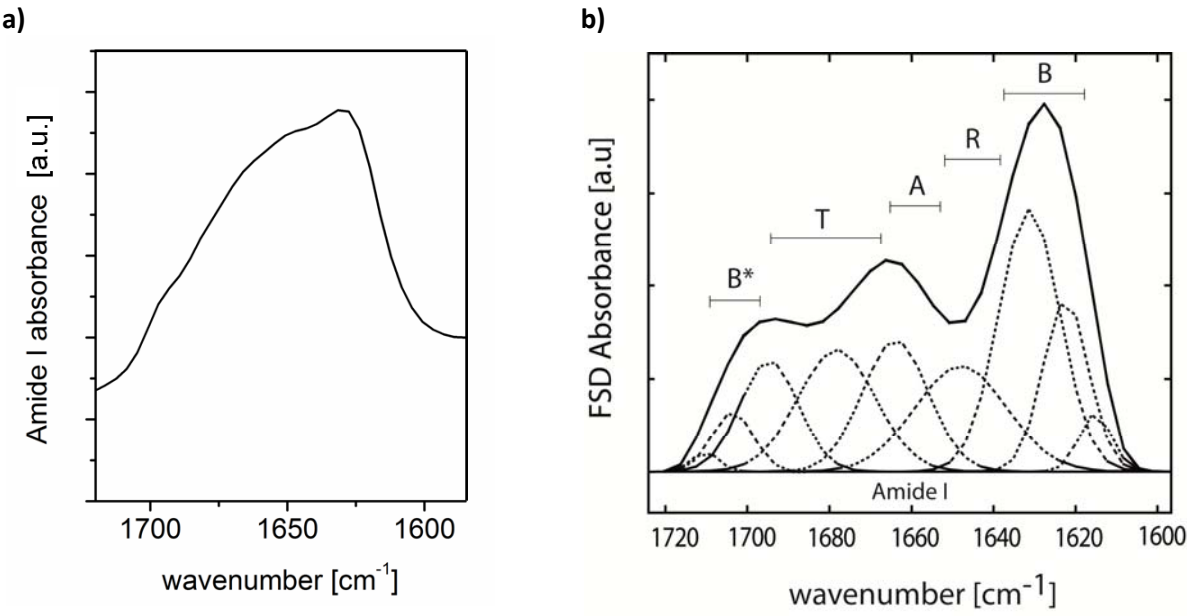

Figure 27. FTIR-Analysis of eADF(C16) particles. **a)** FTIR spectrum of eADF(C16) particles produced by salting out with potassium phosphate (1M, pH8). **b)** Fourier self deconvolution (FSD) of FTIR spectrum shown on the left. The peaks are marked with abbreviations that stand for: turns (T), alpha helix (A), random coil (R), inter- and intramolecular beta sheets (B), intramolecular beta sheets (B*).

Table 8. Secondary structure elements of eADF4(C16) particles produced by salting out with potassium phosphate (1 M, pH 8).

Beta-sheets [%] (±2%) (1610–1635 cm^{-1}, 1695–1700 cm^{-1})	Alpha-Helix [%] (±2%) (1647–1664 cm^{-1})	Random-coil [%] (±1%) (1635–1645 cm^{-1})	Beta-turns [%] (±2%) (1666–1695 cm^{-1})
45.1	13.9	15.5	25.5

3.2.4.2 Colloidal stability in solution

Particles employed as vehicles for drug delivery should not flocculate under conditions of physiological ionic strength. Generally, aggregation of particles occurs when attractive van der Waals interactions between particles dominate over repulsive forces. The ζ-potential which generates repulsive electrostatic interactions between particles was determined to be -22 ±2 mV for the eADF4(C16) particles produced by salting out with 1 M potassium phosphate (pH8). In order to investigate the colloidal stability of eADF4(C16) particles in suspension we studied the aggregation of silk particles as a function of $(NH_4)_2SO_4$ ionic strength which is associated with the salvation power of the medium due to the strong destructive effect of SO_4^{2-} anions on the structure of the water in its immediate vicinity. We found that eADF4(C16) particles are colloidally stable within the complete studied concentration range from 0 to 2.0 M $(NH_4)_2SO_4$ (Figure 28). Based on Mie theory the intensity of scattered light in forward direction increases with increasing particle size (Morrison and Ross, 2002). Therefore, the onset of electrolyte induced flocculation in dilute dispersions can be detected by an increase in intensity of scattered light in forward direction (Riley et al., 1999) The slight linear decrease of intensity with increasing concentration of $(NH_4)_2SO_4$ can be explained by the linear increase in ion concentration yielding a decrease of number of particles per volume.

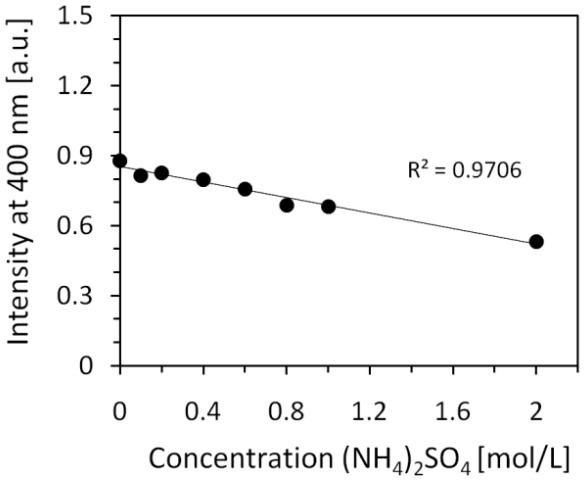

Figure 28. Investigation of colloidal stability assessed by intensity of scattered light at 400 nm. R^2 is the correlation coefficient of the linear fit.

3.2.5 Loading of spider silk particles

To study the loading of eADF4(C16) particles systematically we prepared a stock dispersion which was characterized by SEM and laser diffraction spectrometry. As shown in Figure 29 particles of spherical shape with diameters from 170 nm to 700 nm were obtained. The average diameter of particles was d_{avg} = 332 ± 95 nm. The yield of particle formation by salting out was higher than 99% with remaining soluble protein below the detection limit.

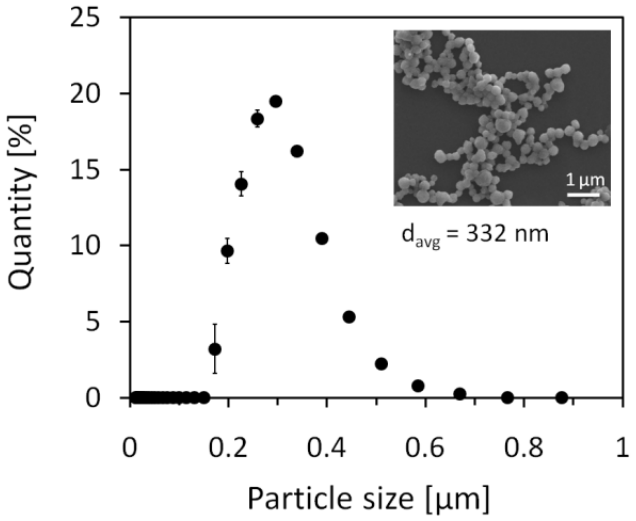

Figure 29. eADF4(C16) particle stock dispersion characterization. Size distribution of eADF4(C16) particles analyzed using laser diffraction spectrometry. The inset shows a scanning electron micrograph of corresponding eADF4(C16) particles. The average diameter of the particle ensemble was d_{avg} = 332 ± 95 nm.

Due to its negative charge at pH 7, eADF4(C16) can form complexes with positively charged molecules based on electrostatic interactions. In order to elucidate if small molecules attach to the particle surface or are able to permeate into the interior, we compared loading efficiencies of glass beads with that of eADF4(C16) particles assuming that permeation processes of drug molecules into the dense glass matrix cannot occur. Due to the high negative zeta-potential (≈ -50 mV) of glass beads, the loading efficiency of glass beads should be higher than that of spider silk particles (zeta-potential ≈ -22 mV) in case no diffusion into the protein matrix occurs.

For this experiment methyl violet (MV) was employed with loading efficiencies above 95% at molar ratios of MV : eADF4(C16) of 10 : 1. Online zeta potential measurements during methyl violet loading revealed that the change of zeta-potential during eADF4(C16) particle loading is a triphasic process (Figure 30a). First, the zeta-potential changes gradually after addition of methyl violet solution. After an initial constant slope, the zeta-potential curve exhibits a plateau phase indicating no further change of surface loading upon increasing methyl violet concentration. Finally the zeta-potential decreases further. The reduction of the zeta-potential, as seen in the titration curve, is a direct consequence of the interaction of the silk particles with molecules of opposite charge. The initial lowering of surface charge can be explained by the charge compensation due to the addition of opposite charged methyl violet molecules. The plateau region indicates an equilibrium state of drug adsorbed at the solid-liquid particle interface and a diffusion of molecules into the hydrophobic core of the protein sphere. After the core matrix is saturated the influx of methyl violet molecules is reduced and eventually terminated. At that point the zeta-potential starts to decrease again, as can be seen by the second slope in Figure 30a, due to further loading of the particle surface. Interestingly, this decrease occurs at a methyl violet concentration corresponding to the molar ratio of MV : eADF4(C16) of 10 : 1 which was identified to be the molar ratio at which the loading efficiency decreases. Figure 30b shows the obtained loading and loading efficiencies employing eADF4(C16) particles as a function of molar ratio. Up to a molar ratio of MV : eADF4(C16) ≈ 10 the loading increases linearly with the amount of methyl violet added. Above a molar ratio of 10 the loading reaches a plateau leading to a decrease of loading efficiency.

In contrast, the zeta-potential of glass microparticles during methyl violet addition showed no distinctive changes (inset Figure 30a). The initial assumption that methyl violet cannot permeate into the glass particle matrix was confirmed by analyzing the supernatant after completing the titration experiment. While the surface charge of glass particles is approximately two times higher compared to silk particles, the determined loading efficiency was only 0.03%. Furthermore the loaded methyl violet could be easily washed off the surface of glass particles by three washing steps using Millipore water.

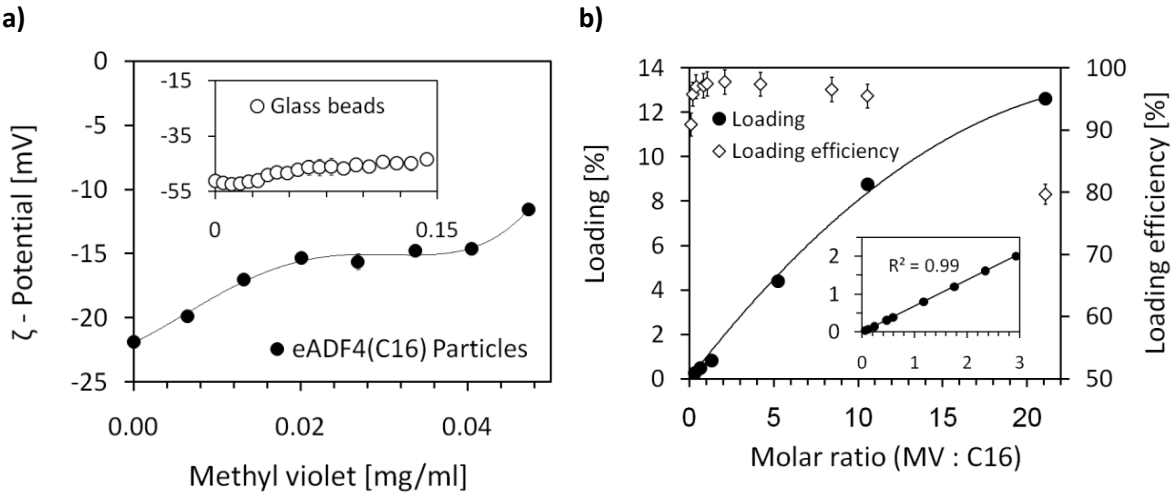

Figure 30. Characterization of loading procedure. **a)** Zeta-potential of eADF4(C16) particles as a function of added methyl violet. For comparison the inlay shows the Zeta-potential of glass beads with methyl violet. **b)** Loading and loading efficiency of methyl violet on eADF4(C16) particles as a function of molar ratio.

In order to investigate the influence of molecular parameters on the loading efficiency, twelve different small molecular drugs were used in this study (Table 9). Since an individual eADF4(C16) molecule is amphiphilic with a dominating hydrophobic character (hydropathicity index = -0.46) exhibiting 17 negative charges (one at each C module and one at the carboxy terminus) and one positive charge at the amino terminus, we concluded that loading of eADF4(C16) particles with drugs is mainly driven by three parameters: the charge of the drug molecule determined by its proton dissociation constant K_a (accounted for BH^+ or HA); the octanol water partition coefficient ($logP_{o/w}$) as an indicator of solubility of the model drug; the molecular weight (*MW*) which plays an important role in diffusion driven mass transport processes. Further, the distribution between a hydrophobic and a hydrophilic phase of two different species of a specific drug, i.e. the native and the protonated form, can be described by its apparent distribution coefficient (*logD*), which can be calculated using equations (5) and (6), respectively (Dossou, 2005).

for acids: $\log D = \log P - \log (1 + 10^{pH-pKa})$ (5)

for bases: $\log D = \log P - \log (1 + 10^{pKa-pH})$ (6)

The *logP* and *pKa* values of individual species used for calculation of *logD* are listed in Table 9. Table 10 summarizes the determined loading efficiencies, maximal (calculated by employing loading efficiencies of 100%) and experimental amount of entrapped drug, as well as the calculated distribution coefficient (*logD*) at pH 7.

Table 9. List of small molecular weight model drugs used for eADF4(C16) sphere loading. Values for molecular weight, dissociation constants (*pKa*) and partition coefficients (*logP*) are taken from literature (Auterhoff H, 1999; CAS, 2009; Chemspider, 2009; National library of medicine, 2009). The partition coefficient (*logP*) accounts for the individual unprotonated forms. The absorption wavelength λ_{Abs} was determined experimentally for each substance. All substances were purchased from Sigma-Aldrich (Deisenhofen, Germany).

Model drug	Molecular weight [Da]	λ_{Abs} [nm]	Dissociation constant of BH^+ (pKa)	Dissociation constant of HA (pKa)	*log P*	Predominant charge at pH7	Permanently charged
Chlorthalidone	338	276	---	8.9	-0.03	uncharged	no
Nipagin	152	254	---	8.3	1.86	uncharged	no
Acetaminophen	151	242		9.3	0.38	uncharged	no
Phenol red	354	510	---	1.7; 7.7	3.00	negative	yes
Tetracaine*HCl	301	310	8.20	---	4.00	positive	no
Procaine*HCl	272	290	8.05	---	2.40	positive	no
Papaverine*HCl	376	248	8.07	---	3.50	positive	no
Ephedrine*HCl	202	256	9.60	---	1.30	positive	no
Propranolol*HCl	295	290	9.10	---	3.18	positive	no
Biperiden*HCl	347	210	9.60	---	3.50	positive	no
Ethacridine lactate	343	365	11.00	---	2.50	positive	no
Methyl violet	407	590	---	---	3.20	positive	yes

Protonated weak organic bases could be loaded onto eADF4(C16) particles with efficiencies ranging between 20.7% and 53.0%. For this class of small molecular model drugs the quotient of calculated *logD* divided by the molecular mass of the individual molecule correlates linearly with the obtained loading efficiencies (Figure 31). This linear relationship clearly indicates that the combination of charge and solubility (expressed by the apparent distribution coefficient *logD*) and diffusion coefficient (expressed by the inverse proportionality of molecular weight) are the dominating factors responsible for effective loading of small weakly alkaline molecules onto eADF4(C16) particles.

Table 10. List of employed model drugs classified according to their chemical nature. The table provides an overview of theoretical and experimental model drug content of loaded spider silk particles (expressed as percentage of wt drug / wt spider silk protein particles), corresponding encapsulation efficiencies and calculated distribution coefficients (*logD*).

Model drug	Chemical nature	Maximal drug content [w/w%]	Experimental drug content [w/w%]	Encapsulation efficiency [%]	*log D*
Ephedrin*HCl	base	4.23	0.88	20.7	-1.321
Procain*HCl	base	5.71	2.16	38.0	0.396
Biperiden*HCl	base	7.28	3.05	42.0	0.899
Propranolol*HCl	base	6.19	2.78	45.0	1.197
Papaverine*HCl	base	7.89	3.71	47.0	2.395
Tetracaine*HCl	base	6.30	3.34	53.0	2.773
Ethacridine lactat	strong base	7.20	7.07	98.2	2.899
Acetaminophen	weak acid	3.16	0.06	0.2	0.378
Chlortalidon	weak acid	7.09	0.68	9.7	-0.315
Nipagin	weak acid	3.19	0.55	17.3	0.544
Phenol red	strong acid	7.12	0.00	0.0	-
Methyl violet	---	8.54	8.37	98.1	-

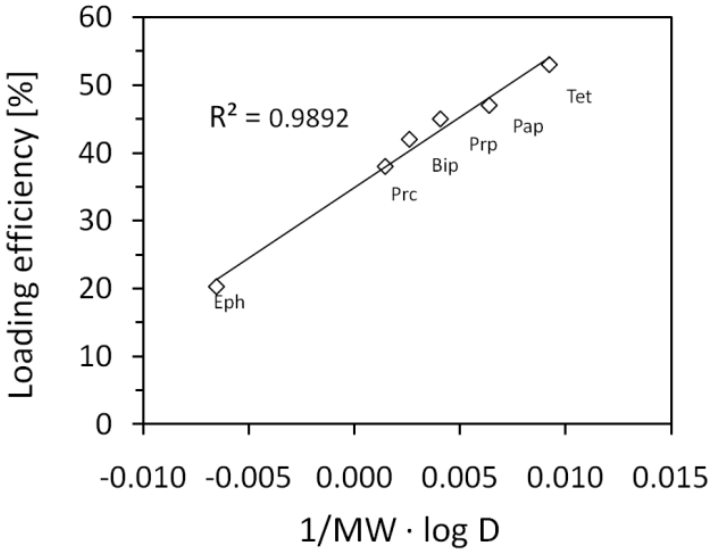

Figure 31. Loading efficiencies for model drugs of weak alkaline nature such as Ephedrin (Eph), Procain (Prc), Biperiden (Bip), Propranolol (Prp), Papaverine (Pap) and Tetracaine (Tet) plotted over *logD* MW^{-1}.

Investigation of molecules with permanent charge revealed that positively charged molecules such as methyl violet were most successfully incorporated whereas negatively charged molecules such as phenol red could not be incorporated using eADF4(C16), and slightly acidic molecules exhibited relatively low loading efficiencies from 0.2 to 17.3%. Strongly alkaline molecules like ethacridine lactate showed a loading efficiency of more than 98%. Despite the relatively high *logD* of acetaminophen (comparable to Nipagin), a loading efficiency of only 0.2% was determined which might be explained by its structure acting as weak phenolic base leading to the appearance of negatively charged acetaminophen species. We suspect that due to electrostatic repulsion of the negative charges these species cannot diffuse into the sphere matrix.

According to our results the distribution coefficient *logD* can be used to estimate the obtainable loading efficiency for weak organic bases without permanent charge. Molecules with permanent charge cannot be included in this model since it is not possible to calculate the corresponding *logD* value. Due to the physicochemical properties of eADF4(C16) for an effective loading of protein particles made thereof, drug molecules should ideally feature a positive charge combined with a certain degree of hydrophobicity and a molecular weight enabling diffusion into the spider silk protein matrix.

3.2.6 In vitro release

The in vitro release behavior of model drugs from eADF4(C16) particles was exemplarily studied with methyl violet and ethacridine lactate. Cumulative release profiles showed that both molecules were released over a period of 30 days (Figure 32a). Most interestingly, only a very small drug burst could be detected, i.e. an initial higher drug release within the first 24 hours of incubation. The release of ethacridine lactate and methyl violet within the first 24 hours was 11% of the total amount encapsulated. Subsequently, eADF4(C16) particles released approximately 5% of the entrapped molecules per day within the first week (Figure 32 a, b). To characterize the release behavior, the semi empirical power law equation was used (equation (7)) (Siepmann and Peppas, 2001),

$$\frac{M_t}{M_\infty} = kt^n \qquad (7)$$

where M_t / M_∞ is the fractional amount of the drug released at time *t*, *k* is a characteristic constant of the system, and exponent *n* is related to the geometrical shape of the formulation and is indicative of the mechanism of drug release. The semi-empirical power law can be seen as a generalization of two independent mechanisms of drug transport, Fickian diffusion and Case II transport, reflecting the influence of polymer relaxation on molecules' movement in the matrix (Polakovic et al., 1999; Rinaki et al., 2003). For spherical systems the limiting value of n, when pure Fickian diffusion or pure Case II transport is operating, were determined to be equal to 0.43 and 0.85, respectively (Kosmidis et al., 2003; Siepmann and Peppas, 2001). When *n* is between 0.43 and 0.85, a superposition of both transport processes occurs which is known as anomalous transport. In order to obtain a linear fit for the drug release data, equation (5) was modified leading to equation (8),

$$log\left(\frac{M_t}{M_\infty}\right) = \log(k) + n \cdot log(t) \qquad (8)$$

where *n* can be calculated from the slope of the log-log plot of release M_t / M_∞ versus time *t* by linear fitting (Figure 32d). Therefrom, three time intervals with different dominating release mechanisms could be identified excluding the initial burst region (< 24h). To distinguish between different time intervals, the criterion that the coefficient r^2 had to be above 0.99 for the individual linear fits was employed. The values of release exponent (*n*), correlation coefficient (r^2), and characteristic constant (*k*) are summarized in Table 11. For validation of the determined release parameters, the experimental release data were compared with theoretical data obtained by the semi-empirical power law employing the determined values for *k* and *n*. A very good agreement from post-initial burst stage (>24 hours) up to 100% release was obtained (Figure 32a). Since only release data after 24 hours were considered for calculation of release parameters (*k* and *n*) the initial burst is underestimated by theoretical data (Figure 32b).

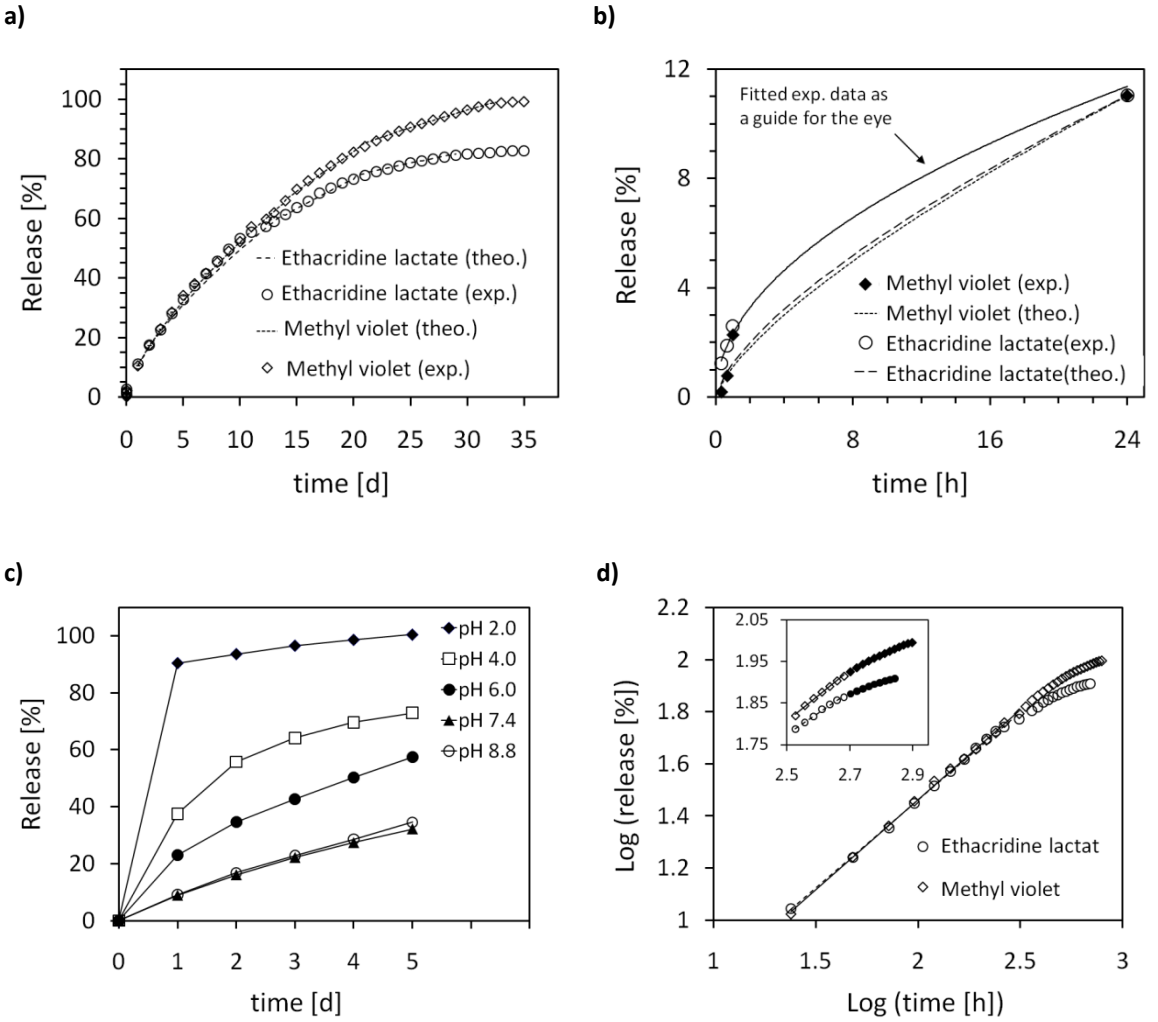

Figure 32. Release studies of ethacridine lactate and methyl violet. **a)** Experimental and theoretical release kinetics of both model drugs over a period of 35 days. **b)** Experimental and theoretical release kinetics in the initial burst region (release < 11%). **c)** Release of ethacridine lactate as a function of pH as indicated. (Buffer capacity PBS: pH 5.8 – pH 8; non buffered conditions for pH 2.0, pH 4.0 and pH 8.8) **d)** Experimental release data of ethacridine lactate and methyl violet based on the power law model. A linear fit with a correlation parameter (r^2) above 0.99 was determined for three distinct time intervals. The linear fit for the interval from day 1 to day 13 is depicted in the main plot, whereas the inset shows the data and linear fits for the time intervals from day 14 to day 20 (open symbols) and day 21 to day 35 (filled symbols) respectively.

Table 11. Drug release parameters (*n*: release exponent; r^2: correlation coefficient; *k*: characteristic constant) for methyl violet and ethacridine lactate for defined release intervals.

Model drug	time [d]	Release [%]	*n*	r^2	*k*
Methyl violet	0-13	≤ 60	0.6920	0.998	1.17
	14-20	60 - 82	0.6079	0.994	1.92

	>20	≥ 82	0.3537	0.993	9.20
Ethacridine lactate	0-13	≤ 60	0.6754	0.998	1.25
	14-20	60 - 73	0.5083	0.994	3.18
	>20	≥ 73	0.2641	0.992	14.4

Within the first two weeks of release, the exponents *n* for ethacridine lactate (EL) and methyl (MV) violet are almost identical (n_{EL} = 0.6754, n_{MV} = 0.692) indicating an anomalous diffusional release (Ritger and Peppas, 1987b). In the second time interval between day 14 and day 20 release profiles diverge from each other with the release exponent of ethacridine lactate dropping to 0.51 and that of methyl violet to *n* = 0.61. In this second time interval fickian transport begins to dominate for ethacridine lactate. After 20 days, release exponent *n* values for methyl violet and ethacridine lactate fall below the limiting value of *n* = 0.43 indicating a fickian release behavior for both (Table 11) (Ritger and Peppas, 1987a).

Next, the influence of pH on drug release was evaluated. Release experiments with ethacridine lactate loaded eADF4(C16) particles incubated in PBS at 37°C, 40 rpm and different pH values showed a strong pH influence on the release rates (Figure 32c) with an acidic environment accelerating drug release. Almost 80% of the loaded drug was released after 24 hours from silk spheres incubated at pH 2 (non buffered conditions). For silk particles incubated at pH 4 (non buffered conditions) an initial release rate of almost 40% was obtained after the first day of incubation. Particles incubated at pH 6 showed two times higher release with a similar release profile as seen at pH 7.4 or 8.8, which were indistinguishable. The observed results confirm the predicted importance of electrostatic interactions between eADF4(C16) and drug molecules. Presumably an influx of protons into the biopolymer leads to a displacement of drug molecules from the matrix. In addition the decreased pH influences the distribution of charged drug species by shifting the equilibrium towards the charged species. As these species are driven towards the negatively charged surface of the protein, they can easily be washed away by the solvent.

3.2.7 In vitro degradation of spider silk particles

Degradability of drug depot systems is a highly desirable property, since the risk of inflammation and intoxication is dramatically lower than for non-degradable systems (Schlosser et al., 2002; Shard and Tomlins, 2006). As most biopolymers feature the ability of enzymatic degradation (Nair and Laurencin, 2007), degradation studies were conducted using proteases (trypsin and elastase) (Del Favero et al., 1985; Shimizu et al., 1998) naturally occurring in vertebrates to simulate a native-like degradation of eADF4(C16) drug carriers. Degradation by elastase is of special interest, since it is mainly secreted by neutrophils and macrophages which are important components of the human innate immune system (Jones et al., 1990; Sonawane et al., 2006). Elastase and trypsin, i.e. serine proteases can cleave peptide bonds on the carboxy side of small, hydrophobic amino acids such as glycine, alanine, and valine (Page and DiCera, 2008). Due to the relative high content of glycin and alanin in eADF4(C16) (≈ 50 % of the total amino acid composition) such proteases may cleave peptide bonds at several sites in the amino acid backbone of eADF4(C16).

Size and morphology analysis of particle ensembles drawn from degradation experiments using LDS and SEM showed that after two days of degradation particles form clusters (Figure 33a). Comparing the mode value which represents the particle size most commonly found in the distribution with the mean size of the particles leads to the conclusion that bigger particles of the ensemble are degraded preferentially (Figure 33b). At t=0 the mean is larger than the mode indicating an asymmetric size distribution towards larger particles. Upon enzymatic degradation for two days mean and mode approach each other indicating that larger particles disappear and the particle distribution becomes symmetric. The particle distribution remains symmetrical up to day 8 on which the mean falls below the mode indicating an asymmetric size distribution towards smaller particles. Analysis of the relative relation of single particles to agglomerations indicates an oscillatory agglomerative behavior (Figure 33a, c). The oscillatory behavior is presumably due to changes in surface structure upon degradation. Seemingly, upon enzymatic degradation there is a dynamic equilibrium between an intermediate surface structure state which cannot be recognized by the chosen enzymes (elastase and trypsin) and a state which can readily be degraded.

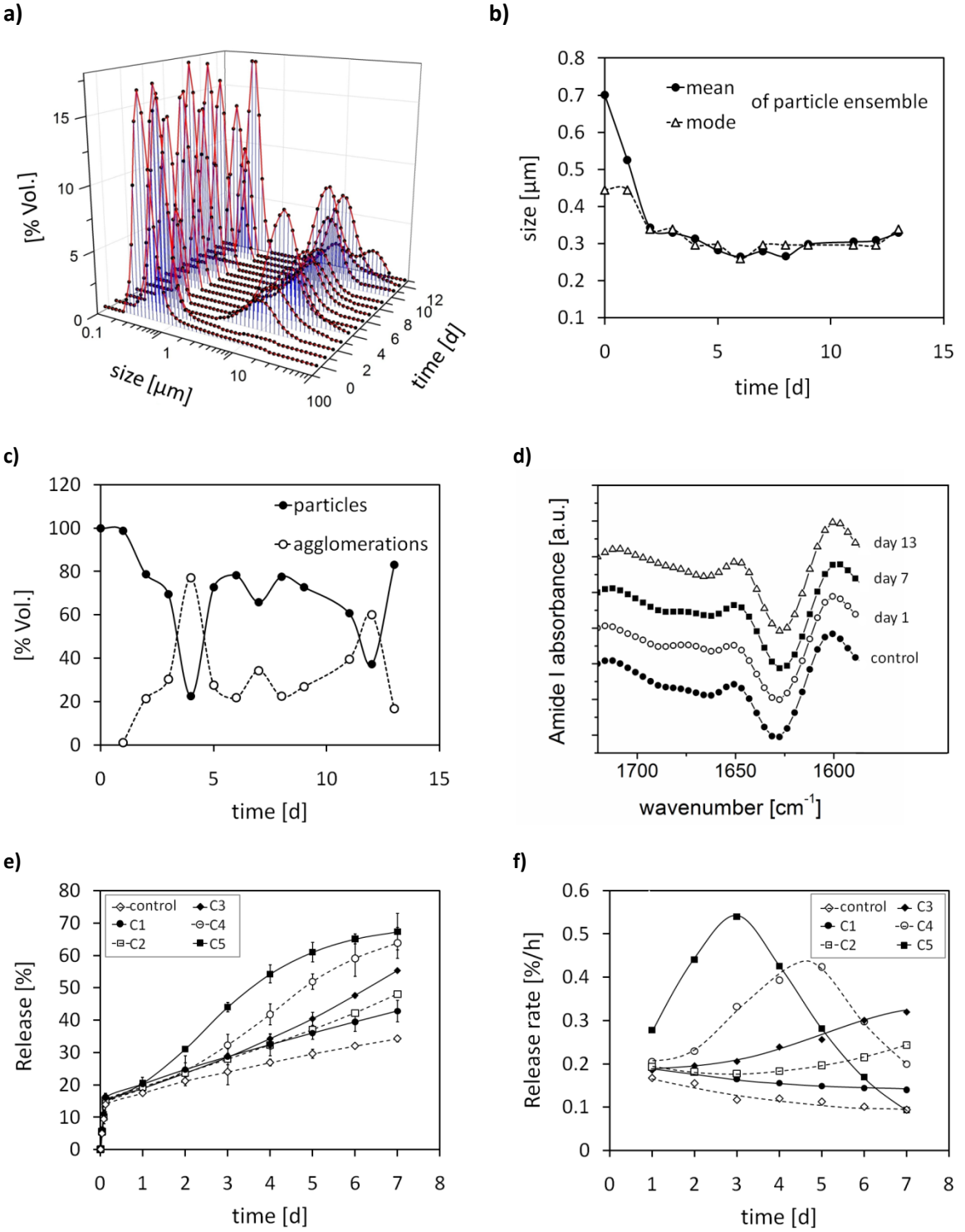

Figure 33. Characterization of eADF4(C16) particles upon enzymatic degradation. **a)** Size distribution of eADF4(C16) particles upon enzymatic degradation. **b)** Mean and mode of eADF4(C16) particles distribution over time. **c)** Percentage of particles and agglomerations of eADF4(C16) particles after degradation with elastase (c = 4 µg/ml) and trypsin (c = 50 µg/ml). **d)** Second derivative of FTIR spectra of eADF4(C16) particles upon degradation. **e)** Cumulative release of methyl violet upon degradation with elastase and trypsin at different concentrations as indicated*****. **f)** Averaged release rate between two successive measurements of methyl violet upon degradation with elastase and trypsin at different concentrations as indicated*****. *****[*control:* no enzymes; *C1:* (0.8 µg elastase + 12.5 µg trypsin)/ 1mg eADF4(C16); *C2:* (1.6 µg elastase + 25 µg trypsin)/ 1mg eADF4(C16); *C3:* (2.4 µg elastase + 37.5 µg trypsin)/ 1mg eADF4(C16); *C4:*

(4.0 µg elastase + 62.5 µg trypsin)/ 1mg eADF4(C16); *C5:* (8.0 µg elastase + 125 µg trypsin)/ 1mg eADF4(C16)].

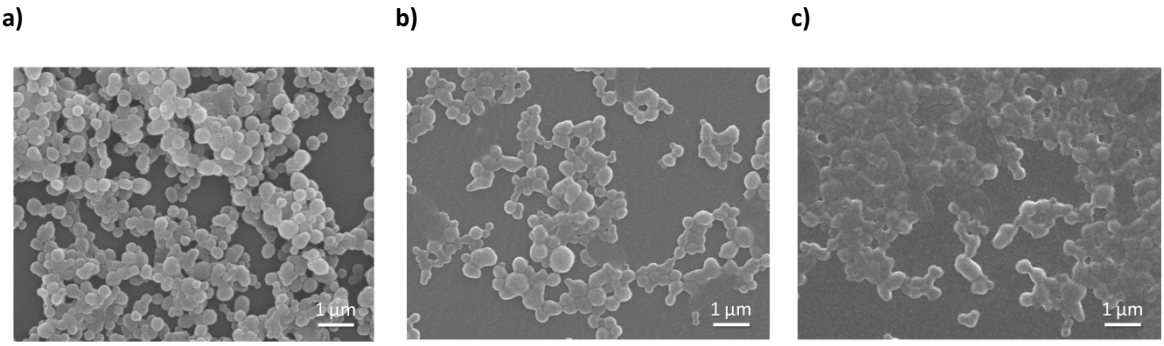

Figure 34. Scanning electron micrographs of eADF4(C16) particles upon degradation. **a)** eADF4(C16) particles after 14 days of incubation in bidistilled Q water (control sample) **b)** eADF4(C16) particles after degradation with elastase (c = 4 µg/ml) and trypsin (c = 50 µg/ml) for 4 days **c)** for 14 days.

Presumably, in a first step enzymatic degradation renders the initial hydrophilic surface more hydrophobic. Therefore, particle agglomeration is fostered in order to minimize particles surface free energy. Upon time, the particles surface structure changes due to protein rearrangement until a new surface exhibits again enzymatic degradation sites and agglomerated particles can be further degraded. SEM micrographs of eADF4(C16) particles upon degradation taken at distinct time intervals confirmed the observed agglomerative behavior (Figure 34). Furthermore, the secondary structure was investigated. Changes of secondary structure of eADF(C16) particles can be most effectively detected by 2nd derivative changes of FTIR spectra at the wavenumbers 1648-1660 cm^{-1} and 1625-1640 cm^{-1}. Our results indicate that only minor changes in percental β-sheet and α-helical content occur. Overall the structure of eADF4(C16) particles is conserved.

The release study upon degradation employing methyl violet loaded eADF(C16) particles revealed that during the first day the total release is apparently independent of the amount of enzyme added (Figure 33e). From day two on, a clear trend can be seen that increasing enzyme concentration yields an accelerated release behavior. Figure 33f illustrates the average release rate between two successive release measurements. The

results show that for higher enzyme concentrations (C3, C4, and C5) the release rate increases upon incubation time (Figure 33f). Furthermore, the higher the enzyme concentration the earlier the maximum release rate is reached (Figure 33f).

3.3 Spider silk films for coatings or therapeutic systems

In contrast to particles, which can be used as mobile carriers, films are more suitable for applications in which a stationary phase is interesting. For example, in the area of biomedical technology silk films are envisioned for applications like functionalized implant coatings by which biomaterial interfacial properties could be improved (Schultz et al., 2005; Thierry et al., 2003; Wang et al., 2007a; Wang et al., 2005). Furthermore, silk membranes could be employed as diffusion controlling membranes in therapeutic systems (Ratana et al., 2003; Stropnik et al., 2000). Crucial for the successful development of any application of silk films is their mechanical stability. Furthermore, it is desired that properties like elasticity, permeability and degradation can be designed according to specific needs. A common technique to produce membranes is the controlled phase separation of a polymer solution by which a polymer rich and polymer poor phase is generated. After phase separation the concentrated phase cures and constitutes the membrane. The four main techniques to produce polymer membranes differ in the employed desolvation mechanism: Thermal induced phase separation, casting and subsequent solvent evaporation, condensation from the vapour phase and immersion phase separation (Cheng et al., 2001; McHugh, 2005; Stropnik et al., 1996; van de Witte et al., 1996; Wienk et al., 1996; Young et al., 2000). In the following sections initial results regarding the characterization of eADF4(C16) films produced by casting and solvent evaporation are summarized. We report on the control of mechanical properties by addition of glycerol and discuss a technique to fabricate porous membranes to potentially design and control the permeability of membranes.

3.3.1 Control of secondary structure upon posttreatments

A conformational change of secondary structure of silk from α-helical rich to β-sheet rich can be induced by methanol (MeOH) treatment (Hae Yong and Young Hwan, 1999; Lawrence et al., 2008; Masuhiro et al., 1995; Metwalli et al., 2007; Slotta et al., 2006). In order to analyze the influence of posttreatments with different methanol concentrations on eADF4(C16) films casted from water (c = 6.2 mg/ml) light microscopic images and FTIR spectra were taken to investigate the effect surface morphology (Figure 35a- 35g) and secondary structure (Figure 35h).

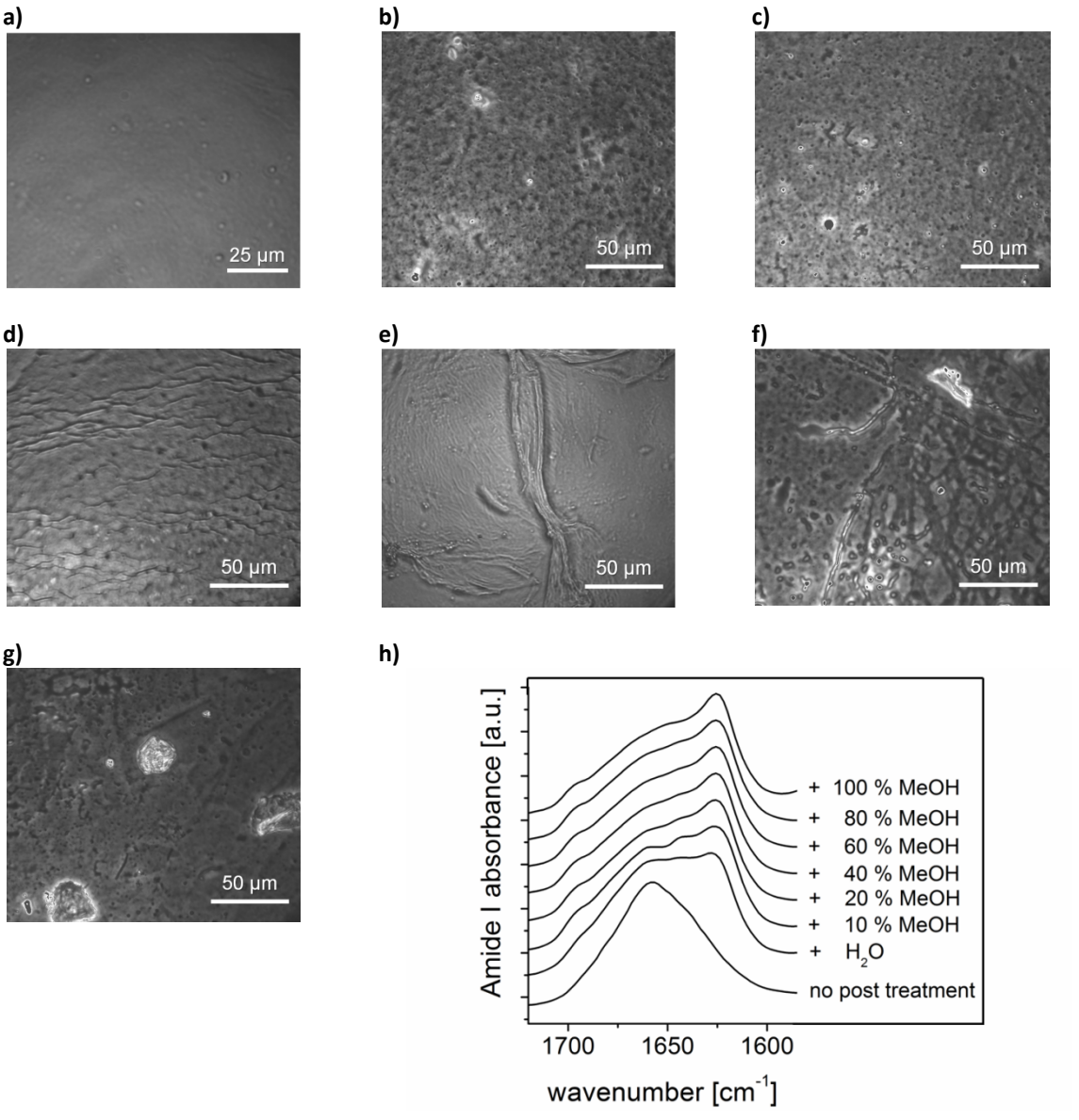

Figure 35. Influence of posttreatment on surface morpholgy and secondary structure of eADF4(C16) films casted from water. **a)** water treatment **b)** 10% MeOH treatment **c)** 20% MeOH treatment **d)** 40% MeOH treatment **e)** 60% MeOH treatment **f)** 80% MeOH treatment **g)** 100% MeOH treatment **h)** FTIR spectra of differently treated eADF4(C16) films casted from water as indicated.

Generally, posttreatment with increasing methanol concentration yielded a more prominent surface structure (Figure 35a- g) whereas for posttreatment with pure water a relatively smooth surface could be observed (Figure 35a). For posttreatments with MeOH <20% predominantly spherical structures occur. Above 20% methanol string like structures can be observed (Figure 35b-e), whereas above 80% methanol treatment clusters were detected (Figure 35f,g). FTIR analysis revealed that with increasing methanol concentration β-sheet conformations are promoted (Figure 35h). Strikingly, posttreatment with water also induced β-sheet formation (Figure 35h).

3.3.2 Mechanical characterization of films with different glycerol content

Due to the low solubility of eADF4(C16) in water (maximal ca. 1%) films casted from water are very thin and difficult to handle for mechanical testing. Therefore films were casted from HFIP by which concentrations of more than 100 mg/ml can be reached. Additionally the low vapor pressure of HFIP allows fast film formation and therefore a reduction of the influence of the evaporation process (evaporation velocity) on the film properties. Therefore inhomogeneities like thickness variations resulting from concentration gradient driven diffusion processes can be avoided. Generally, the membrane thickness can be controlled by the silk concentration in the solvent (Ismail and Hassan, 2006; Wang et al., 2007a). Additionally, the homogeneity of the film depends on the fugacity of the solvent and spreadability of the silk solution on the substrate on to which the film is casted (Shojaie et al., 1994a; Shojaie et al., 1994b; Tanny, 1974; Young et al., 2002). Preliminary experiments showed that the best films fulfilling afore mentioned requirements are obtained using HFIP as a solvent due to its low vapor pressure and low surface tension. The films containing different amounts of glycerol were prepared as described in section 2.2.4. The addition of glycerol showed no

macroscopical influence on the morphology of eADF4(C16) films on scanning electron micrographs. Figure 36 shows a typical SEM image of a eADF4(C16) film from which the thickness has been determined. The average membrane thickness was determined to be 14±1 µm (Figure 36 a).

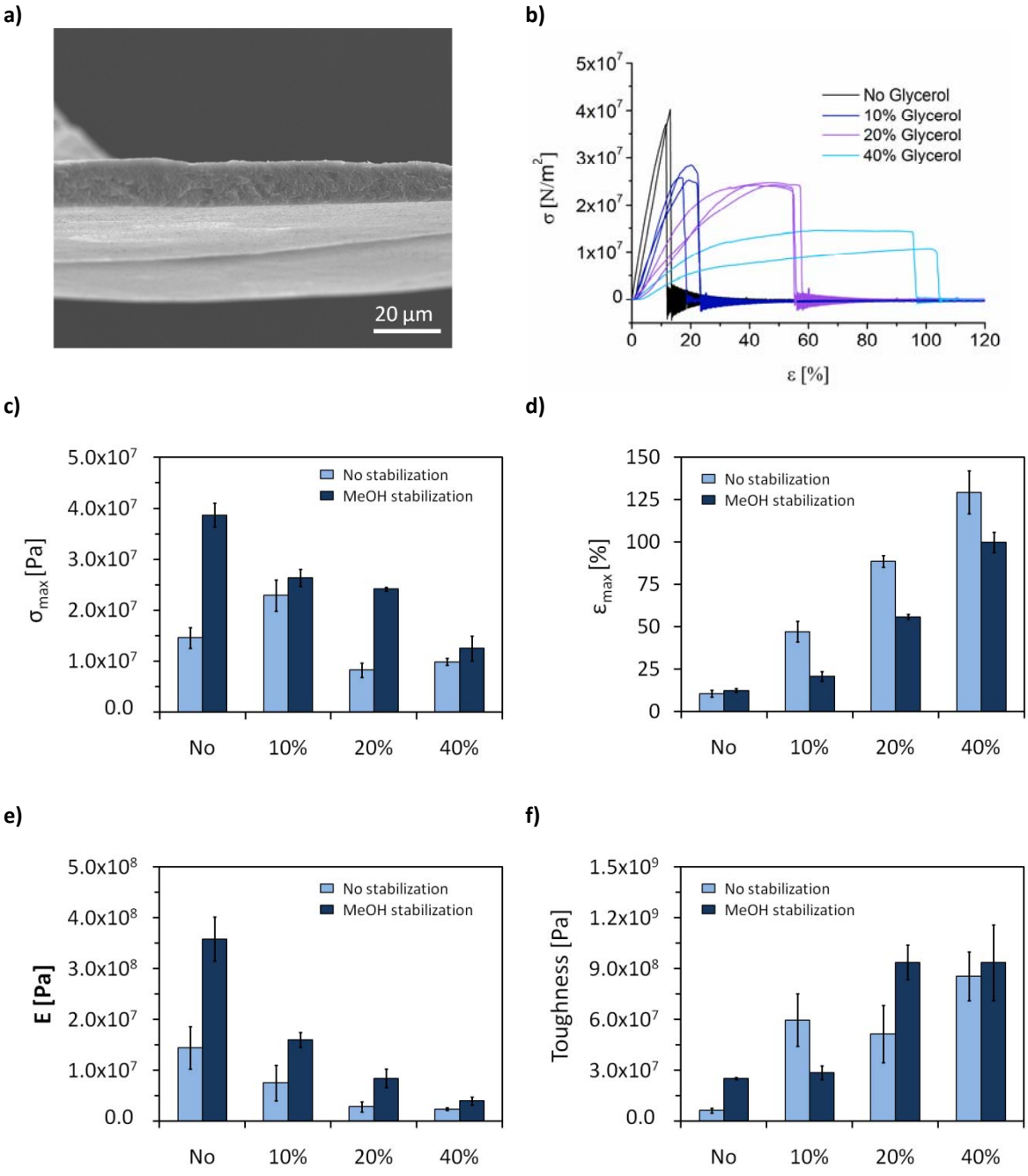

Figure 36: Mechanical characterization of eADF4(C16) films. **a)** Typical SEM micrograph of a eADF4(C16) film cross section for determination of membrane thickness **b)** Typical stress-strain plots of MeOH posttreated eADF4(C16) films with different content of glycerol as indicated (0%, 10%, 20%, 40%). **c)-f)**

From stress strain plots calculated mechanical properties of eADF4(C16) films with different content of glycerol with and without posttreatment: c) Tensile strength d) Elongation e) E-Modul f) Toughness.

Data analysis showed that post treatment with 50% MeOH generally yields an enhancement of tensile strength and E-Modulus whereas the elongation to break decreases (Figure 36 c-f). Increasing addition of glycerol yields to a decrease of tensile strength and E-modulus whereas the elongation to break and toughness increases (Figure 36 c-f). Interestingly, films containing 10% glycerol were an exception to the afore-mentioned trend with respect to the determined tensile strength. In contrast to all other samples measured, their tensile strength was higher compared to films without glycerol.

3.3.3 Influence of glycerol on secondary structure

Generally the mechanical properties of polymeric materials depend on the intra- and intermolecular forces which are influenced by the molecular mass and the conformation of the polymer in the bulk material (van de Witte et al., 1996). To analyze the influence of silk protein conformation on the observed mechanical properties the secondary structure of the silk films was analyzed using FTIR spectroscopy (Figure 37).

a) **b)**

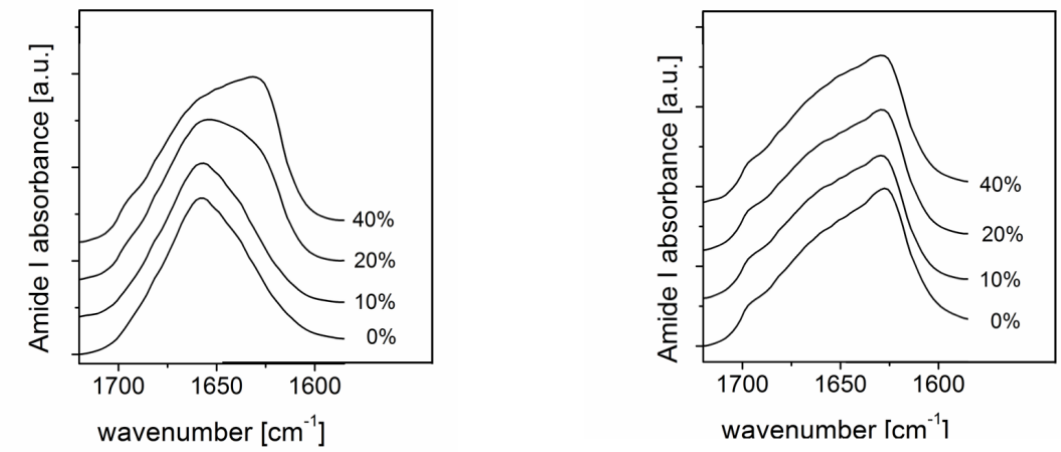

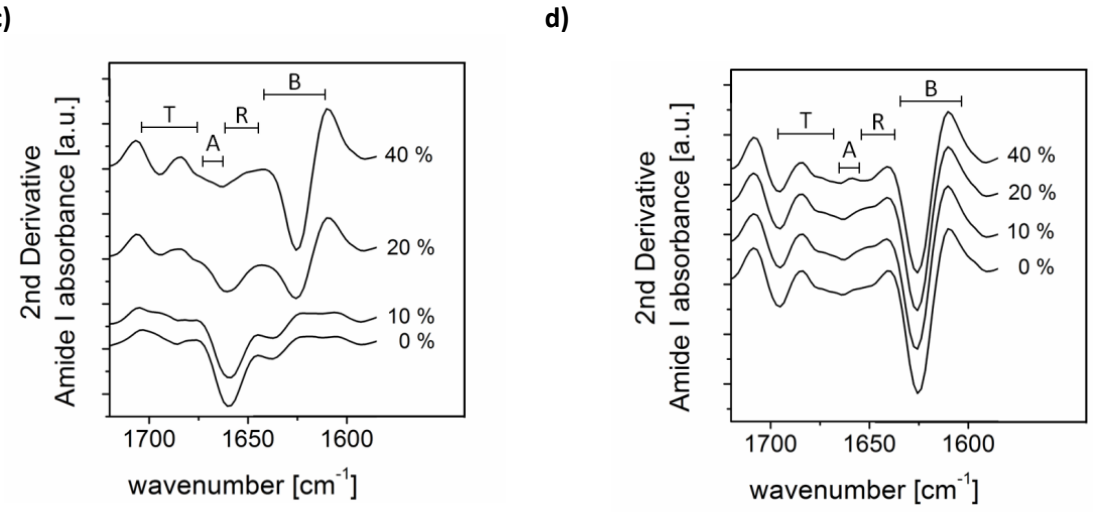

Figure 37: FTIR analysis of eADF4(C16) films with different content of glycerol (0%, 10%, 20%, 40%) with and without post treatment casted from HFIP. **a)** FTIR spectra of eADF4(C16) films without post treatment **b)** FTIR spectra of eADF4(C16) films with 50 % MeOH post treatment. **c)** Second derivative of FTIR spectra for films without post treatment. **d)** Second derivative of FTIR spectra for films with 50% MeOH post treatment

Generally the posttreatment with MeOH yields to conformational change from α-helical rich to *β*-sheet rich films (Figure 37 a, b). Analysis of FTIR data shows that 50% MeOH posttreated glycerol blended films have a slightly increased content of α-helical and random coil conformation whereas the total amount of β-sheets decreases (Figure 37 b, d, e). Interestingly the addition of glycerol (> 10 %) yields an induction of β-sheets as can be seen in Figure 37 a, c. This can be explained by the unpolar glycerol which is incorporated replacing the polar water molecules and therefore yields an enhancement of the intramolecular interactions responsible for structure formation. Although, no significant increase in β-sheet structures was detected for films containing 10 % glycerol, the enhancement of intramolecular interactions could be the reason for the observed increased tensile strength (Figure 36 c).

3.3.4 Comparison to PLGA films

The state of the art polymer used for biomedical application is poly(lactic-*co*-glycolic acid) (PLGA). In order to classify and compare the results obtained for eADF4(C16) films four different PLGA grades similarly produced by casting and solvent evaporation were

tested in the same way (see 2.2.5 and 2.3.10). Macroscopically the films casted from different PLGA grades (RG502H, RG503H, RG504H, RG755S) showed no difference in the scanning electron micrographs. Figure 38a shows a typical SEM of a PLGA film cross section. The average thickness was determined to be 50±5 µm (Figure 38a).

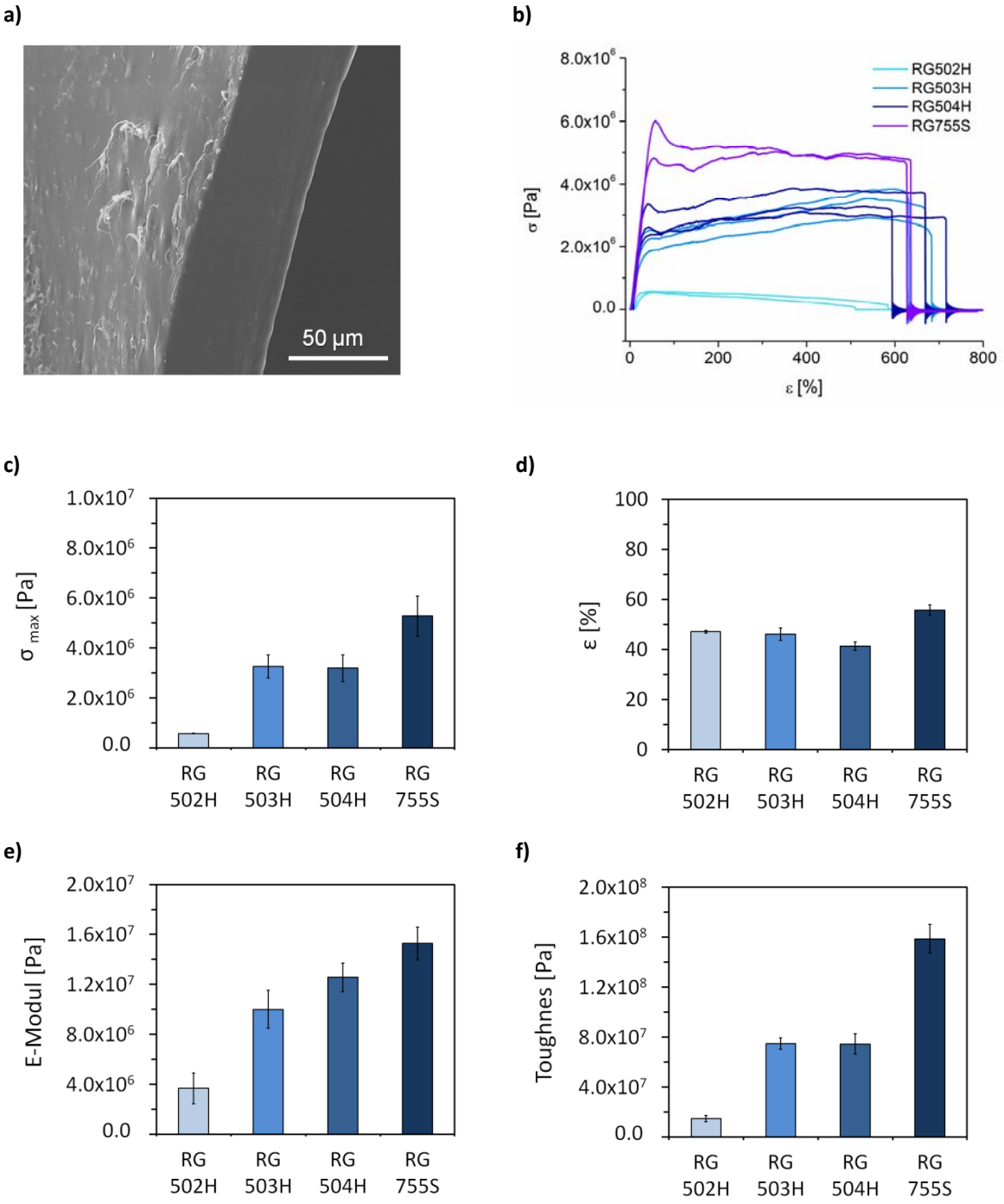

Figure 38: Mechanical characterization of PLGA films. **a)** Typical SEM micrograph of a PLGA film cross section for thickness determination. **b)** Typical stress-strain plots of different PLGA films (RG502H, RG503H, RG504H, RG755S). **c)-f)** From stress strain plots calculated mechanical properties of different PLGA-films: **c)** Tensile strength **d)** Elongation at maximum tensile strength **e)** E-Modulus **f)** Toughness.

Generally, the data shows that tensile strength, E-Moduli and toughness increases with the degree of polymerization reflected by the inherent viscosity (Figure 38 c, e, f and Table 2). All PLGA films tested could be extremely elongated and a lot of energy could be dissipated after the point of maximal tensile strength (Figure 38b). Although films were dried for 7 days at ambient conditions this effect was observed. Most likely this can be explained by remaining solvent (aceton) in the films. For comparison with eADF4(C16) films the elongation at maximal tensile strength was used and employed for toughness calculation. Table 12 summarizes all measured mechanical data obtained for eADF4(C16) and PLGA films. Unfortunately very little information on mechanical data of PLGAs is available. However, despite the high total elongation the determined values for tensile strength and E-modulus agree within the order of magnitude with reported values in literature whereas not sufficient information on sample preparation for mechanical testing is provided (Kranz et al., 2000).

Table 12. Overview of mechanical properties of eADF4(C16) and PLGA films. The mechanical properties for eADF4(C16) films with 0%, 10%, 20% and 40% glycerol with and without 50% MeOH posttreatment are listed. For comparison the determined mechanical properties of films casted from four different PLGA grades (RG502H, RG503H, RG504H, RG755S) are shown in the last section of the table.

Material	Post treatment	Glycerol [%]	σ_{max} [Pa]	ε at σ_{max} [%]	E-Modul [Pa]	Toughness [Pa]
eADF4(C16)	50% MeOH	---	3.9×10^7	12	3.6×10^8	2.5×10^8
eADF4(C16)	50% MeOH	10	2.6×10^7	21	1.6×10^8	2.9×10^8
eADF4(C16)	50% MeOH	20	2.4×10^7	56	8.4×10^7	9.4×10^8
eADF4(C16)	50% MeOH	40	1.2×10^7	100	4.0×10^7	9.4×10^8
eADF4(C16)	---	---	1.5×10^7	11	1.4×10^8	6.2×10^7
eADF4(C16)	---	10	2.3×10^7	47	7.5×10^7	6.0×10^8
eADF4(C16)	---	20	8.3×10^6	89	2.8×10^7	5.1×10^8
eADF4(C16)	---	40	9.9×10^6	129	2.3×10^7	8.5×10^8

RG502H	---	---	5.8 x10^5	47	3.7 x10^6	1.5 x10^7
RG503H	---	---	3.3 x10^5	46	1.0 x10^7	7.5 x10^7
RG504H	---	---	3.2 x10^6	43	1.3 x10^7	7.5 x10^7
RG755S	---	---	5.3 x10^6	56	1.3 x10^7	1.6 x10^8

3.3.5 Porous films by PEO blending

Microphase separation of polymer blends can be used to produce porous films (Jin et al., 2004; Lawrence et al., 2008). The idea is that the polymer in the dispersed phase can be dissolved whereas the polymer constituting the matrix is stable. This technique has been used to produce porous structures in *B. mori* films (Jin et al., 2004; Lawrence et al., 2008). The advantage of using silks is that by changing their conformation by posttreatments (like MeOH or potassiumphosphate), silk can become insoluble in water. PEO is a water soluable polymer approved by the Food and Drug Administration (FDA) for biomedical applications.

To achieve a homogenous distribution of pores throughout the membrane a microphase separation has to be achieved. Therefore, we studied the phase behavior of eADF4(C16) dissolved in HFIP and dissolved in water blended with an aqueous PEO solution (5% (w/v)) at different ratios. Phase contrast microscopic pictures of blended films with different PEO content after drying and without any post treatment are shown in Figure 39. The phase behavior of eADF4(C16) in HFIP blended with PEO is shown in Figure 39 a-d whereas the Figure 39 e-h shows the phase behavior for the water system.

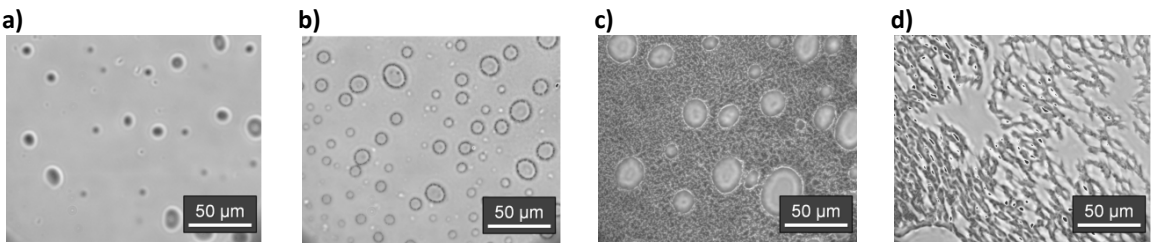

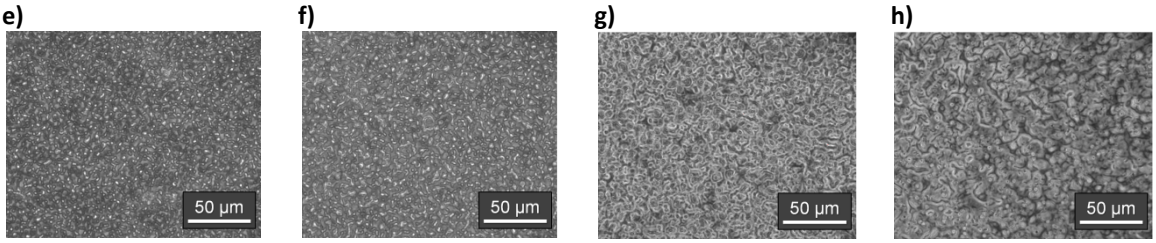

Figure 39: Phase behavior of eADF4(C16)-PEO blendings **a)–e)** Phasecontrastmicroscopic pictures of eADF4(C16)/HFIP Films with: **a)** 4% PEO **b)** 8% PEO **c)** 12% PEO **d)** 16% PEO **e)-h)** Phasecontrastmicroscopic pictures of eADF4(C16)/water films with **e)** 16% PEO **f)** 32% PEO **g)** 48% PEO **h)** 64% PEO.

From the phase contrast micrographs in Figure 39 it can be seen that microphase separation occurs in the water system whereas in the HFIP system macrophase separation was observed. Therefore, eADF4(C16)/PEO/water blendings with different ratios were, casted, dried and posttreated by 50% MeOH and incubated in water for 24 h to dissolve the PEO. SEM analysis showed that above 5% PEO content porous membrane structures were obtained (Figure 40a-f). Generally, an increase in PEO content yield larger pores (Figure 40b-f). In case of 5% PEO pores of about 500 nm to 1 µm could be generated (Figure 40b,c) whereas in the case of 333% PEO foam like structures with a pore sizes above 5 µm were observed (Figure 40f).

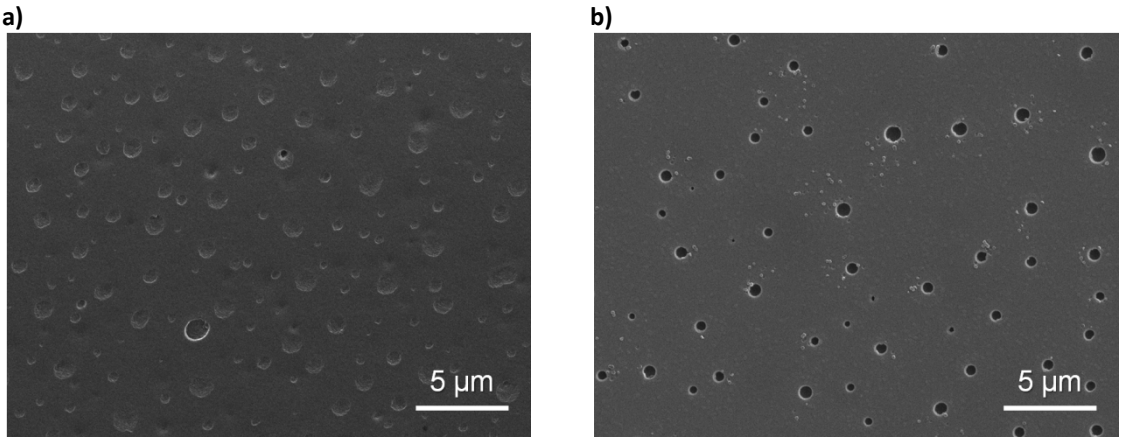

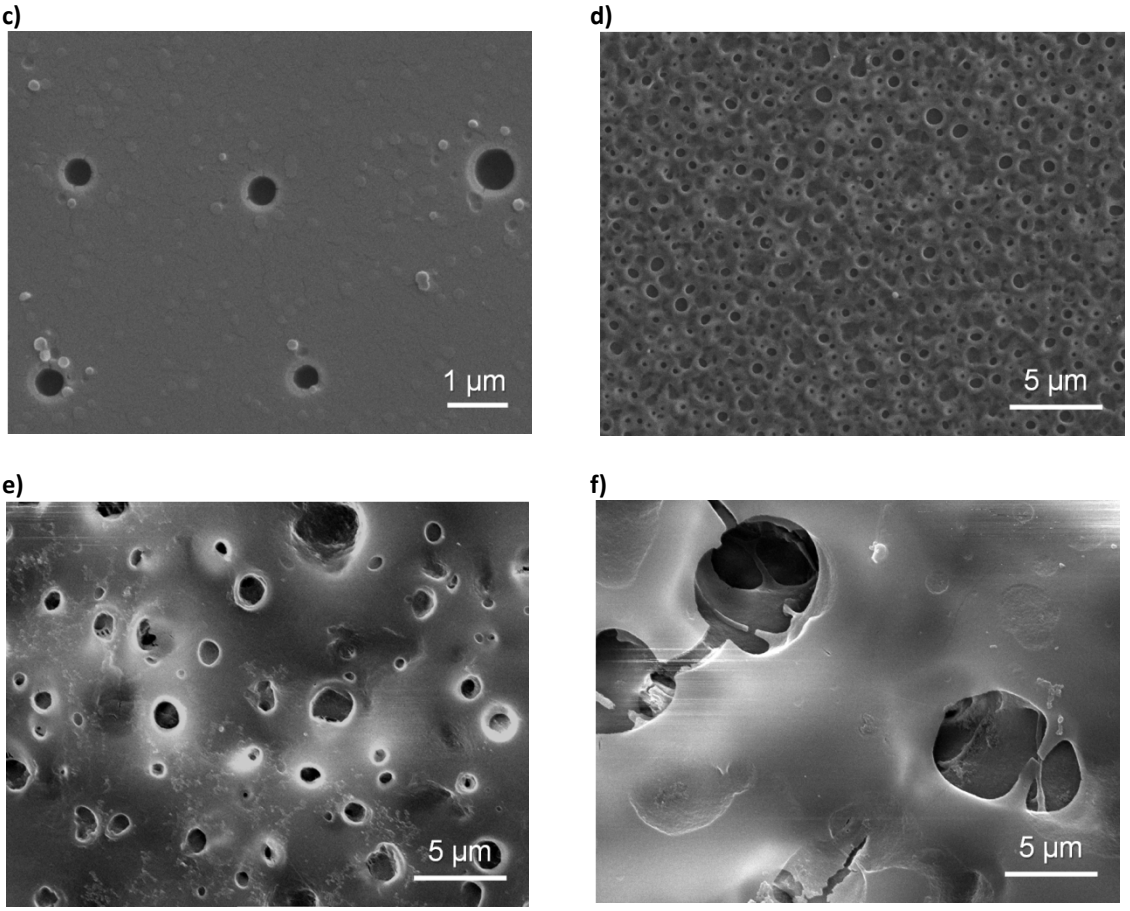

Figure 40. Scanning electron micrographs of porous eADF4(C16) films with different PEO content: **a)** 5% (w/v) PEO **b)** 20% (w/v) PEO **c)** 20% PEO (w/v) zoom **d)** 50% (w/v) PEO **e)** 111% (w/v) PEO **f)** 333% (w/v) PEO.

Furthermore, the surface roughness in the vicinity of the pores was analyzed. Figure 41a shows a typical AFM micrograph of 5.5 µm x 5.5 µm film section with the trajectory (white line) at which the surface analysis was conducted. Figure 41b shows the z-profile of the trajectory and the determined values of average surface roughness (between the red marks). An average maximum height of the profile R_z = 8.9 nm and a maximum roughness depth of R_{max} = 14.5 nm was determined

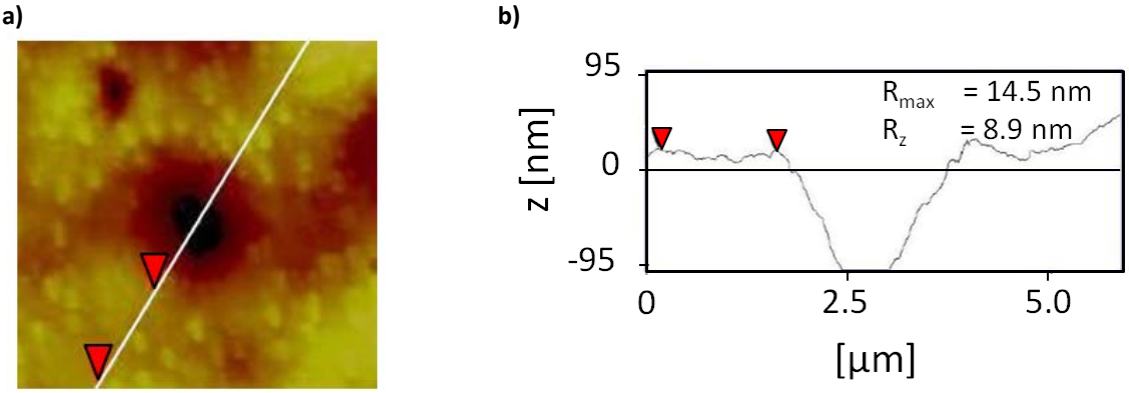

Figure 41. Atomic force microscopic analysis of a porous film. a) AFM micrograph of a 5.5 µm x 5.5 µm film section. The white line indicates the trajectory at which the surface analysis was conducted. b) z-profile of the trajectory. The surface roughness was determined between the red marks yielding values of R_z = 8.9 nm for the average maximum height of the profile and R_{max} = 14.5 nm for the maximum roughness depth.

In order to elucidate if the pores seen in the scanning electron micrograph are transmembrane pores, confocal microscopy has been employed to scan the membranes in z-direction. The left side of Figure 42 shows the top view of a porous membrane. The line A-A indicates the position of the vertical cut in z-direction, as shown on the right side. As shown in Figure 42 transmembrane pores were detected.

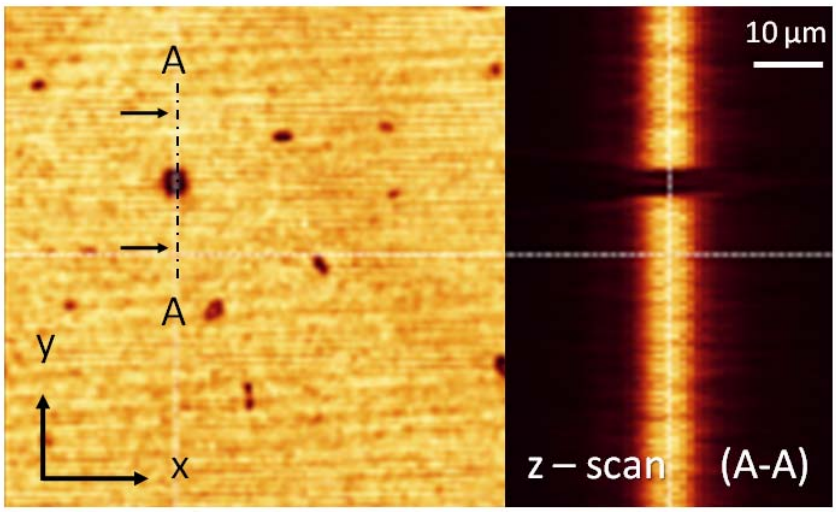

Figure 42. Confocal microscopy of a porous eADF4(C16) film obtained after blending and dissolution of PEO. The left side shows the top view, whereas the line A-A indicates the position of the vertical cut in z-direction, as shown on the right side. The right side shows that the pore is a continuous trans-membrane pore.

3.3.6 Influence of PEO on secondary structure

FTIR analysis of PEO blended eADF4(C16) films casted from water and HFIP revealed that in the water system PEO induces β-sheet formation (Figure 43a) whereas no influence on secondary structure change could be detected for the HFIP system (Figure 43b). This result indicates that PEO behaves as a hygroscopic polymer, reducing the water content in the eADF4(C16) film in therefore enhances intermolecular interactions resulting in β-sheet formation.

a) **b)**

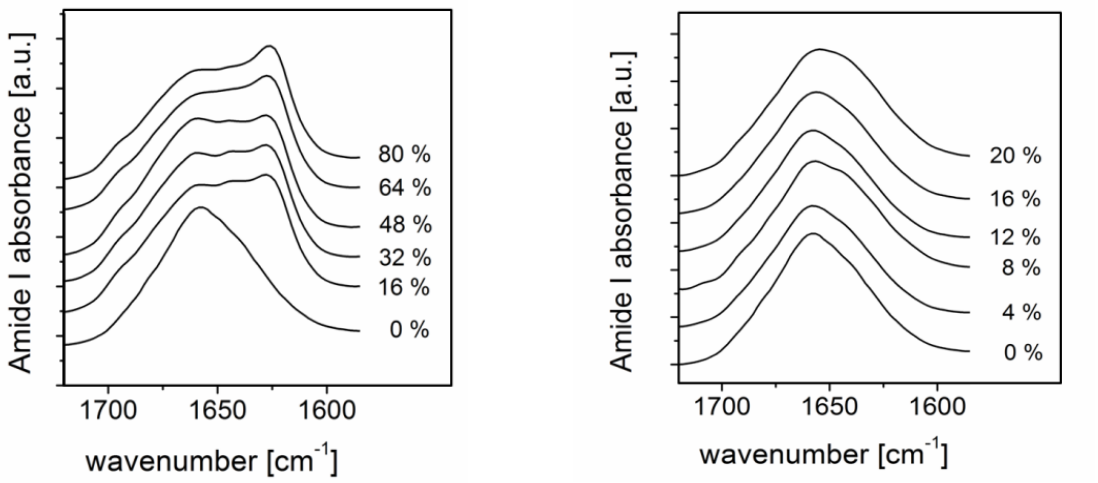

Figure 43. FTIR analysis of eADF4(C16) films blended with different amounts of PEO as indicated for eADF4(C16) casted from **a)** water **b)** and HFIP.

3.3.7 In vitro release from eADF4(C16) films

In order to investigate the release of small molecule model drugs, eADF(C16) films were casted from HFIP and loaded with 5% (w/w) crystal violet. The loading was performed by addition of crystal violet to eADF4(C16) solution prior to film casting. After film stabilization with 50% MeOH the loaded films were incubated in different salt solutions (KCl, NaCl, $MgCl_2$ and $CaCl_2$) of various ionic strength (10 mM, 50 mM and 200 mM) and PBS of various pH (pH 4, 6, 7.4 and 9). The Influence of different salt solutions and ionic strength was examined by determination of crystal violet concentration in the supernatant after 24 h. Figure 44a shows that the release increases with increasing ionic strength and follows the Hofmeister series (see section 3.12). The influence of pH on the

release behavior was studied upon incubation in PBS for 35 days. Generally, release is accelerated for increasing acidic conditions (Figure 44b). Until day 5 the release media was not changed for determination of crystal violet concentration in supernatant. From day 5 on the release media was replaced by fresh PBS at each measurement. Thereby, the kink in the release data (Figure 44b) on day 5 can be explained since the crystal violet concentration gradient between eADF4(C16) matrix and the release media is the driving force for diffusional release.

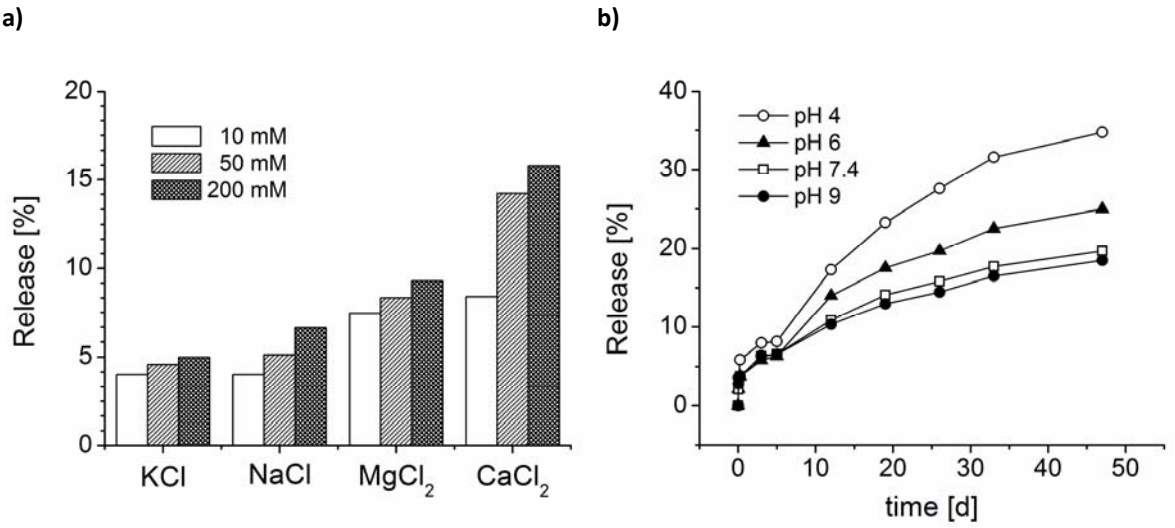

Figure 44. Crystal Violet release from eADF4(C16) films. **a)** Release of crystal violet from eADF4(C16) films after incubation in different salt solutions (KCl, NaCl, $MgCl_2$ and $CaCl_2$) of various ionic strength (10 mM, 50 mM and 200 mM) after 24 h. **b)** Crystal violet release from eADF4(C16) films over time for incubation in PBS as a function of pH as indicated. (Buffer capacity PBS: pH 5.8 – pH 8; non buffered conditions for pH pH 4.0 and pH 9). Until day 5 the release media was not changed for determination of crystal violet concentration in supernatant. From day 5 on the release media was replaced by fresh PBS at each measurement. Thereby, the kink in the release data on day 5 can be explained.

4 DISCUSSION

4.1 Particle formation

Salting out has long been used as an early step in the process of protein purification (Green, 1931; Green, 1932). In aqueous solutions, proteins can be considered as charged polyions. Their charge depends on the hydrogen-ion dissociation constants of each constituent amino acids and the solution pH (Kuehner et al., 1996). Upon addition of kosmotropic salts a supersaturated solution is generated in which the protein in solution exceeds its thermodynamic solubility limit, which gives rise to the minimization of free energy by liquid-liquid phase separation (Broide et al., 1996; Jiang and Prausnitz, 1999). Consequently, a protein rich phase is formed in a protein lean phase (Brick et al., 2003). The degree of separation is characterized by the partition coefficients K_e which is directly related to the salting out efficiency and defined as the ratio of protein concentration in the dense phase to the protein concentration in the supernatant (Chang and Bae, 2003). Our results show, that salting out efficiency of regenerated *B. mori* silk fibroin and eADF4(C16) increases with ionic strength and follows the Hofmeister series (Zhang and Cremer, 2006). Particle formation was detected for strong kosmotropic salts like potassium phosphate at high salt concentrations (> 0.75 M potassium phosphate for *B. mori* silk fibroin and > 0.5 M potassium phosphate for eADF4(C16)). Under such conditions, where silk protein particle formation occurs, the concentration of ions is so high that there is little free volume for protein molecules giving rise to short range osmotic attraction. Additionally, the Debye length is extremely small, and thus coulombic interactions are essentially completely screened. Therefore, the protein molecules in the dense phase are subjected to protein-protein interaction, coalesce and form nuclei.

To a first approximation, the overall perturbation potential between two different protein molecules can be described by a two body potential of mean force $W_{pp}(r)$ comprised of four potentials as shown in equation (9);

$$W_{pp}(r) = W_{elec}(r) + W_{disp}(r) + W_{osmotic}(r) + W_{specific}(r) \qquad (9)$$

where r is the center to center separation. $W_{elec}(r)$ is the electric double layer repulsion potential, $W_{dis}(r)$ is the dispersion potential, $W_{osmotic}(r)$ is an attractive interaction due to the excluded volume effect of salt ions. $W_{specific}(r)$ is an attractive potential between proteins included to represent any specific chemical effects such as hydrophobic interactions (Kuehner et al., 1996; Leckband and Sivasankar, 1999). Details are shown in Appendix A4. Assuming a spherical nucleus with radius r its free energy can be described to a first approximation by equation (10)

$$\Delta G = \Delta G_s + \Delta G_v = 4\pi r^2 \gamma + 4/3\pi r^3 \Delta g_v \qquad (10)$$

where γ stands for the surface tension between the two phases and Δg_v for the difference in free energy per unit volume between the two phases. The two terms on the right of the equation have opposite signs so that ΔG as a function of r passes through a maximum (Figure 41). The critical nucleus radius r* is defined by the position of the maximum of the free energy and given by equation (11).

$$r^* = -2\gamma/\Delta g_v \qquad (11)$$

Particles with a radius smaller than r* redissolve, whilst particles which by reason of statistical fluctuations exceed this size are stable and can grow further (Horn and Rieger, 2001).

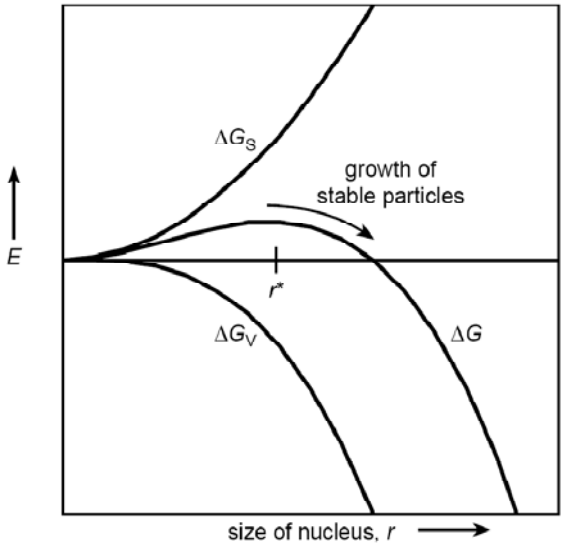

Figure 45. Energy diagram to explain the nucleation process (ΔG: free energy of a particle with radius r, ΔG_s : surface energy, ΔG_v : bulk energy, r*: radius of the critical nucleus). The particle sizes fluctuate because of statistical processes. Particles with a radius r<r* redissolve, those with r>r* grow further.

The particle size distribution (PSD) is the result of several parallel and successive processes: nucleation, growth, and agglomeration (Schwarzer and Peukert, 2004a; Schwarzer and Peukert, 2004b). Figure 42 shows the various influencing parameters on the three mentioned processes.

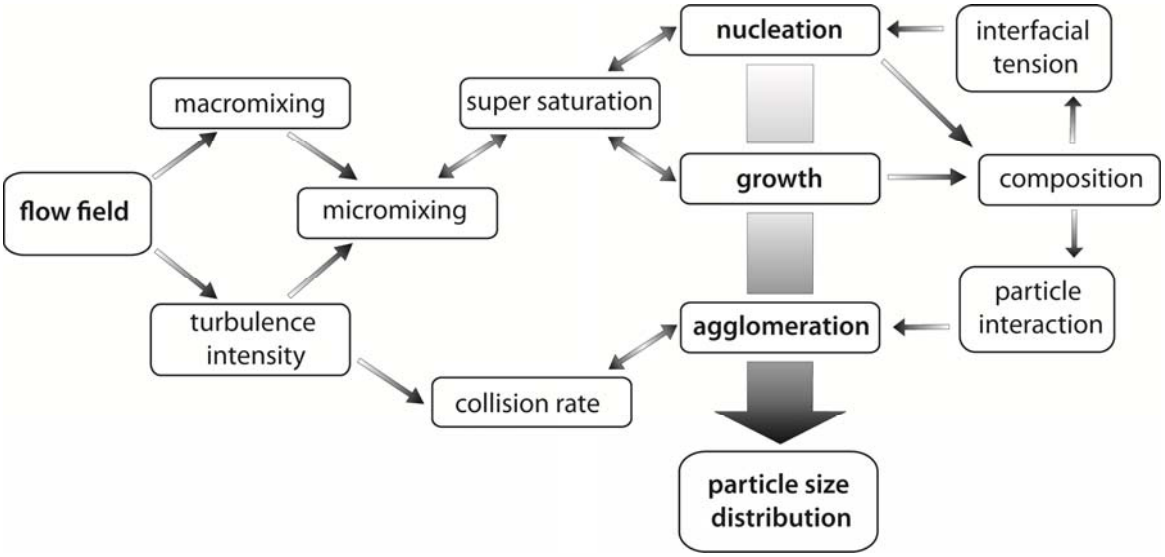

Figure 46. Processing parameters affecting particle size distribution upon salting out. The flow field with which educt solutions are mixed influences the homogeneity of the supersaturation as well as the rate at which particles colloid with each other resulting in agglomerations. The extent of supersaturation has strong influence on nucleation rate and growth. The composition (structure, charge, surface properties etc) of particles depends on the physicochemical properties of macromolecules employed as well as the underlying growth mechanism involving the arrangement and interactions of the molecules constituting the particle.

The mixing flow field by which supersaturation is generated is determined by the mixing method (dialysis, pipettes and micromixing device). The flow field can be described as a function of turbulence intensity, which determines the size of the smallest eddies and thereby the diffusion length necessary for molecular mixing (Haberkorn et al., 2003). Additionally, the mixing intensity influences the rate at which particles colloide with each other and thereby the agglomeration.

Within the scope of a quasi-equilibrium approach (Arrhenius) the number of nuclei which form per unit time and volume can be expressed by equation (12),

$$J = A\exp(-\Delta G^{*}/kT) \qquad (12)$$

where J is the rate of nucleation, A is determined by the frequency of the molecular processes, ΔG* is the free energy needed to form a critical nucleus of radius r*, k is the Boltzmann constant and T the Temperature. In accordance with equation (13)

$$kT\ \ln(S) = 2\sigma v / r \qquad (13)$$

the supersaturation S=c/c* is coupled with the particle radius; v is the molecular volume, c denotes the supersaturated concentration, and c* the concentration at the equilibrium solubility. Therefore combining equation (10), (11), (12) and (13), the rate of nucleation can be expressed in terms of the supersaturation according to equation (14),

$$J = A\exp(-(16\pi\gamma^{3}v^{2})/(3k^{3}T^{3}[\ln S]^{2})) \qquad (14)$$

which shows that nucleation and growth rates depend strongly on the extent of supersaturation (Horn and Rieger, 2001; Sear, 1999). While at high supersaturation a large number of particles are formed that remain small since the available total protein mass is limited, fewer but larger particles are generated at lower supersaturation. Therefore, the particles size distribution depends on the homogeneity of supersaturation throughout the solution and thus the method of educt solution mixing. Additionally to mixing intensity, processing parameters regarding the composition of the educt solutions have influence on the resulting particles. For example, the interfacial tension that influences the nucleation rate is also a function of ionic strength.

As outlined above, salting out is a complex procedure of parallel and subsequent processes with various interacting and changing parameters. Our investigation regarding the particle production of regenerated *B. mori* silk fibroin and engineered spider silk protein eADF4(C16) showed that salting out efficiency correlates with the Hofmeister series and particle formation occurs at high ionic strength of kosmotropic salts such as potassium phosphate. We conclude that for the production of stable silk particles by salting out a high concentration of potassium phosphate is required. Due to the fact that the grand average hydropaticity of eADF4(C16) is lower compared to regenerated *B. mori* silk fibroin the ionic strength threshold necessary for particle formation is at lower.

Particle growth stops, when the protein concentration is below the equilibrium of solubility leading to the fact that the particle diameter does not increase anymore. Generally, with increasing protein concentration particle size is increased. Our results, regarding the investigation of different mixing techniques show that in agreement with theoretical approaches at higher mixing intensities smaller particles with a narrow size distribution can be obtained whereas at very slow mixing particle size and width of size distribution increases (Figure 47).

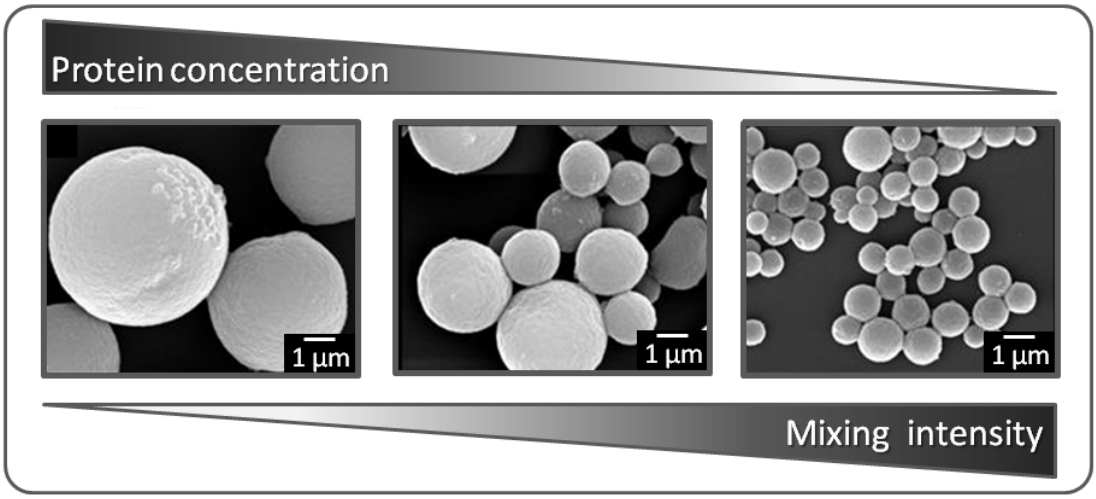

Figure 47. Influence of protein concentration and mixing intensity on silk particle formation produced by salting out with 1 M potassium phosphate (pH 8). With increasing protein concentration larger spheres can be produced whereas with increasing mixing intensity sphere size can be decreased.

4.2 Silk particle characteristics

B. mori silk fibroin and eADF4(C16) particles have been characterized with respect to their zeta potential and secondary structure. Compared to *B. mori* silk particles produced by salting out with 1M potassium phosphate at pH8, eADF4(C16) particles have much higher β-sheet content at the same salting out conditions: 45.1 % β-sheet for eADF4(C16) particles and 15.1 % β-sheet for *B. mori* silk fibroin particles. The zetapotential of eADF4(C16) particles produced at the afore mentioned salting out conditions was determined to be -22±2 mV and -45±2 mV for *B. mori* silk fibroin

particles, respectively. This result can be explained by the architecture of amino acid composition of the different employed silk proteins as discussed in 3.1.1 and 3.2.1. eADF4(C16) carries less negative charges and is very hydrophobic which gives rise to β-sheet structure formation. Due to the fact that the β-sheet content of *B. mori* silk particles was only 15.1% at salting out with potassium phosphate at pH 8, the influence of pH on secondary structure and zeta potential was studied. As shown in 3.1.3.1 and 3.1.3.2 the β-sheet content increases for salting out at lower pH whereas the zeta potential decreases. In the following, we will explain the observed influence of pH on the secondary structure and zeta potential of *B. mori* silk fibroin particles based on its amino acid composition. In agreement with the characterization of *B. mori* silk fibroin in section 3.1.1 Figure 48a shows the derived schematic model of silk fibroin protein heavy(H) and light(L)-chain.

Based on these characteristics of the domains and previously published data regarding the relationships between amino acid composition and silk protein phase separation, salting-out behavior and self-assembly (Bini et al., 2004; Chen et al., 2008; Foo et al., 2006a; Jin and Kaplan, 2003; Mita et al., 1994; Sponner et al., 2004; Terry et al., 2004) a model for particle formation has been developed. The theoretical pI of the domains can be used to describe the influence of pH on the charge distribution of the silk fibroin protein associated with self-assembly due to intra- and intermolecular forces. At pH 9 all charged amino acid side chains except the C-terminus are negatively charged resulting in a likely rather elongated molecular conformation in solution due to repulsive charge-charge interactions along the biopolymer backbone (Figure 48b, right). As the pH is lowered the repulsive interactions along the protein are suppressed, resulting in a less extended and more compact conformation (Figure 48b, middle). At pH 4, electrostatic repulsion is suppressed allowing the approaching of neighboring residues and molecules and the formation of hydrophobic interactions and later hydrogen bonds between molecules (Terry et al., 2004). The formation of particles is based on the salting-out effect of kosmotropic salts like potassium phosphate. In a first step the protein chains form micellar like structures due to the enhancement of hydrophobic interactions. Depending on the structural conformation of the silk fibroin predetermined by pH, different micellar structures with different packing densities are formed. In a second step the micelles form particulate globules by further hydrophobic interactions. The

micelles formed at pH 9 reveal a less dense packing than those made at acidic pH. Therefore, tighter packing of the micelles in the particles is possible due to additional hydrophobic interactions, which might lead to the detected higher chemical stability (although the silk I structure should be thermodynamically less stable than the silk II structure the particles with high silk I content a chemically more stable than those with silk II structure). The theory about the formation of micellar structures is supported by SEM pictures of particles produced by salting with potassium phosphate (pH 8) with a ionic strength of 0.75 M where the transition of particle formation has been observed (Figure 6a,b). The observed micellar structures are approximately 100 nm which corresponds to the length of an elongated silk fibroin protein.

a)

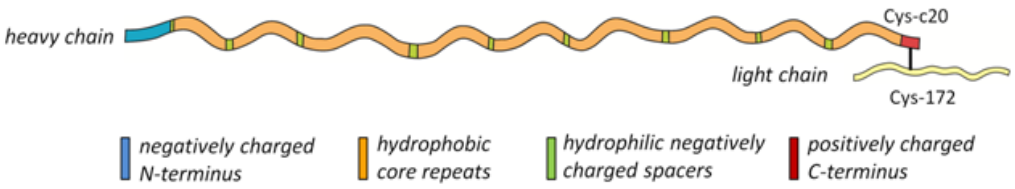

b)

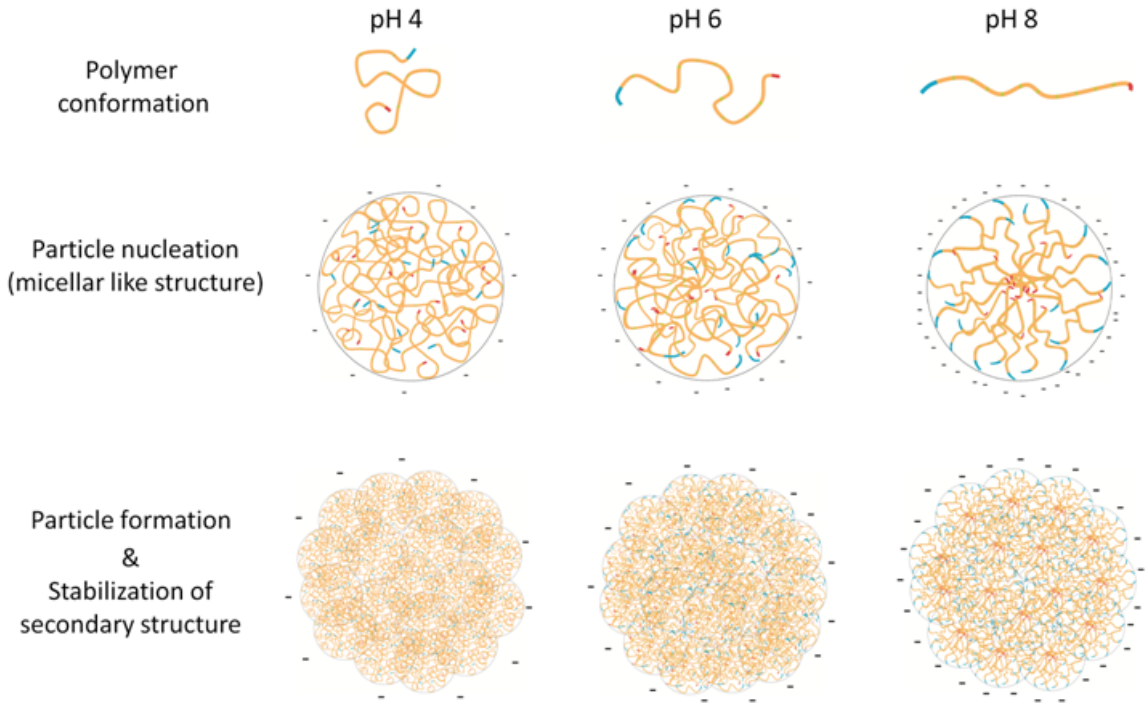

Figure 48. Silk fibroin characteristics and particle formation. **a)** Characteristics of silk fibroin considering the charge distribution along the amino acid chain. **b)** Model for silk fibroin particle formation. *Top:* Assumed configuration of amino acid chains at different pHs. *Middle:* Particle nucleation of micellar like structures. *Bottom:* Particle formation and stabilization of secondary structures through clustering of micellar like structures in the presence of potassium phosphate (>1.0 M).

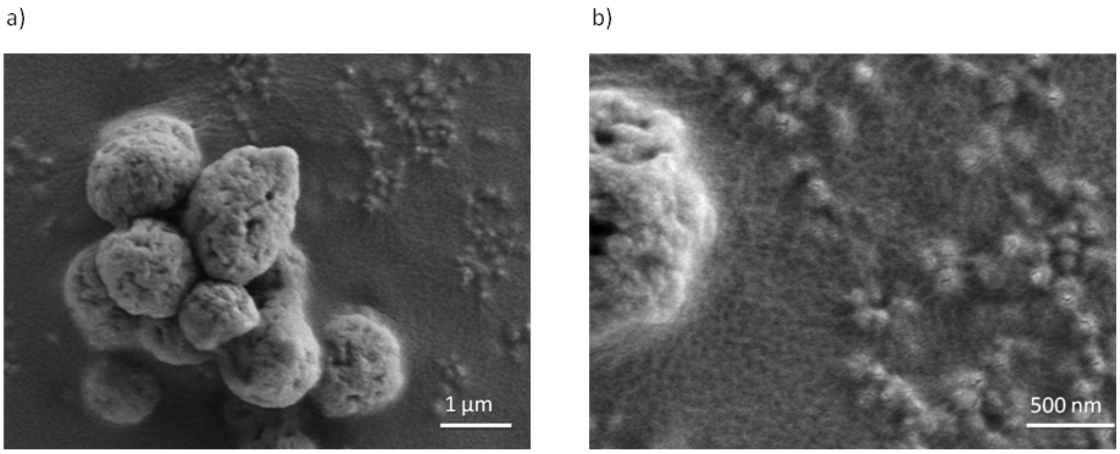

Figure 49. Scanning electron micrograph of particles produced at the transition conditions for particle formation (salting out with 0.75 M potassium phosphate at pH 8). a) Larger particles are comprised of smaller micellar structures (magnification 20,000x). b) Micellar-like structures of approximately 100 nm (magnification 50,000x)

4.3 Loading and Release

Our in vitro loading and release study shows the potential of silk particles produced by salting out of regenerated *B. mori* silk fibroin and engineered spider silk protein eADF4(C16) for drug carriers. Especially, for positively charged and sufficiently hydrophobic drug molecules which represent the majority of drug molecules available today (Couvreur et al., 1990; Gelperina et al., 2005; Lee et al., 2004; Meng et al., 2009; Nakanishi et al., 2001; Zhu and McShane, 2005) silk carriers seem to be very promising. Our detailed investigation of the loading procedure including the parameters like the octanol / water partition coefficient (*logP*) and dissociation constants (*pKa*) of twelve different model drugs emphasized the applicability of the encapsulation procedure. Additionally, using an online zeta potential measurement during particle loading allowed

monitoring of the loading processes and facilitated the determination of the loading endpoint. In case of *B. mori* silk fibroin particles the influence of the secondary structure of the particles on their release behavior was studied with crystal violet (CV). Particles with a higher content of silk II structure showed an increased initial burst with release of 29% CV for particles produced at pH 7, 17% CV for particles produced at pH 8, and 11% CV for particles produced at pH 9 (Figure 20). Particles produced at pH 7 show an increased release rate over the whole period of time compared to particles produced at pH 8 and pH 9. Furthermore we showed that the release is pH sensitive with accelerated release rates at lower pH. We conclude that silk particle loading and release follows the following mechanism: In a first step drug molecules are attracted to the particle by electrostatic forces. After particle surface saturation small molecular drugs start to diffuse into the biopolymer matrix. Drug molecules are bonded by attractive hydrophobic and electrostatic interactions. After complete loading and incubation in release media drug molecules are transported to the particle surface due to concentration gradient driven transport processes. Upon time drug molecules are slowly released from the surface by which constant release rates can be realized (Figure 50).

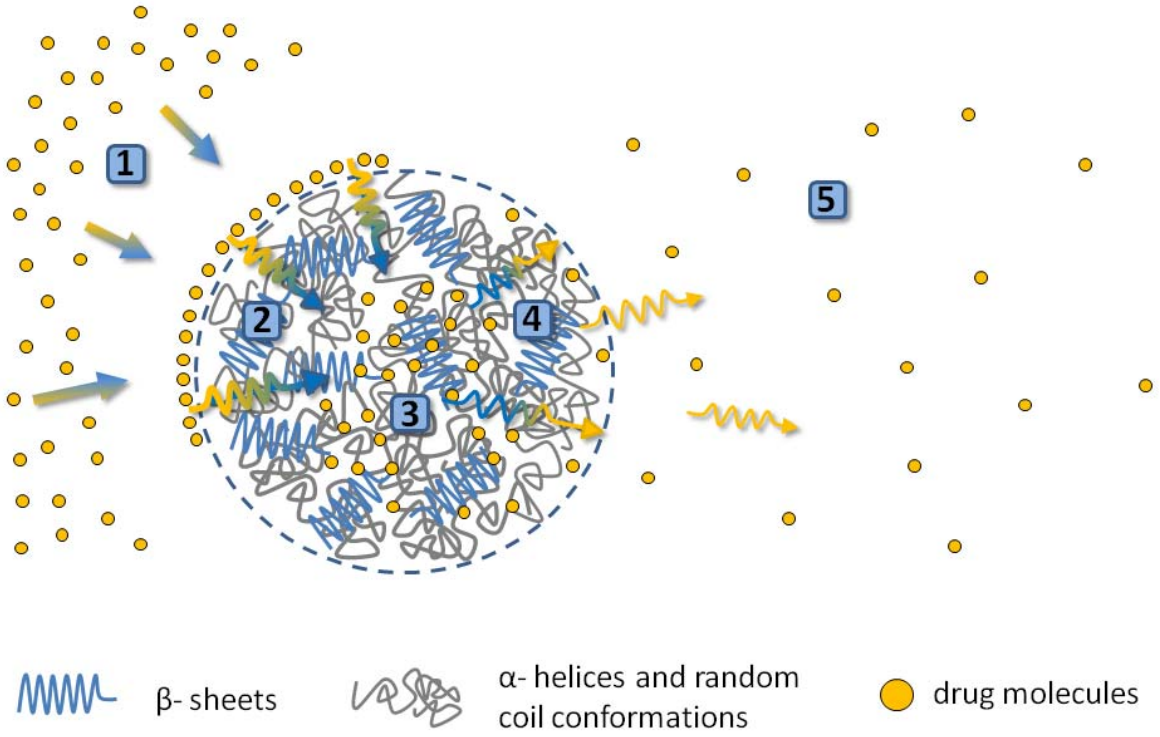

Figure 50. . Loading and release mechanism for silk particles. 1) Drug molecules are attracted to the particle by electrostatic forces. 2) After particle surface saturation small molecular drugs start to diffuse into the biopolymer matrix. 3) Drug molecules are bonded by attractive hydrophobic and electrostatic interactions. 4) After complete loading and incubation in release media drug molecules are transported to the particle surface due to concentration gradient driven transport processes. 5) Upon time drug molecules are slowly released from the surface by which constant release rates can be realized.

4.4 Comparison of *Bombyx mori* silk fibroin and eADF4(C16) carriers

Generally, our results show that colloidal particles from aqueous solution of *B. mori* silk fibroin and engineered spider silk eADF4(C16) can be produced by salting out with potassium phosphate. However, for *B. mori* silk fibroin particle production a higher potassium phosphate concentration is required (ionic strength > 0.75 M for *B. mori* silk fibroin compared to > 0.4 M for eADF4(C16)). This can be explained by the fact that *B. mori* silk fibroin contains hydrophilic spacers in its amino acid sequence and therefore more ions are needed to reduce the quality of the hydration layer necessary for protein destabilization and salting out. As discussed in 4.2 the secondary structure of *B. mori* silk fibroin particles can be controlled by pH of potassium phosphate due the presence of hydrophilic spacers in the amino acid sequence. The conformation of secondary structure is also associated with the zetapotential of particle produced by salting out potassium phosphate of different pH. In contrast, due to the very simple and repetitive sequence of eADF4(C16) and the lack of hydrophilic spacers in combination with the high hydrophobicity, intermolecular interactions are very strong upon salting out leading to the observed high β sheet content (> 45%) of eADF4(C16) particles compared to *B. mori* silk fibroin particles (β sheet content ca. 15 %) at the same salting out conditions at pH 8. However, compared to *B. mori* silk particles eADF4(C16) particles have a smoother surface (Figure 15e and Figure 25b) which can be explained by the smaller molecular weight and by the afore mentioned difference in primary structure. Our results indicate that both *B. mori* silk particles and eADF4(C16) particles can be loaded by the same strategy based on charge-charge interaction and diffusion into the particle matrix. In case of *B. mori* silk particles, release could be controlled by the secondary structure of the particles whereas in case of eADF4(C16) particles pH sensitive release was observed.

Due the fact that the interaction of small molecule model drugs with the silk protein matrix is based on electrostatic and hydrophobic interactions, generally an increase in ionic strength and decrease of pH yields accelerated release behavior. One major advantage of eADF4(C16) particles might be that due to the recombinant production the protein can be engineered and produced in a controllable fashion with constant material quality whereas the quality of regenerated *B. mori* silk depends on the silk quality of the cocoon and the degumming process. Furthermore, engineered spider silk offers the possibility of incorporation of functional groups or attachment of marker molecules which might be of interest for future studies in terms of specific targeting.

4.5 Potential of silk films for biomedical applications

Silk films can be employed for a great variety of biomedical applications such as wound dressings, devices for controlled release, self supporting implantable therapeutic multilayer systems, functionalized coating for implants or scaffolds in tissue engineering (Akira et al., 2000; Lawrence et al., 2009; Liu et al., 2009; Lvov et al., 2002; Wang et al., 2007a). Due to the limited availability of engineered spider silk, most of the silk film studies have been carried out with *B. mori* silk fibroin. However, similar applications can be envisioned for recombinant spider silk proteins due to the similarity in their physicochemical properties. Engineered spider silk proteins might be preferable due to the potential of silk protein design according to specific requirements and eventually improved mechanical properties (Metwalli et al., 2007; Slotta et al., 2006).

Our initial results regarding the characterization of eADF4(C16) films are promising in respect to the control of film features required for its application as biomaterial. The experimental data regarding the mechanics showed that eADF4(C16) membranes are comparable to commonly used biomaterials such as different PLGA grades (Table 12). Additionally, mechanical properties can be controlled by addition of hygroscopic plasticizers like glycerol which alter intermolecular interactions and renders eADF4(C16) films more elastic (Table 12). As an example, a content of 40 % (v/w) glycerol increases the elasticity of a eADF4(C16) film about 10 fold, accompanied by a 10 fold decrease in elastic modulus and a slight decrease in strength (Table 12). Furthermore, porous

eADF4(C16) films can be produced by PEO blending, film stabilization and subsequent dissolution of PEO. The size of the pores as well as their interconnectivity can be varied by the concentration of PEO (Figure 40). Initial experiments showed that matrixloaded eADF4(C16) films exhibit a similar prolonged pH sensitive release behavior as the studied eADF4(C16) particles. The film permeability for certain molecules depends on parameters such as charge, hydrophobicity and crystallinity (secondary structure) of the membranes. Crystalline domains have a higher density and therefore exhibit a permeation barrier. Future studies regarding the permeability of engineered spider silk membranes considering molecular weight, charge and hydrophobicity of drug molecules as well as the secondary structure and pore size will reveal additional valuable information for their application as diffusion controlling membranes.

In summary, the combination of processing parameters seems promising for the generation of tailored silk films. However, for specific applications in tissue engineering, additional features might be necessary, for example combining silk films with additional functional groups such as components of the extracellular matrix for better cell adhesion or differentiation (Bini et al., 2006; Colin D. Heyes, 2007; Sofia et al., 2001). Our established recombinant production technology of spider silk proteins offers various possibilities to introduce new and additional amino acid side chains by genetic engineering, which can be utilized for further functionalization.

5. Conclusion

The aim of this study was to develop a simple method to produce silk protein based drug carriers which can be produced and loaded within an all-aqueous process. Therefore, regenerated *B. mori* silk fibroin and recombinantly produced spider silk eADF4(C16) were characterized with respect to their phase behavior and processing. The produced particles were characterized with respect to their features and applicability as controlled drug delivery systems.

We showed that solid *B. mori* silk fibroin and eADF4(C16) particles of controllable sizes (500 nm --2 µm for *B. mori* silk particles and 250 nm -2 µm for eADF4(C16) particles) can be obtained in an all-aqueous process by salting out with potassium phosphate. We conclude that for stable silk particle formation a high concentration of potassium phosphate (>0.75 M) is required. Spherical growth stops when the protein concentration is below the equilibrium of solubility, leading to the fact that the sphere diameter does not increase anymore. Analysis of morphology and structure of the obtained silk particles showed that eADF4(C16) particles compared to *B. mori* silk fibroin particles have a smoother surface and higher β-sheet content (>45% compared to ≈15% for *B. mori* silk particles) at the same salting out conditions. Generally, silk particle size could be controlled by protein concentration whereas the concentration has to be below 15 mg/ml to avoid particle agglomeration. Further studies of the process parameters of eADF4(C16) particle formation revealed that sphere size and size distribution can be controlled by mixing intensity. Higher mixing intensity yields smaller particles with a narrow size distribution. In contrast to eADF4(C16) particles, secondary structure and the zeta potential of *B. mori* silk fibroin particles can be controlled by varying the pH upon salting out. Particles produced by salting out with 1.25 M potassium phosphate pH 6 showed a dominating silk II (crystalline) structure whereas particles produced at pH 9 were mainly composed of silk I (less crystalline). The stability of silk particles in denaturating agents (Urea, GdmHCl, GdmSCN) as well as the stability of secondary structure upon post treatments (EtOH and MeOH) indicate that the particles with silk I structure are very stable and can be sterilized without affecting their secondary structure. We propose a model to explain the observed influence of pH on secondary

structure and zeta potential and conclude that larger particles produced by salting out are comprised of smaller micellar like structures. We showed the applicability of the particles for controlled release. The negative surface charge of the particles enables loading with positively charged small molecules by simple charge -charge interaction and diffusion into the particle matrix. *In vitro* release revealed that the release of small molecules from *B. mori* silk fibroin particles depends on their charge as well as the silk structure. The same loading procedure was performed for eADF4(C16) particles and investigated in more detail by determination of loading efficiencies of twelve different model drugs in dependence of drug molecule properties such as octanol/water partition coefficient (*logP*) and dissociation constants (*pKa*). Our results show the potential of silk protein particles for sustained controlled delivery of positively charged and sufficiently hydrophobic drug molecules which represent the majority of drug molecules available today (Couvreur et al., 1990; Gelperina et al., 2005; Lee et al., 2004; Meng et al., 2009; Nakanishi et al., 2001; Zhu and McShane, 2005), emphasizing the general applicability of our loading procedure. Additionally, using an online zeta potential measurement during particle loading allowed monitoring of the loading processes and facilitated the determination of the loading endpoint. Especially for intravenous administration of highly potent cancer chemotherapeutic agents the silk carrier system may be ideal. Most drugs used in cytostatics therapy (e.g. doxorubicin*HCl, paclitaxel or docetaxel) exhibit a low solubility in aqueous milieu (Nakanishi et al., 2001). Our results indicate that eADF4(C16) particles are very well suited for encapsulation of small hydrophobic drugs. The molecules are concentrated in the particles matrix and released in a prolonged manner due to hydrophobic interactions between drug molecules and particle matrix. Since our complete process of particle production and loading only involve aqueous solvent conditions and potassium phosphate at room temperature and neutral pH, and since the processing conditions can be easily scaled-up, protein particles made of engineered spider silk or regenerated *B. mori* silk fibroin are *per se* suitable for the encapsulation of sensitive drugs. Due to their size, eADF4(C16) and *B. mori* silk fibroin particles are applicable for drug targeting in humans since the diameter of the particles is appropriate for phagocytosis by macrophages or cellular uptake by carcinoma cells (Bartlett DW, 2007; Chavanpatil MD, 2006). We conclude that silk particles have the

potential for diverse applications where controlled release from biocompatible, mechanically tough, and slowly biodegradable carriers is desirable

Further, we showed that engineered spider silk protein eADF4(C16) film features can be controlled. Our results show that the secondary structure can be influenced by post casting treatments and that macroscopic properties like porosity and mechanical stability can be influenced by additives like PEO and glycerol. Therefore engineered spider silk films may potentially be useful for the design of implant coatings or scaffolds for tissue engineering.

In summary, this work indicates that due to the processability of silk proteins into various morphologies, control of properties on the molecular and macroscopic level along with their biocompatibility and biodegradability silk proteins may play an important role for future applications in novel biomaterials.

Bibliography

Adachi, T., Tomita, M., Shimizu, K., Ogawa, S., Yoshizato, K., 2006. Generation of hybrid transgenic silkworms that express Bombyx mori prolyl-hydroxylase α-subunits and human collagens in posterior silk glands: Production of cocoons that contained collagens with hydroxylated proline residues. Journal of Biotechnology 126, 205-219.

Akira, S., Kikuya, S., Haruo, M., Takashi, N., Kouzou, T., Ryuukichi, T., Mamoru, I., Takeshi, H., Nader, G.A., Susumu, I., 2000. Promotive effects of a silk film on epidermal recovery from full-thickness skin wounds. Proceedings of the Society for Experimental Biology and Medicine 225, 58-64.

Allen, T.M., Cullis, P.R., 2004. Drug delivery systems: Entering the mainstream. Science 303, 1818-1822.

Allmeling, C., Jokuszies, A., Reimers, K., Kall, S., Choi, C.Y., Brandes, G., Kasper, C., Scheper, T., Guggenheim, M., Vogt, P.M., 2008. Spider silk fibres in artificial nerve constructs promote peripheral nerve regeneration. Cell Proliferation 41, 408-420.

Altman, G.H., Diaz, F., Jakuba, C., Calabro, T., Horan, R.L., Chen, J., Lu, H., Richmond, J., Kaplan, D.L., 2003. Silk-based biomaterials. Biomaterials 24, 401-416.

Arshady, R., 1990. Review : Biodegradable microcapsular drug delivery systems: Manufacturing methodology, release control and targeting prospects. Journal of Bioactive and Compatible Polymers 5, 315-342.

Assender, H., Bliznyuk, V., Porfyrakis, K., 2002. How surface topography relates to materials' properties. Science 297, 973-976.

Aubry, J., Ganachaud, F., Cohen Addad, J.-P., Cabane, B., 2009. Nanoprecipitation of polymethylmethacrylate by solvent shifting. Langmuir 25, 1970-1979.

Auterhoff H, K.J., Höltje H-D, 1999. Lehrbuch der Pharmazeutischen Chemie. Wissenschaftliche Verlagsgesellachaft mbH Stuttgart.

Bartlett DW, S.H., Hildebrandt IJ, Weber WA, Davis ME, 2007. Impact of tumor-specific targeting on the biodistribution and efficacy of siRNA particles measured by multimodality in vivo imaging. Proceedings of the National Academy of Sciences of the United States of America 104, 15549-15554.

Bartus, R.T., Tracy, M.A., Emerich, D.F., Zale, S.E., 1998. Drug delivery: Sustained delivery of proteins for novel therapeutic products. Science 281, 1161-1162.

Berthold, A., Cremer, K., Kreuter, J., 1996. Preparation and characterization of chitosan microspheres as drug carrier for prednisolone sodium phosphate as model for anti-inflammatory drugs. Journal of Controlled Release 39, 17-25.

Bilati, U., Allémann, E., Doelker, E., 2005a. Development of a nanoprecipitation method intended for the entrapment of hydrophilic drugs into nanoparticles. European Journal of Pharmaceutical Sciences 24, 67-75.

Bilati, U., Allémann, E., Doelker, E., 2005b. Nanoprecipitation versus emulsion-based techniques for the encapsulation of proteins into biodegradable nanoparticles and process-related stability issues. AAPS Pharmaceutical Science and Technology 6, 594-604.

Bini, E., Foo, C.W.P., Huang, J., Karageorgiou, V., Kitchel, B., Kaplan, D.L., 2006. RGD-functionalized bioengineered spider dragline silk biomaterial. Biomacromolecules 7, 3139-3145.

Bini, E., Knight, D.P., Kaplan, D.L., 2004. Mapping domain structures in silks from insects and spiders related to protein assembly. Journal of Molecular Biology 335, 27-40.

Bioinformatics, S.I.o., ExPASy Proteomics Server Vol. 2009.

Bogush, V., Sokolova, O., Davydova, L., Klinov, D., Sidoruk, K., Esipova, N., Neretina, T., Orchanskyi, I., Makeev, V., Tumanyan, V., Shaitan, K., Debabov, V., Kirpichnikov, M., 2009. A novel model system for design of biomaterials based on recombinant analogs of spider silk proteins. Journal of Neuroimmune Pharmacology 4, 17-27.

Boyer, P.D., 1971. The Enzymes. In: Boyer, P.D. (Ed.), Academic Press, New York, pp. 323-373.

Braun, F.N., Viney, C., 2003. Modelling self assembly of natural silk solutions. International Journal of Biological Macromolecules 32, 59-65.

Brick, M.C., Palmer, H.J., Whitesides, T.H., 2003. Formation of colloidal dispersions of organic materials in aqueous media by solvent shifting. Langmuir 19, 6367-6380.

Broide, M.L., Tominc, T.M., Saxowsky, M.D., 1996. Using phase transitions to investigate the effect of salts on protein interactions. Physical Review E 53, 6325.

Brooks, A.E., Stricker, S.M., Joshi, S.B., Kamerzell, T.J., Middaugh, C.R., Lewis, R.V., 2008. Properties of synthetic spider silk fibers based on Argiope aurantia MaSp2. Biomacromolecules 9, 1506-1510.

Calvo, P., Remunan-Lopez, C., Vila-Jato, J.L., Alonso, M.J., 1997a. Chitosan and chitosan/ethylene oxide-propylene: Oxide block copolymer nanoparticles as novel carriers for proteins and vaccines. Pharmaceutical Research 14, 1431-1436.

Calvo, P., Remuñán-López, C., Vila-Jato, J.L., Alonso, M.J., 1997b. Novel hydrophilic chitosan-polyethylene oxide nanoparticles as protein carriers. Journal of Applied Polymer Science 63, 125-132.

CAS, d., 2009. American Chemical Society: CAS database Vol. 2009.

Cbreve, Stropnik, Germi, L., B, Zbreve, erjal, 1996. Morphology variety and formation mechanisms of polymeric membranes prepared by wet phase inversion. Journal of Applied Polymer Science 61, 1821-1830.

Chang, B.H., Bae, Y.C., 2003. Salting-out in the aqueous single-protein solution: the effect of shape factor. Biophysical Chemistry 104, 523-533.

Chavanpatil MD, K.A., Panyam J, 2006. Particles for cellular drug delivery: Mechanisms and factors influencing delivery. Journal of Nanoscience and Nanotechnology 6, 2651-2663.

Cheema, S.K., Gobin, A.S., Rhea, R., Lopez-Berestein, G., Newman, R.A., Mathur, A.B., 2007. Silk fibroin mediated delivery of liposomal emodin to breast cancer cells. International Journal of Pharmaceutics 341, 221-229.

Chemspider, 2009. Online database Vol. 2009.

Chen, H., Suk, K., Chi-Young, P., Hun-Sik, K., In-Joo, C., Hyoung-Joon, J., 2008. pH-triggered transition of silk fibroin from spherical micelles to nanofibrils in water. Macromolecular Research 16, 539-543.

Cheng, L.-P., Young, T.-H., Chuang, W.-Y., Chen, L.-Y., Chen, L.-W., 2001. The formation mechanism of membranes prepared from the nonsolvent-solvent-crystalline polymer systems. Polymer 42, 443-451.

Chenhua, Z., Juming, Y., Hiromi, M., Raghuvansh, K., Tetsuo, A., 2003. Structural characterization and artificial fiber formation of Bombyx mori silk fibroin in hexafluoro-iso-propanol solvent system. Biopolymers 69, 253-259.

Chickering, D.E., Jacob, J.S., Desai, T.A., Harrison, M., Harris, W.P., Morrell, C.N., Chaturvedi, P., Mathiowitz, E., 1997. Bioadhesive microspheres: III. An in vivo transit and bioavailability study of drug-loaded alginate and poly(fumaric-co-sebacic anhydride) microspheres. Journal of Controlled Release 48, 35-46.

Chorny, M., Fishbein, I., Danenberg, H.D., Golomb, G., 2002. Lipophilic drug loaded nanospheres prepared by nanoprecipitation: effect of formulation variables on size, drug recovery and release kinetics. Journal of Controlled Release 83, 389-400.

Colin D. Heyes, J.G., Martin Möller and G. Ulrich Nienhaus, 2007. Synthesis, patterning and applications of star-shaped poly(ethylene glycol) biofunctionalized surfaces. Molecular Biosystems 3, 419-430.

Coombes, A.G.A., Tasker, S., Lindblad, M., Holmgren, J., Hoste, K., Toncheva, V., Schacht, E., Davies, M.C., Illum, L., Davis, S.S., 1997. Biodegradable polymeric microparticles for drug delivery and vaccine formulation: the surface attachment of hydrophilic species using the concept of poly(ethylene glycol) anchoring segments. Biomaterials 18, 1153-1161.

Couvreur, P., Puisieux, F., 1993. Nano- and microparticles for the delivery of polypeptides and proteins. Advanced Drug Delivery Reviews 10, 141-162.

Couvreur, P., Roblot-Treupel, L., Poupon, M.F., Brasseur, F., Puisieux, F., 1990. Nanoparticles as microcarriers for anticancer drugs. Advanced Drug Delivery Reviews 5, 209-230.

Crampton, H.L., Simanek, E., 2007. Dendrimers as drug delivery vehicles: non-covalent interactions of bioactive compounds with dendrimers. Polymer International 56, 489-496.

Del Favero, G., Fabris, C., Plebani, M., Panucci, A., Piccoli, A., Perobelli, L., Burlina, A., Naccarato, R., 1985. Serum elastase 1 in chronic pancreatic disease. Journal of Molecular Medicine 63, 603-606.

Desai, M.P., Labhasetwar, V., Amidon, G.L., Levy, R.J., 1996. Gastrointestinal uptake of biodegradable microparticles: Effect of particle size. Pharmaceutical Research 13, 1838-1845.

Dicko, C., Porter, D., Bond, J., Kenney, J.M., Vollrath, F., 2007. Structural disorder in silk proteins reveals the emergence of elastomericity. Biomacromolecules 9, 216-221.

Digenis, G.A., Gold, T.B., Shah, V.P., 1994. Cross-linking of gelatin capsules and its relevance to their in vitro-in vivo performance. Journal of Pharmaceutical Sciences 83, 915-921.

Dossou, U., 2005. Vorhersage intestinaler Absorption auf der Basis von physikalisch-chemischen Parametern und Verbesserung von Absorptionseigenschaften potenzieller Arzneistoffe, Naturwissenschaftlich-Technische Fakultät III Vol. PhD, Universität des Saarlandes, Saarbrücken, pp. 322.

Edlund, U., Albertsson, A., 2002. Degradable polymer microspheres for controlled drug delivery, Degradable Aliphatic Polyesters, pp. 67-112.

Edwin, D., Gleb, B.S., Frank, C., Sean, A.D., Helmuth, M., 1998. Novel hollow polymer shells by colloid-templated assembly of polyelectrolytes. Angewandte Chemie International Edition 37, 2201-2205.

Esmaeili, F., Ghahremani, M.H., Esmaeili, B., Khoshayand, M.R., Atyabi, F., Dinarvand, R., 2008. PLGA nanoparticles of different surface properties: Preparation and evaluation of their body distribution. International Journal of Pharmaceutics 349, 249-255.

Exler, J.H., Hummerich, D., Scheibel, T., 2007. The amphiphilic properties of spider silks are important for spinning. Angewandte Chemie International Edition 46, 3559-3562.

Foo, C.W.P., Bini, E., Hensman, J., Knight, D.P., Lewis, R.V., Kaplan, D.L., 2006a. Role of pH and charge on silk protein assembly in insects and spiders. Applied Physics A 82, 223-233.

Foo, C.W.P., Bini, E., Huang, J., Lee, S.Y., Kaplan, D.L., 2006b. Solution behavior of synthetic silk peptides and modified recombinant silk proteins. Applied Physics A: Materials Science & Processing 82, 193-203.

Freddi, G., Mossotti, R., Innocenti, R., 2003. Degumming of silk fabric with several proteases. Journal of Biotechnology 106, 101-112.

Freiberg, S., Zhu, X.X., 2004. Polymer microspheres for controlled drug release. International Journal of Pharmaceutics 282, 1-18.

Gatesy, J., Hayashi, C., Motriuk, D., Woods, J., Lewis, R., 2001. Extreme diversity, conservation, and convergence of spider silk fibroin sequences. Science 291, 2603-2605.

Gellynck, K., Verdonk, P., Forsyth, R., Almqvist, K., Van Nimmen, E., Gheysens, T., Mertens, J., Van Langenhove, L., Kiekens, P., Verbruggen, G., 2008. Biocompatibility and biodegradability of spider egg sac silk. Journal of Materials Science: Materials in Medicine 19, 2963-2970.

Gelperina, S., Kisich, K., Iseman, M.D., Heifets, L., 2005. The potential advantages of nanoparticle drug delivery systems in chemotherapy of tuberculosis. Am. J. Respir. Crit. Care Med. 172, 1487-1490.

George, A.D., Thomas, B.G., Vinod, P.S., 1994. Cross-linking of gelatin capsules and its relevance to their in vitro-in vivo performance. Journal of Pharmaceutical Sciences 83, 915-921.

George, M., Abraham, T.E., 2006. Polyionic hydrocolloids for the intestinal delivery of protein drugs: Alginate and chitosan -- a review. Journal of Controlled Release 114, 1-14.

Glišović, A., Salditt, T., 2007. Temperature dependent structure of spider silk by X-ray diffraction. Applied Physics A: Materials Science & Processing 87, 63-69.

Gobin, A.S., Rhea, R., Newman, R.A., Mathur, A.B., 2006. Silk-fibroin-coated liposomes for long-term and targeted drug delivery. International Journal of Nanomedicine 1, 81– 87.

Gosline, J.M., Denny, M.W., DeMont, M.E., 1984. Spider silk as rubber. Nature 309, 551-552.

Gosline, J.M., Guerette, P.A., Ortlepp, C.S., Savage, K.N., 1999. The mechanical design of spider silks: from fibroin sequence to mechanical function. Journal of Experimental Biology 202, 3295-3303.

Govender, T., Riley, T., Ehtezazi, T., Garnett, M.C., Stolnik, S., Illum, L., Davis, S.S., 2000. Defining the drug incorporation properties of PLA-PEG nanoparticles. International Journal of Pharmaceutics 199, 95-110.

Govender, T., Stolnik, S., Garnett, M.C., Illum, L., Davis, S.S., 1999. PLGA nanoparticles prepared by nanoprecipitation: drug loading and release studies of a water soluble drug. Journal of Controlled Release 57, 171-185.

Green, A.A., 1931. Studies in the physical chemistry of the proteins, VIII: The solubility of hemoglobin in concentrated salt solutions. A study of the salting-out of proteins. Journal of Biological Chemistry. 93.

Green, A.A., 1932. Studies in the Physical chemistry of the proteins, X: The solubility of hemoglobin in solutions of chlorides and sulfates of varying concentration. Journal of Biological Chemistry 95, 47.

Guerette, P.A., Ginzinger, D.G., Weber, B.H.F., Gosline, J.M., 1996. Silk properties determined by gland-specific expression of a spider fibroin gene family. Science 272, 112-115.

Haberkorn, H., Franke, D., Frechen, T., Goesele, W., Rieger, J., 2003. Early stages of particle formation in precipitation reactions--quinacridone and boehmite as generic examples. Journal of Colloid and Interface Science 259, 112-126.

Hae Yong, K., Young Hwan, P., 1999. Structural and conformational changes of regenerated Antheraea pernyi silk fibroin films treated with methanol solution. Journal of Applied Polymer Science 73, 2887-2894.

Hagn, F., Eisoldt, L., Hardy, J., Vendrely, C., Coles, M., Scheibel, T., Kessler, H., 2010. A highly conserved spider silk domain acts as a molecular switch that controls fiber assembly. Nature in press.

Hardy, J.G., Römer, L.M., Scheibel, T.R., 2008. Polymeric materials based on silk proteins. Polymer 49, 4309-4327.

Heim, M., Keerl, D., Scheibel, T., 2009. Spider Silk: From Soluble Protein to Extraordinary Fiber. Angewandte Chemie International Edition 48, 3584-3596.

Heim, M., Römer, L., Scheibel, T., 2010. Hierarchical structures made of proteins. The complex architecture of spider webs and their constituent silk proteins. Chemical Society Reviews 39, 156-164.

Hermanson, K.D., Harasim, M.B., Scheibel, T., Bausch, A.R., 2007a. Permeability of silk microcapsules made by the interfacial adsorption of protein. Physical Chemistry Chemical Physics 9, 6442-6446.

Hermanson, K.D., Huemmerich, D., Scheibel, T., Bausch, A.R., 2007b. Engineered microcapsules fabricated from reconstituted spider silk. Advanced Materials 19, 1810-1815.

Hofmann, S., Wong Po Foo, C.T., Rossetti, F., Textor, M., Vunjak-Novakovic, G., Kaplan, D.L., Merkle, H.P., Meinel, L., 2006. Silk fibroin as an organic polymer for controlled drug delivery. Journal of Controlled Release 111, 219-227.

Holland, C., Terry, A.E., Porter, D., Vollrath, F., 2007. Natural and unnatural silks. Polymer 48, 3388-3392.

Holland, G.P., Jenkins, J.E., Creager, M.S., Lewis, R.V., Yarger, J.L., 2008a. Quantifying the fraction of glycine and alanine in [small beta]-sheet and helical conformations in spider dragline silk using solid-state NMR. Chemical Communications, 5568-5570.

Holland, G.P., Jenkins, J.E., Creager, M.S., Lewis, R.V., Yarger, J.L., 2008b. Solid-state NMR investigation of major and minor ampullate spider silk in the native and hydrated states. Biomacromolecules 9, 651-657.

Horan, R.L., Antle, K., Collette, A.L., Wang, Y., Huang, J., Moreau, J.E., Volloch, V., Kaplan, D.L., Altman, G.H., 2005. In vitro degradation of silk fibroin. Biomaterials 26, 3385-3393.

Horn, D., Rieger, J., 2001. Organic nanoparticles in the aqueous phase - Theory, experiment, and use. Angewandte Chemie International Edition 40, 4330-4361.

Hu, X., Kaplan, D., Cebe, P., 2006a. Determining β-sheet crystallinity in fibrous proteins by thermal analysis and infrared spectroscopy. Macromolecules 39, 6161-6170.

Hu, X., Vasanthavada, K., Kohler, K., McNary, S., Moore, A., Vierra, C., 2006b. Molecular mechanisms of spider silk. Cellular and Molecular Life Sciences (CMLS) 63, 1986-1999.

Huang, F., Sun, L., Zheng, J., 2008. In vitro and in vivo characterization of a silk fibroin-coated polyester vascular prosthesis. Artificial Organs 32, 932-941.

Huemmerich, D., Helsen, C.W., Quedzuweit, S., Oschmann, J., Rudolph, R., Scheibel, T., 2004a. Primary structure elements of spider dragline silks and their contribution to protein solubility. Biochemistry 43, 13604-13612.

Huemmerich, D., Scheibel, T., Vollrath, F., Cohen, S., Gat, U., Ittah, S., 2004b. Novel assembly properties of recombinant spider dragline silk proteins. Curr Biol 14, 2070-2074.

Huemmerich, D., Slotta, U., Scheibel, T., 2006. Processing and modification of films made from recombinant spider silk proteins. Applied Physics A 82, 219-222.

Ibrahim, H., Bindschaedler, C., Doelker, E., Buri, P., Gurny, R., 1992. Aqueous nanodispersions prepared by a salting-out process. International Journal of Pharmaceutics 87, 239-246.

Inoue, S., Tanaka, K., Arisaka, F., Kimura, S., Ohtomo, K., Mizuno, S., 2000. Silk fibroin of Bombyx mori is secreted, assembling a high molecular mass elementary unit consisting of H-chain, L-chain, and P25, with a 6:6:1 Molar Ratio. Journal of Biological Chemistry 275, 40517-40528.

Ismail, A.F., Hassan, A.R., 2006. Formation and characterization of asymmetric nanofiltration membrane: Effect of shear rate and polymer concentration. Journal of Membrane Science 270, 57-72.

Ittah, S., Michaeli, A., Goldblum, A., Gat, U., 2007. A model for the structure of the C-terminal domain of dragline spider silk and the role of its conserved cysteine. Biomacromolecules 8, 2768-2773.

Jain, R.A., 2000. The manufacturing techniques of various drug loaded biodegradable poly(lactide-co-glycolide) (PLGA) devices. Biomaterials 21, 2475-2490.

Jelinski, L.W., 1998. Establishing the relationship between structure and mechanical function in silks. Current Opinion in Solid State and Materials Science 3, 237-245.

Jiang, J., Prausnitz, J.M., 1999. Molecular thermodynamics for protein precipitation with a polyelectrolyte. The Journal of Physical Chemistry B 103, 5560-5569.

Jin, H.-J., Fridrikh, S.V., Rutledge, G.C., Kaplan, D.L., 2002. Electrospinning Bombyx mori silk with poly(ethylene oxide). Biomacromolecules 3, 1233-1239.

Jin, H.-J., Kaplan, D.L., 2003. Mechanism of silk processing in insects and spiders. Nature 424, 1057-1061.

Jin, H.J., Park, J., Valluzzi, R., Cebe, P., Kaplan, D.L., 2004. Biomaterial films of Bombyx mori silk fibroin with poly(ethylene oxide). Biomacromolecules 5, 711-717.

Jin, N., Young Hwan, P., 2001. Morphology of regenerated silk fibroin: Effects of freezing temperature, alcohol addition, and molecular weight. Journal of Applied Polymer Science 81, 3008-3021.

Jones, M.M., Seilheimer, D.K., Pier, G.B., Rossen, R.D., 1990. Increased elastase secretion by peripheral blood monocytes in cystic fibrosis patients. Clinical and Experimental Immunology. 80, 344-349.

Jung, T., Kamm, W., Breitenbach, A., Kaiserling, E., Xiao, J.X., Kissel, T., 2000. Biodegradable nanoparticles for oral delivery of peptides: is there a role for polymers to affect mucosal uptake? European Journal of Pharmaceutics and Biopharmaceutics 50, 147-160.

Kaplan, D.L., 1998. Fibrous proteins--silk as a model system. Polymer Degradation and Stability 59, 25-32.

Kaplan, D.L., Mello, C.M., Arcidiacono, S., Fossey, S., Senecal, K., Muller, W., 1997. Silk. In: Kevin McGrath, D.K. (Ed.), Protein-Based Materials, Birkhäuser, Boston, Basel, Berlin, pp. 103-131.

Keten, S., Xu, Z., Ihle, B., Buehler, M.J., 2010. Nanoconfinement controls stiffness, strength and mechanical toughness of β-sheet crystals in silk. Nature Materials 9, 359-367.

Kohane, D.S., 2007. Microparticles and nanoparticles for drug delivery. Biotechnology and Bioengineering 96, 203-209.

Kosmidis, K., Rinaki, E., Argyrakis, P., Macheras, P., 2003. Analysis of Case II drug transport with radial and axial release from cylinders. International Journal of Pharmaceutics 254, 183-188.

Kranz, H., Ubrich, N., Maincent, P., Bodmeier, R., 2000. Physicomechanical properties of biodegradable poly(D,L-lactide) and poly(D,L-lactide-co-glycolide) films in the dry and wet states. Journal of Pharmaceutical Sciences 89, 1558-1566.

Krasnov, I., Diddens, I., Hauptmann, N., Helms, G., Ogurreck, M., Seydel, T., Funari, S.S., Muller, M., 2008. Mechanical Properties of Silk: Interplay of Deformation on Macroscopic and Molecular Length Scales. Physical Review Letters 100, 048104-048104.

Kreuter, J., 2001. Nanoparticulate systems for brain delivery of drugs. Advanced Drug Delivery Reviews 47, 65-81.

Kuehner, D.E., Blanch, H.W., Prausnitz, J.M., 1996. Salt-induced protein precipitation: Phase equilibria from an equation of state. Fluid Phase Equilibria 116, 140-147.

Kummerlen, J., van Beek, J.D., Vollrath, F., Meier, B.H., 1996. Local structure in spider dragline silk investigated by two-dimensional spin-diffusion nuclear magnetic resonance. Macromolecules 29, 2920-2928.

Kyte, J., Doolittle, R.F., 1982. A simple method for displaying the hydropathic character of a protein. Journal of Molecular Biology 157, 105-132.

Lammel, A., Keerl, D., Römer, L., Scheibel, T., 2008a. Proteins: Polymers of natural origin. In: Hu, J. (Ed.), Recent Advances in Biomaterials Research, Transworld Research Network, pp. 1-22.

Lammel, A., Schwab, M., Hofer, M., Winter, G., Scheibel, T., 2010. Spider silk submicroparticles for controlled drug delivery. Journal of Controlled Release Ms. Ref. No.: JCR-D-10-00069, in revision.

Lammel, A., Schwab, M., Slotta, U., Winter, G., Scheibel, T., 2008b. Processing conditions for the formation of spider silk microspheres. ChemSusChem 1, 413-416.

Langer, R., 1990. New methods of drug delivery. Science 249, 1527-1533.

Langer, R., Peppas, N.A., 2003. Advances in biomaterials, drug delivery, and bionanotechnology. AIChE Journal 49, 2990-3006.

Latha, M.S., Rathinam, K., Mohanan, P.V., Jayakrishnan, A., 1995. Bioavailability of theophylline from glutaraldehyde cross-linked casein microspheres in rabbits following oral administration. Journal of Controlled Release 34, 1-7.

Lawrence, B., Omenetto, F., Chui, K., Kaplan, D., 2008. Processing methods to control silk fibroin film biomaterial features. Journal of Materials Science 43, 6967-6985.

Lawrence, B.D., Marchant, J.K., Pindrus, M.A., Omenetto, F.G., Kaplan, D.L., 2009. Silk film biomaterials for cornea tissue engineering. Biomaterials 30, 1299-1308.

Lazaris, A., Arcidiacono, S., Huang, Y., Zhou, J.-F., Duguay, F., Chretien, N., Welsh, E.A., Soares, J.W., Karatzas, C.N., 2002. Spider silk fibers spun from soluble recombinant silk produced in mammalian cells. Science 295, 472-476.

Leckband, D., Sivasankar, S., 1999. Forces controlling protein interactions: theory and experiment. Colloids and Surfaces B: Biointerfaces 14, 83-97.

Lee, J., Cho, E.C., Cho, K., 2004. Incorporation and release behavior of hydrophobic drug in functionalized poly(lactide)-block-poly(ethylene oxide) micelles. Journal of Controlled Release 94, 323-335.

Lefèvre, T., Boudreault, S., Cloutier, C., Pelì zolet, M., 2008. Conformational and orientational transformation of silk proteins in the major ampullate gland of Nephila clavipes spiders. Biomacromolecules 9, 2399-2407.

Lefèvre, T., Rousseau, M.-E., Pézolet, M., 2007. Protein secondary structure and orientation in silk as revealed by Raman spectromicroscopy. Biophysical Journal 92, 2885-2895.

Liebmann, B., Hümmerich, D., Scheibel, T., Fehr, M., 2008. Formulation of poorly water-soluble substances using self-assembling spider silk protein. Colloids and Surfaces A: Physicochemical and Engineering Aspects 331, 126-132.

Liso, P.A., Rebuelta, M., Román, J.S., Gallardo, A., Villar, A.M., 1995. Antinociceptive and antipyretic properties of a new conjugated ibuprofen-methacrylic polymeric controlled delivery system. Journal of Controlled Release 33, 429-436.

Liu, X.-Y., Zhang, C.-C., Xu, W.-L., Ouyang, C.-x., 2009. Controlled release of heparin from blended polyurethane and silk fibroin film. Materials Letters 63, 263-265.

Liu, X., Sun, Q., Wang, H., Zhang, L., Wang, J.-Y., 2005. Microspheres of corn protein, zein, for an ivermectin drug delivery system. Biomaterials 26, 109-115.

Liu, Y., Shao, Z., Zhou, P., Chen, X., 2004. Thermal and crystalline behaviour of silk fiborin/nylon 66 blend films. Polymer 45, 7705-7710.

Lück, M., Pistel, K.-F., Li, Y.-X., Blunk, T., Müller, R.H., Kissel, T., 1998. Plasma protein adsorption on biodegradable microspheres consisting of poly(-lactide-co-glycolide), poly(-lactide) or ABA triblock copolymers containing poly(oxyethylene): Influence of production method and polymer composition. Journal of Controlled Release 55, 107-120.

Lun, B., Jianmei, X., Qilong, S., Chuanxia, D., Jiangchao, S., Zhengyu, W., 2007. On the growth model of the capillaries in the porous silk fibroin films. Journal of Materials Science: Materials in Medicine 18, 1917-1921.

Lvov, Y., Ariga, K., Ichinose, I., Kunitake, T., 2002. Assembly of multicomponent protein films by means of electrostaticlayer-by-layer adsorption. Journal of the American Chemical Society 117, 6117-6123.

MacAdam, A.B., Shafi, Z.B., James, S.L., Marriott, C., Martin, G.P., 1997. Preparation of hydrophobic and hydrophilic albumin microspheres and determination of surface carboxylic acid and amino residues. International Journal of Pharmaceutics 151, 47-55.

Masuhiro, T., Giuliano, F., Patrizia, M., Alessandro, B., Nobutami, K., 1995. Structure and molecular conformation of tussah silk fibroin films: Effect of methanol. Journal of Polymer Science Part B: Polymer Physics 33, 1995-2001.

Mathiowitz, E., Jacob, J.S., Jong, Y.S., Carino, G.P., Chickering, D.E., Chaturvedi, P., Santos, C.A., Vijayaraghavan, K., Montgomery, S., Bassett, M., Morrell, C.N., 1997. Biologically erodable microspheres as potential oral drug delivery systems. Nature 386, 410-414.

Matsumoto, A., Chen, J., Collette, A.L., Kim, U.-J., Altman, G.H., Cebe, P., Kaplan, D.L., 2006. Mechanisms of silk fibroin sol-gel transitions. The Journal of Physical Chemistry B 110, 21630-21638.

Matsumoto, A., Lindsay, A., Abedian, B., Kaplan, D.L., 2008. Silk fibroin solution properties related to assembly and structure. Macromolecular Bioscience 8, 1006-1018.

McGrath, K., Kaplan, D.L., 2004. Protein-Based Materials. Birkhäuser.

McHugh, A.J., 2005. The role of polymer membrane formation in sustained release drug delivery systems. Journal of Controlled Release 109, 211-221.

Megeed, Z., Cappello, J., Ghandehari, H., 2002. Genetically engineered silk-elastinlike protein polymers for controlled drug delivery. Advanced Drug Delivery Reviews 54, 1075-1091.

Mei, N., Zhou, P., Pan, L.-F., Chen, G., Wu, C.-G., Chen, X., Shao, Z.-Z., Chen, G.-Q., 2006. Biocompatibility of poly (3-hydroxybutyrate-co-3-hydroxyhexanoate) modified by silk fibroin. Journal of Materials Science: Materials in Medicine 17, 749-758.

Meinel, L., Hofmann, S., Karageorgiou, V., Kirker-Head, C., McCool, J., Gronowicz, G., Zichner, L., Langer, R., Vunjak-Novakovic, G., Kaplan, D.L., 2005. The inflammatory responses to silk films in vitro and in vivo. Biomaterials 26, 147-155.

Meng, X., Chen, Y., Chowdhury, S.R., Yang, D., Mitra, S., 2009. Stabilizing dispersions of hydrophobic drug molecules using cellulose ethers during anti-solvent synthesis of micro-particulates. Colloids and Surfaces B: Biointerfaces 70, 7-14.

Metwalli, E., Slotta, U., Darko, C., Roth, S.V., Scheibel, T., Papadakis, C.M., 2007. Structural changes of thin films from recombinant spider silk proteins upon post-treatment. Applied Physics A 89, 655-661.

Mi, F.-L., Shyu, S.-S., Lin, Y.-M., Wu, Y.-B., Peng, C.-K., Tsai, Y.-H., 2003. Chitin/PLGA blend microspheres as a biodegradable drug delivery system: a new delivery system for protein. Biomaterials 24, 5023-5036.

Mingzhong, L., Norihiko, M., Lixing, D., Linsen, Z., 2002. Preparation of porous poly(vinyl alcohol)-silk fibroin blend membranes. Membrane Technology 2002, 15-15.

Mita, K., Ichimura, S., James, T.C., 1994. Highly repetitive structure and its organization of the silk fibroin gene. Journal of Molecular Evolution 38, 583-592.

Morlock, M., Koll, H., Winter, G., Kissel, T., 1997. Microencapsulation of rh-erythropoietin, using biodegradable poly(lactide-co-glycolide): protein stability and the effects of stabilizing excipients. European Journal of Pharmaceutics and Biopharmaceutics 43, 29-36.

Morrison, I.D., Ross, S., 2002. Colloidal dispersions – Suspensions, Emulsions and Foams. New York: John Wiley & Sons.

Mukhopadhyay, S., Sakthivel, J.C., 2005. Spider silk - Providing new insights in the field of high performance materials. Journal of Industrial Textiles 35, 91-113.

Nair, L.S., Laurencin, C.T., 2007. Biodegradable polymers as biomaterials. Progress in Polymer Science 32, 762-798.

Nakanishi, T., Fukushima, S., Okamoto, K., Suzuki, M., Matsumura, Y., Yokoyama, M., Okano, T., Sakurai, Kataoka, K., 2001. Development of the polymer micelle carrier system for doxorubicin. Journal of Controlled Release 74, 295-302.

National library of medicine, U., 2009. ChemIDplus Vol. 2009.

Nazarov, R., Jin, H.-J., Kaplan, D.L., 2004. Porous 3-D scaffolds from regenerated silk fibroin. Biomacromolecules 5, 718-726.

Numata, K., Kaplan, D.L., 2010. Silk-based delivery systems of bioactive molecules. Advanced Drug Delivery Reviews In Press, Accepted Manuscript.

Numata, K., Subramanian, B., Currie, H.A., Kaplan, D.L., 2009. Bioengineered silk protein-based gene delivery systems. Biomaterials 30, 5775-5784.

Page, M.J., DiCera, E., 2008. Serine Proteases and Serine Protease Inhibitors. John Wiley & Sons.

Panilaitis, B., Altman, G.H., Chen, J., Jin, H.-J., Karageorgiou, V., Kaplan, D.L., 2003. Macrophage responses to silk. Biomaterials 24, 3079-3085.

Panya, W., Yasuhiko, T., Ratana, R., 2007. Miscibility and biodegradability of silk fibroin/carboxymethyl chitin blend films. Macromolecular Bioscience 7, 1258-1271.

Panyam, J., Labhasetwar, V., 2003. Biodegradable nanoparticles for drug and gene delivery to cells and tissue. Advanced Drug Delivery Reviews 55, 329-347.

Papadopoulos, P., Sölter, J., Kremer, F., 2007. Structure-property relationships in major ampullate spider silk as deduced from polarized FTIR spectroscopy. The European Physical Journal E: Soft Matter and Biological Physics 24, 193-199.

Park, W., Ha, W., Ito, H., Miyamoto, T., Inagaki, H., Noishiki, Y., 2001. Relationships between antithrombogenicity and surface free energy of regenerated silk fibroin films. Fibers and Polymers 2, 58-63.

Parkhe, A.D., Seeley, S.K., Gardner, K., Thompson, L., Lewis, R.V., 1997. Structural studies of spider silk proteins in the fiber. Journal of Molecular Recognition 10, 1-6.

Phillips, D.M., Drummy, L.F., Conrady, D.G., Fox, D.M., Naik, R.R., Stone, M.O., Trulove, P.C., De Long, H.C., Mantz, R.A., 2004. Dissolution and regeneration of Bombyx mori silk fibroin using ionic liquids. Journal of the American Chemical Society 126, 14350-14351.

Pilar, C., José, L.V.-J., María, J.A., 1996. Comparative in vitro evaluation of several colloidal systems, nanoparticles, nanocapsules, and nanoemulsions, as ocular drug carriers. Journal of Pharmaceutical Sciences 85, 530-536.

Pitt, C.G., Gratzl, M.M., Jeffcoat, R.A., Zweidinger, R., Schindler, A., 1979. Sustained drug delivery systems II: Factors affecting release rates from poly(epsilon-caprolactone) and related biodegradable polyesters. Journal of Pharmaceutical Sciences 68, 1534-1538.

Polakovic, M., Gorner, T., Gref, R., Dellacherie, E., 1999. Lidocaine loaded biodegradable nanospheres - II. Modelling of drug release. Journal of Controlled Release 60, 169-177.

Porter, D., Vollrath, F., 2009. Silk as a Biomimetic Ideal for Structural Polymers. Advanced Materials 21, 487-492.

Quintanar-Guerrero, D., Fessi, H., Allémann, E., Doelker, E., 1996. Influence of stabilizing agents and preparative variables on the formation of poly(-lactic acid) nanoparticles by an emulsification-diffusion technique. International Journal of Pharmaceutics 143, 133-141.

R. Mossotti, R.I.M.Z.A.A.G.F., 2006. The degumming of silk fabrics: a preliminary near infrared spectroscopy study. Journal of Near Infrared Spectroscopy 14, 201-208.

Rammensee, S., Huemmerich, D., Hermanson, K.D., Scheibel, T., Bausch, A.R., 2006. Rheological characterization of hydrogels formed by recombinantly produced spider silk. Applied Physics A: Materials Science & Processing 82, 261-264.

Rammensee, S., Slotta, U., Scheibel, T., Bausch, A.R., 2008. Assembly mechanism of recombinant spider silk proteins. Proceedings of the National Academy of Sciences 105, 6590-6595.

Ratana, R., Sopon, K., Alexander, M.J., Seiichi, T., 2003. Preparation of crosslinked chitosan/silk fibroin blend films for drug delivery systems. Macromolecular Bioscience 3, 604-611.

Reza, A., 1990a. Microspheres and microcapsules, a survey of manufacturing techniques Part II: Coacervation. Polymer Engineering & Science 30, 905-914.

Reza, A., 1990b. Microspheres and microcapsules, a survey of manufacturing techniques: Part III: Solvent evaporation. Polymer Engineering & Science 30, 915-924.

Ribeiro, H.S., Chu, B.-S., Ichikawa, S., Nakajima, M., 2008. Preparation of nanodispersions containing [beta]-carotene by solvent displacement method. Food Hydrocolloids 22, 12-17.

Riley, T., Govender, T., Stolnik, S., Xiong, C.D., Garnett, M.C., Illum, L., Davis, S.S., 1999. Colloidal stability and drug incorporation aspects of micellar-like PLA-PEG nanoparticles. Colloids and Surfaces B: Biointerfaces 16, 147-159.

Rinaki, E., Valsami, G., Macheras, P., 2003. The power law can describe the entire drug release curve from HPMC-based matrix tablets: a hypothesis. International Journal of Pharmaceutics 255, 199-207.

Ritger, P.L., Peppas, N.A., 1987a. A simple equation for description of solute release I. Fickian and non-fickian release from non-swellable devices in the form of slabs, spheres, cylinders or discs. Journal of Controlled Release 5, 23-36.

Ritger, P.L., Peppas, N.A., 1987b. A simple equation for description of solute release II. Fickian and anomalous release from swellable devices. Journal of Controlled Release 5, 37-42.

Römer, L., Scheibel, T., 2008. The elaborate structure of spider silk: Structure and function of a natural high performance fiber. Prion 2, 1-8.

Roser, M., Fischer, D., Kissel, T., 1998. Surface-modified biodegradable albumin nano- and microspheres. II: effect of surface charges on in vitro phagocytosis and biodistribution in rats. European Journal of Pharmaceutics and Biopharmaceutics 46, 255-263.

Rubino, O.P., Kowalsky, R., Swarbrick, J., 1993. Albumin microspheres as a drug delivery system: Relation among turbidity ratio, degree of cross-linking, and drug release. Pharmaceutical Research 10, 1059-1065.

Ruxandra, G., Grégory, M., Édith, D., 1999. Polyoxyethylene-coated nanospheres: effect of coating on zeta potential and phagocytosis. Polymer International 48, 251-256.

Sahin, S., Selek, H., Ponchel, G., Ercan, M.T., Sargon, M., Hincal, A.A., Kas, H.S., 2002. Preparation, characterization and in vivo distribution of terbutaline sulfate loaded albumin microspheres. Journal of Controlled Release 82, 345-358.

Sakuma, S., Matsumoto, T., Yamashita, S., Wang, Y., Lu, Z.-R., 2007. Conjugation of poorly absorptive drugs with mucoadhesive polymers for the improvement of oral absorption of drugs. Journal of Controlled Release 123, 195-202.

Santos, D.E.S., Neto, C.G.T., Fonseca, J.L.C., Pereira, M.R., 2008. Chitosan macroporous asymmetric membranes - Preparation, characterization and transport of drugs. Journal of Membrane Science 325, 362-370.

Scheibel, T., 2004. Spider silks: recombinant synthesis, assembly, spinning, and engineering of synthetic proteins. Microb Cell Fact 3, 14.

Scheibel, T., 2005. Protein fibers as performance proteins: new technologies and applications. Curr Opin Biotechnol 16, 427-433.

Schlosser, M., Wilhelm, L., Urban, G., Ziegler, B., Ziegler, M., Zippel, R., 2002. Immunogenicity of polymeric implants: Long-term antibody response against polyester (Dacron) following the implantation of vascular prostheses into LEW.1A rats. Journal of Biomedical Materials Research 61, 450-457.

Schultz, P., Vautier, D., Richert, L., Jessel, N., Haikel, Y., Schaaf, P., Voegel, J.-C., Ogier, J., Debry, C., 2005. Polyelectrolyte multilayers functionalized by a synthetic analogue of an anti-inflammatory peptide, α-MSH, for coating a tracheal prosthesis. Biomaterials 26, 2621-2630.

Schwarzer, H.C., Peukert, W., 2004a. Combined experimental/numerical study on the precipitation of nanoparticles. AIChE Journal 50, 3234-3247.

Schwarzer, H.C., Peukert, W., 2004b. Tailoring particle size through nanoparticle precipitation. Chemical Engineering Communications 191, 580 - 606.

Sear, R.P., 1999. Classical nucleation theory for the nucleation of the solid phase of spherical particles with a short-ranged attraction. The Journal of Chemical Physics 111, 2001-2007.

Semmrich, C., Bausch, A.R., 2010. Protein crystals: How the weak become strong. Nature Materials 9, 293-295.

Shard, A.G., Tomlins, P.E., 2006. Biocompatibility and the efficacy of medical implants. Regenerative Medicine 1, 789.

Sheng, Y., Liu, C., Yuan, Y., Tao, X., Yang, F., Shan, X., Zhou, H., Xu, F., 2009. Long-circulating polymeric nanoparticles bearing a combinatorial coating of PEG and water-soluble chitosan. Biomaterials 30, 2340-2348.

Shimizu, T., Yamashiro, Y., Igarashi, J., Fujita, H., Ishimoto, K., 1998. Increased serum trypsin and elastase-1 levels in patients undergoing L-asparaginase therapy. European Journal of Pediatrics 157, 561-563.

Shojaie, S.S., Krantz, W.B., Greenberg, A.R., 1994a. Dense polymer film and membrane formation via the dry-cast process part I. Model development. Journal of Membrane Science 94, 255-280.

Shojaie, S.S., Krantz, W.B., Greenberg, A.R., 1994b. Dense polymer film and membrane formation via the dry-cast process part II. Model validation and morphological studies. Journal of Membrane Science 94, 281-298.

Siepmann, J., Peppas, N.A., 2001. Modeling of drug release from delivery systems based on hydroxypropyl methylcellulose (HPMC). Advanced Drug Delivery Reviews 48, 139-157.

Simmons, A., Ray, E., Jelinski, L.W., 1994. Solid-State 13C NMR of Nephila clavipes dragline silk establishes structure and identity of crystalline regions. Macromolecules 27, 5235-5237.

Slotta, U., Tammer, M., Kremer, F., Koelsch, P., Scheibel, T., 2006. Structural analysis of spider silk films. Supramolecular Chemistry 18, 465-471.

Slotta, U.K., Rammensee, S., Gorb, S., Scheibel, T., 2008. An engineered spider silk protein forms microspheres. Angewandte Chemie International Edition 47, 4592-4594.

Smith, A.M., Scheibel, T.R., 2010. Functional amyloids used by organisms: A lesson in controlling assembly. Macromolecular Chemistry and Physics 211, 127-135.

Sofia, S., McCarthy, M.B., Gronowicz, G., Kaplan, D.L., 2001. Functionalized silk-based biomaterials for bone formation. Journal of Biomedical Materials Research 54, 139-148.

Sokolsky-Papkov, M., Agashi, K., Olaye, A., Shakesheff, K., Domb, A.J., 2007. Polymer carriers for drug delivery in tissue engineering. Advanced Drug Delivery Reviews 59, 187-206.

Somnath, S., Jagdish, S., 2007. Phase-sensitive polymer-based controlled delivery systems of leuprolide acetate: In vitro release, biocompatibility, and in vivo absorption in rabbits. International Journal of Pharmaceutics 328, 42-48.

Sonawane, A., Jyot, J., During, R., Ramphal, R., 2006. Neutrophil elastase, an innate immunity effector molecule, represses flagellin transcription in pseudomonas aeruginosa. Infection and Immunity 74, 6682-6689.

Soppimath, K.S., Aminabhavi, T.M., Kulkarni, A.R., Rudzinski, W.E., 2001. Biodegradable polymeric nanoparticles as drug delivery devices. Journal of Controlled Release 70, 1-20.

Speer, D.P., Chvapil, M., Eskelson, C.D., Ulreich, J., 1980. Biological effects of residual glutaraldehyde in glutaraldehyde-tanned collagen biomaterials. Journal of Biomedical Materials Research 14, 753-764.

Sponner, A., Unger, E., Grosse, F., Weisshart, K., 2004. Conserved C-termini of Spidroins are secreted by the major ampullate glands and retained in the silk thread. Biomacromolecules 5, 840-845.

Sponner, A., Vater, W., Monajembashi, S., Unger, E., Grosse, F., Weisshart, K., 2007. Composition and hierarchical organisation of a spider silk. PLoS ONE 2, e998.

Sponner, A., Vater, W., Rommerskirch, W., Vollrath, F., Unger, E., Grosse, F., Weisshart, K., 2005. The conserved C-termini contribute to the properties of spider silk fibroins. Biochemical and Biophysical Research Communication 338, 897-902.

Stephens, J.S., Fahnestock, S.R., Farmer, R.S., Kiick, K.L., Chase, D.B., Rabolt, J.F., 2005. Effects of electrospinning and solution casting protocols on the secondary structure of a genetically engineered dragline spider silk analogue investigated via Fourier Transform Raman Spectroscopy. Biomacromolecules 6, 1405-1413.

Stropnik, C., Germi, L., Zerjal, B., 1996. Morphology variety and formation mechanisms of polymeric membranes prepared by wet phase inversion. Journal of Applied Polymer Science 61, 1821-1830.

Stropnik, C., Musil, V., Brumen, M., 2000. Polymeric membrane formation by wet-phase separation; turbidity and shrinkage phenomena as evidence for the elementary processes. Polymer 41, 9227-9237.

Tamber, H., Johansen, P., Merkle, H.P., Gander, B., 2005. Formulation aspects of biodegradable polymeric microspheres for antigen delivery. Advanced Drug Delivery Reviews 57, 357-376.

Tanaka, K., Kajiyama, N., Ishikura, K., Waga, S., Kikuchi, A., Ohtomo, K., Takagi, T., Mizuno, S., 1999. Determination of the site of disulfide linkage between heavy and light chains of silk fibroin

produced by Bombyx mori. Biochimica et Biophysica Acta (BBA) - Protein Structure and Molecular Enzymology 1432, 92-103.

Tanaka, T., Magoshi, J., Magoshi, Y., ichi Inoue, S., Kobayashi, M., Tsuda, H., Becker, M., Nakamura, S., 2002. Thermal properties of Bombyx mori and several wild silkworm silks: Phase transition of liquid silk. Journal of Thermal Analysis and Calorimetry 70, 825-832.

Tanny, G.B., 1974. The surface tension of polymer solutions and asymmetric membrane formation. Journal of Applied Polymer Science 18, 2149-2163.

Terry, A.E., Knight, D.P., Porter, D., Vollrath, F., 2004. pH induced changes in the rheology of silk fibroin solution from the middle division of Bombyx mori silkworm. Biomacromolecules 5, 768-772.

Teule, F., Cooper, A.R., Furin, W.A., Bittencourt, D., Rech, E.L., Brooks, A., Lewis, R.V., 2009. A protocol for the production of recombinant spider silk-like proteins for artificial fiber spinning. Nature Protocols 4, 341-355.

Thierry, B., Winnik, F.M., Merhi, Y., Silver, J., Tabrizian, M., 2003. Bioactive coatings of endovascular stents based on polyelectrolyte multilayers. Biomacromolecules 4, 1564-1571.

Tongwen, X., Binglin, H., 1998. Mechanism of sustained drug release in diffusion-controlled polymer matrix-application of percolation theory. International Journal of Pharmaceutics 170, 139-149.

Uebersax, L., Mattotti, M., Papaloïzos, M., Merkle, H.P., Gander, B., Meinel, L., 2007. Silk fibroin matrices for the controlled release of nerve growth factor (NGF). Biomaterials 28, 4449-4460.

Uhrich, K.E., Cannizzaro, S.M., Langer, R.S., Shakesheff, K.M., 1999. Polymeric systems for controlled drug release. Chemical Reviews 99, 3181-3198.

Um, I.C., Kweon, H., Park, Y.H., Hudson, S., 2001. Structural characteristics and properties of the regenerated silk fibroin prepared from formic acid. International Journal of Biological Macromolecules 29, 91-97.

van Beek, J.D., Hess, S., Vollrath, F., Meier, B.H., 2002. The molecular structure of spider dragline silk: Folding and orientation of the protein backbone. Proceedings of the National Academy of Sciences 99, 10266-10271.

van de Witte, P., Dijkstra, P.J., van den Berg, J.W.A., Feijen, J., 1996. Phase separation processes in polymer solutions in relation to membrane formation. Journal of Membrane Science 117, 1-31.

Vandelli, M.A., Rivasi, F., Guerra, P., Forni, F., Arletti, R., 2001. Gelatin microspheres crosslinked with glyceraldehyde as a potential drug delivery system: preparation, characterisation, in vitro and in vivo studies. International Journal of Pharmaceutics 215, 175-184.

Vasir, J.K., Tambwekar, K., Garg, S., 2003. Bioadhesive microspheres as a controlled drug delivery system. International Journal of Pharmaceutics 255, 13-32.

Vendrely, C., Ackerschott, C., Romer, L., Scheibel, T., 2008. Molecular design of performance proteins with repetitive sequences: Recombinant flagelliform spider silk as basis for biomaterials. Methods in Molecular Biology 474, 3-14.

Vendrely, C., Scheibel, T., 2007. Biotechnological production of spider-silk proteins enables new applications. Macromolecular Bioscience 7, 401-409.

Vepari, C., Kaplan, D.L., 2007. Silk as a Biomaterial. Progress in Polymer Science 32, 991-1007.

Vila, A., Sánchez, A., Tobío, M., Calvo, P., Alonso, M.J., 2002. Design of biodegradable particles for protein delivery. Journal of Controlled Release 78, 15-24.

Vladimir, N.U., 2002. What does it mean to be natively unfolded? European Journal of Biochemistry 269, 2-12.

Vollrath, F., 1999. Biology of spider silk. International Journal of Biological Macromolecules 24, 81-88.

Vollrath, F., 2000. Strength and structure of spiders' silks. Reviews in Molecular Biotechnology 74, 67-83.

Vollrath F, B.P., Basedow A, Engström W, List H, 2002. Local tolerance to spider silks and protein polymers in vivo. In Vivo 16, 229-234.

Vollrath, F., Porter, D., 2006. Spider silk as a model biomaterial. Applied Physics A 82, 205-212.

Wang, J.-N., Yan, S.-Q., Lu, C.-D., Bai, L., 2009. Biosynthesis and characterization of typical fibroin crystalline polypeptides of silkworm Bombyx mori. Materials Science and Engineering: C 29, 1321-1325.

Wang, X., Hu, X., Daley, A., Rabotyagova, O., Cebe, P., Kaplan, D.L., 2007a. Nanolayer biomaterial coatings of silk fibroin for controlled release. Journal of Controlled Release 121, 190-199.

Wang, X., Kim, H.J., Xu, P., Matsumoto, A., Kaplan, D.L., 2005. Biomaterial coatings by stepwise deposition of silk fibroin. Langmuir 21, 11335-11341.

Wang, X., Kluge, J.A., Leisk, G.G., Kaplan, D.L., 2008. Sonication-induced gelation of silk fibroin for cell encapsulation. Biomaterials 29, 1054-1064.

Wang, X., Wenk, E., Matsumoto, A., Meinel, L., Li, C., Kaplan, D.L., 2007b. Silk microspheres for encapsulation and controlled release. Journal of Controlled Release 117, 360-370.

Wang, Y., Kim, H.-J., Vunjak-Novakovic, G., Kaplan, D.L., 2006. Stem cell-based tissue engineering with silk biomaterials. Biomaterials 27, 6064-6082.

Wang, Y., Rudym, D.D., Walsh, A., Abrahamsen, L., Kim, H.-J., Kim, H.S., Kirker-Head, C., Kaplan, D.L., In vivo degradation of three-dimensional silk fibroin scaffolds. Biomaterials 29, 3415-3428.

Washington, C., 1990. Drug release from microdisperse systems: a critical review. International Journal of Pharmaceutics 58, 1-12.

Wenk, E., Wandrey, A.J., Merkle, H.P., Meinel, L., 2008. Silk fibroin spheres as a platform for controlled drug delivery. Journal of Controlled Release 132, 26-34.

Wienk, I.M., Boom, R.M., Beerlage, M.A.M., Bulte, A.M.W., Smolders, C.A., Strathmann, H., 1996. Recent advances in the formation of phase inversion membranes made from amorphous or semi-crystalline polymers. Journal of Membrane Science 113, 361-371.

Winkler, S., Kaplan, D.L., 2000. Molecular biology of spider silk. Reviews in Molecular Biotechnology 74, 85-93.

Winkler, S., Szela, S., Avtges, P., Valluzzi, R., Kirschner, D.A., Kaplan, D., 1999. Designing recombinant spider silk proteins to control assembly. International Journal of Biological Macromolecules 24, 265-270.

Wong Po Foo, C., Kaplan, D.L., 2002. Genetic engineering of fibrous proteins: spider dragline silk and collagen. Advanced Drug Delivery Reviews 54, 1131-1143.

Yang, G., Zhang, L., Cao, X., Liu, Y., 2002. Structure and microporous formation of cellulose/silk fibroin blend membranes: Part II. Effect of post-treatment by alkali. Journal of Membrane Science 210, 379-387.

Yang, M., Kawamura, J., Zhu, Z., Yamauchi, K., Asakura, T., 2009. Development of silk-like materials based on Bombyx mori and Nephila clavipes dragline silk fibroins. Polymer 50, 117-124.

Yang, Y., Chen, X., Ding, F., Zhang, P., Liu, J., Gu, X., 2007. Biocompatibility evaluation of silk fibroin with peripheral nerve tissues and cells in vitro. Biomaterials 28, 1643-1652.

Yasutomo, N., Yoshiharu, N., Masahisa, W., Shigenori, K., Jun, M., 2002. Mechanical properties of silk fibroin-microcrystalline cellulose composite films. Journal of Applied Polymer Science 86, 3425-3429.

Yonemura, N., Mita, K., Tamura, T., Sehnal, F., 2009. Conservation of silk genes in Trichoptera and Lepidoptera. Journal of Molecular Evolution 68, 641-653.

Young, T.-H., Huang, J.-H., Chuang, W.-Y., 2002. Effect of evaporation temperature on the formation of particulate membranes from crystalline polymers by dry-cast process. European Polymer Journal 38, 63-72.

Young, T.-H., Huang, Y.-H., Chen, L.-Y., 2000. Effect of solvent evaporation on the formation of asymmetric and symmetric membranes with crystallizable EVAL polymer. Journal of Membrane Science 164, 111-120.

Zambaux, M.F., Bonneaux, F., Gref, R., Maincent, P., Dellacherie, E., Alonso, M.J., Labrude, P., Vigneron, C., 1998. Influence of experimental parameters on the characteristics of poly(lactic acid) nanoparticles prepared by a double emulsion method. Journal of Controlled Release 50, 31-40.

Zax, D.B., Armanios, D.E., Horak, S., Malowniak, C., Yang, Z., 2004. Variation of mechanical properties with amino acid content in the silk of nephila clavipes. Biomacromolecules 5, 732-738.

Zbilut, J.P., Scheibel, T., Huemmerich, D., Webber Jr, C.L., Colafranceschi, M., Giuliani, A., 2006. Statistical approaches for investigating silk properties. Applied Physics A: Materials Science & Processing 82, 243-251.

Zhang, Y.-Q., Shen, W.-D., Xiang, R.-L., Zhuge, L.-J., Gao, W.-J., Wang, W.-B., 2007. Formation of silk fibroin nanoparticles in water-miscible organic solvent and their characterization. Journal of Nanoparticle Research 9, 885-900.

Zhang, Y., Cremer, P.S., 2006. Interactions between macromolecules and ions: the Hofmeister series. Current Opinion in Chemical Biology 10, 658-663.

Zhao, H.-P., Feng, X.-Q., Shi, H.-J., 2007. Variability in mechanical properties of Bombyx mori silk. Materials Science and Engineering: C 27, 675-683.

Zhao, H.-P., Feng, X.-Q., Yu, S.-W., Cui, W.-Z., Zou, F.-Z., 2005. Mechanical properties of silkworm cocoons. Polymer 46, 9192-9201.

Zhu, H., McShane, M.J., 2005. Loading of hydrophobic materials into polymer particles: Implications for fluorescent nanosensors and drug delivery. Journal of the American Chemical Society 127, 13448-13449.

Zolnik, B.S., Burgess, D.J., 2007. Effect of acidic pH on PLGA microsphere degradation and release. Journal of Controlled Release 122, 338-344.

Abbreviations, Symbols & Units

Abbriviations

ADF	*Araneus diatematus fibroin*
AFM	atomic force microscopy
B. mori	*Bombyx mori*
FTIR	fourier transform infrared spectrometry
GdmScn	Guanidiniumthiocyanat
GdmHCl	Guanidiniumhydrochlorid
HFIP	hexafluoroisopropanol
LDS	laser diffraction spectrometry
MWCO	molecular weight cut off
PBS	phosphate buffered saline
SEM	scanning electron microscopy
UV	ultraviolett
Vis	Visuell
c.a.	circa
pH	Pondus Hydrogenii
pI	Isoelectric point
p.a.	pro analysis
LMW	Low molecular weigt
Tris	Tris-(hydroxymethyl)-aminomethan
ln	logarithm

Symbols

ε_{max}	elongation	[%]
σ_{max}	tensile strength	[Pa]
E	Elastic modulus	[Pa]
λ	Wavelength	[nm]
M_w	molecular weight	[Da]
g	Gravitation constant	9.81 [m/s^2]

Units

mm	milli meter	g	Gramm
µm	micro meter	µg	Micro gramm
nm	nanometer	kDa	kilo Dalton
M	mol	Da	Dalton
mM	milli mol	N	Newton
µM	micro mol	Pa	Pascal
nM	nano mol	h	hours
l	liter	min	minutes
ml	Milli liter	s	seconds
µl	Micro liter		

Publications

Peer reviewed publications

A. Lammel, X. Hu, S.-H. Park, D. L. Kaplan, T. Scheibel. Controlling silk fibroin particle features for drug delivery. Biomaterials 2010, 31(16): 4583-91.

A. Lammel *, M. Schwab*, M. Hofer, G. Winter, T. Scheibel. Spider silk submicroparticles for controlled drug delivery. 2009. in revision.

A. Lammel*, K. Spiess*, T. Scheibel. Recombinant spider silk proteins employed in novel biomaterials. accepted.

A. Lammel, M. Schwab, U. Slotta, G. Winter and T. Scheibel. Processing conditions for spider silk microsphere formation. ChemSusChem 2008; 1(5): 413-416.

* contributed equally

Book chapters

A. Lammel, D. Keerl, L. Römer, and T. Scheibel. Proteins: Polymers of natural origin. In: Hu J., editor. Recent Advances in Biomaterials Research. Trivandrum: Transworld Research Network; 2008, p. 1-22.

A. Lammel, K. Spieß, C. Blüm, M. Schwab, G. Winter, T. Scheibel. Spinnenseidenproteine – Biopolymerische Materialien für medizintechnische Anwendungen. In: Krenkel W., editor. Verbundwerkstoffe. Wiley-VCH; 2009, p. 683-688.

Patent

A. Lammel, M. Schwab, G. Winter, T. Scheibel. (2009) Spider silk particles for controlled and sustained delivery of compounds. Provisional application, USA, 61/265,344

Conference presentations

Oral presentation

A. Lammel, K. Spieß, C. Blüm, M. Schwab, G. Winter, T. Scheibel. Spider Silk Proteins - Biopolymeric Materials for Medical Applications. Verbundwerkstoffe und Werkstoffverbunde, Bayreuth, Germany, 1st -3rd April, 2009

Poster presentations

M. Hofer, **A. Lammel** , M. Schwab , J. Myschik, T. Scheibel , G. Winter. Spider Silk Proteins – A New Biopolymer for Drug Delivery Applications. Science to Market EAPB Conference, October 6th-7th 2009, Hannover, Germany.

A. Lammel, M. Schwab, G. Winter, T. Scheibel. Spider Silk Proteins - New biopolymeric Materials for Medical Applications. Materials Science and Engineering, September 1st-4th 2008, Nürnberg, Germany.

A. Lammel, U. Mayer, S. Rammensee, A. Bausch, T. Scheibel, W. Wall. Materials from Spider Silk - Experimental and Numerical Approaches for Silk Assembly. DynaSoft 08 – Dynamics in Soft Condensed Matter, July 28th - August 9th 2008, Cargese -Institute of Scientific Studies, France.

A. Lammel, U. Mayer, S. Rammensee, A. Bausch, T. Scheibel, W. Wall. Materials from Spider Silk.
Forum 2008 - International Graduate School of Science and Engineering, July 27th-28th 2008, Raitenhasslach, Germany. (Award for Best Poster Presentation)

A. Lammel, M. Schwab, U. Slotta, G. Winter, T. Scheibel. Engineerd spider silk microspheres: Formation mechanisms and Processing conditions, Particles 2008 - Particle Synthesis, Characterization, and Particle-Based Advanced Materials. Orlando, USA, 10th - 13th May 2008

M. Schwab, **A. Lammel**, U. Slotta, T. Scheibel, G. Winter. Characterization of spider silk protein films for application in pharmaceutical technology. 6th World Meeting on Pharmaceutics, Biopharmaceutics and Pharmaceutical Technology, Barcelona, Spain 7th-10th April 2008

Appendix

A1 Silk fobroin heavy chain (*B. mori*)

Number of amino acids: 5263

Accession number: P05790

Aminoacid sequence:

1 MRVKTFVILC CALQYVAYTN ANINDFDEDY FGSDVTVQSS NTTDEIIRDA SGAVIEEQITT
61 KKMQRKNKN HGILGKNEKM IKTFVITTDS DGNESIVEED VLMKTLSDGT VAQSYVAADA
121 GAYSQSGPYV SNSGYSTHQG YTSDFSTSAA VGAGAGAGAA AGSGAGAGAG YGAASGAGAG
181 AGAGAGAGYG TGAGAGAGAG YGAGAGAGAG AGYGAGAGAG AGAGYGAGAG AGAGAGYGAG
241 AGAGAGAGYG AGAGAGAGAG YGAASGAGAG AGYGQGVGSG AASGAGAGAG AGSAAGSGAG
301 AGAGTGAGAG YGAGAGAGAG AGYGAASGTG AGYGAGAGAG YGGASGAGAG AGAGAGAGAG
361 AGYGTGAGYG AGAGAGAGAG AGAGYGAGAG AGYGAGYGVG AGAGYGAGYG AGAGSGAASG
421 AGSGAGAGSG AGAGSGAGAG SGAGAGSGAG AGSGAGAGSG AGAGSGAGAG SGTGAGSGAG
481 AGYGAGAGAG YGAGAGSGAA SGAGAGSGAG AGSGAGAGSG AGAGSGAGAG SGAGAGYGAG
541 AGAGYGAGAG AGYGAGAGVG YGAGAGSGAA SGAGAGSGAG AGSGAGAGSG AGAGSGAGAG
601 SGAGAGSGAG AGSGAGAGSG AGAGSGAGVG YGAGVGAGYG AGYGAGAGAG YGAGAGSGAA
661 SGAGAGAGAG AGTGSSGFGP YVANGGYSRS DGYEYAWSSD FGTGSGAGAG SGAGAGSGAG
721 AGSGAGAGSG AGAGSGAGAG YGAGVGVGYG AGYGAGAGAG YGAGAGSGAA SGAGAGSGAG
781 AGSGAGAGSG AGAGSGAGAG SGAGAGSGAG AGSGAGAGSG AGAGSGAGAG SGAGVGSGAG
841 AGSGAGAGVG YGAGAGVGYG AGAGSGAASG AGAGSGAGAG SGAGAGSGAG AGSGAGAGSG
901 AGAGSGAGAG SGAGAGSGAG AGSGAGVGYG AGVGAGYGAG YGAGAGAGYG AGAGSGAASG
961 AGAGSGAGAG SGAGAGSGAG AGSGAGAGSG AGAGSGAGAG SGAGAGSGAG AGSGAGAGSG
1021 AGAGSGAGAG YGAGAGAGYG AGYGAGAGAG YGAGAGSGAA SGAGSGAGAG SGAGAGAGSG
1081 AGAGSGAGAG SGAGAGSGAG AGSGAGAGSG AGAGYGAGVG AGYGAGYGAG AGAGYGAGAG
1141 SGAASGAGAG SGAGAGSGAG AGSGAGAGSG AGAGSGAGAG SGAGAGSGAG VGYGAGYGAG
1201 AGAGYGAGAG SGAASGAGAG AGAGAGTGSS GFGPYVAHGG YSGYEYAWSS ESDFGTGSGA
1261 GAGSGAGAGS GAGAGSGAGA GSGAGYGAGV GAGYGAGYGA GAGAGYGAGA GSGAGSGAGA
1321 GSGAGAGSGA GAGSGAGAGS GAGAGSGAGA GSGAGAGSGA GAGSGAGAGY GAGYGAGAGA
1381 GYGAGAGSGA GSGAGAGSGA GAGSGAGAGS GAGAGSGAGA GSGAGAGSGA GAGSGAGAGY
1441 GAGVGAGYGA GYGAGAGAGY GAGAGSGAGS GAGAGSGAGA GSGAGAGSGA GVGSGAGAGS
1501 GAGAGSGAGA GSGAGAGYGA GYGAGAGAGY GAGAGSGAGS GAGAGSGAGA GSGAGAGSGA
1561 GAGSGAGAGS GAGAGSGAGA GSGAGVGYGA GVGAGYGAGY GAGAGAGYGA GAGSGAASGA
1621 GAGAGAGAGT GSSGFGPYVA NGGYSGYEYA WSSESDFGTG SGAGAGSGAG AGSGAGAGSG
1681 AGAGSGAGAG YGAGYGAGAG AGYGAGAGSG AGSGAGAGSG AGAGSGAGAG SGAGAGSGAG
1741 AGSGAGAGSG AGAGSGAGSG SGAGAGSGAG AGSGAGAGYG AGVGAGYGVG YGAGAGAGYG
1801 AGAGSGAASG AGAGAGAGAG TGSSGFGPYV AHGGYSGYEY AWSSESDFGT GSGAGAGSGA
1861 GAGSGAGAGS GAGAGSGAGA GSGAGAGSGA GAGYGAGVGA GYGAAYGAGA GAGYGAGAGS
1921 GAASGAGAGS GAGAGSGAGA GSGAGAGSGA GAGSGAGAGS GAGAGSGAGA GSGAGAGSGA
1981 GAGSGAGAGY GAGAGAGYGA GAGSGAGSGA GAGSGAGAGS GAGAGSGAGA GSGAGAGSGA
2041 GSGSGAGAGS GAGAGSGAGA GYGAGVGAGY GAGYGAGAGA GYGAGAGSGA GSGAGAGSGA
2101 GAGYGAGAGA GYGAGYGAGA GAGYGAGAGT GAGSGAGAGS GAGAGSGAGA GSGAGAGSGA
2161 GAGSGAGAGS GAGSGSGAGA GSGAGAGSGA GAGSGAGAGS GAGAGSGAGA GYGAGAGAGY
2221 GAGYGAGAGA GYGAGAGSGA GSGAGAGSGA GAGSGAGAGS GAGAGYGAGY GAGAGSGAAS
2281 GAGAGAGAGA GTGSSGFGPY VAHGGYSGYE YAWSSESDFG TGSGAGAGSG AGAGAGAGAG
2341 SGAGAGYGAG VGAGYGAGYG AGAGAGYGAG AGSGTGSGAG AGSGAGAGYG AGVGAGYGAG
2401 AGSGAAFGAG AGAGAGSGAG AGSGAGAGSG AGAGSGAGAG SGAGAGYGAG YGAGVGAGYG
2461 AGAGSGAASG AGAGSGAGAG SGAGAGSGAG AGSGAGAGSG AGAGYGAGVG AGYGAGYGAG

2521 AGAGYGAGAG SGAASGAGAG SGAGAGAGSG AGAGSGAGAG SGAGAGSGAG SGAGAGSGAG
2581 AGSGAGAGYG AGAGSGAASG AGAGAGAGAG TGSSGFGPYV ANGGYSGYEY AWSSESDFGT
2641 GSGAGAGSGA GAGSGAGAGS GAGAGSGAGA GYGAGVGAGY GAGYGAGAGA GYGAGAGSGA
2701 GSGAGAGSGA GAGSGAGAGS GAGAGSGAGA GSGAGAGSGA GAGYGAGAGS GAASGAGAGS
2761 GAGAGSGAGA GSGAGAGSGA GAGSGAGAGS GAGAGYGAGV GAGYGVGYGA GAGAGYGAGA
2821 GSGAGSGAGA GSGAGAGSGA GAGSGAGAGS GAGSGAGAGS GAGAGSGAGA GSGAGSGAGA
2881 GSGAGAGYGV GYGAGAGAGY GAGAGSGAGS GAGAGSGAGA GSGAGAGSGA GSGAGAGSGA
2941 GAGSGAGAGS GAGAGYGAGV GAGYGVGYGA GAGAGYGAGA GSGAGSGAGA GSGAGAGSGA
3001 GAGSGAGAGS GAGAGSGAGA GSGAGAGSGA GSGAGAGSGA GAGSGAGAGS GAGAGSGAGS
3061 GAGAGSGAGA GSGAGAGSGA GAGYGAGVGA GYGVGYGAGV GAGYGAGAGS GAASGAGAGS
3121 GAGAGAGSGA GAGSGAGAGS GAGAGSGAGA GSGAGAGSGA GAGYGAGYGA GVGAGYGAGA
3181 GVGYGAGAGA GYGAGAGSGA ASGAGAGAGS GAGAGTGAGA GSGAGAGYGA GAGSGAASGA
3241 GAGAGAGAGT GSSGFGPYVA NGGYSGYEYA WSSESDFGTG SGAGAGSGAG AGSGAGAGSG
3301 AGAGSGAGAG YGAGVGAGYG AGAGSGAGSG AGAGSGAGAG SGAGAGSGAG AGSGAGAGYG
3361 AGAGSGTGSG AGAGSGAGAG SGAGAGSGAG AGSGAGAGSG AGAGSGVGAG YGVGYGAGAG
3421 AGYGVGYGAG AGAGYGAGAG SGTGSGAGAG SGAGAGSGAG AGSGAGAGSG AGAGSGAGAG
3481 SGAGAGYGAG VGAGYGVGYG AGAGAGYGAG AGSGAGSGAG AGSGAGAGSG AGAGSGAGAG
3541 SGAGSGAGAG SGAGAGSGAG AGSGAGSGAG AGSGAGAGYG VGYGAGAGAG YGAGAGSGAG
3601 SGAGAGSGAG AGSGAGAGSG AGSGAGAGSG AGAGSGAGAG SGAGAGYGAG VGAGYGVGYG
3661 AGAGAGYGAG AGSGAGSGAG AGSGAGAGSG AGAGSGAGAG SGAGAGSGAG AGSGAGAGSG
3721 AGSGAGAGSG AGAGSGAGAG SGAGAGYGAG VGAGYGVGYG AGAGAGYGAG AGSGAASGAG
3781 AGAGAGAGTG SSGFGPYVAN GGYSGYEYAW SSESDFGTGS GAGAGSGAGA GSGAGAGYGA
3841 GYGAGVGAGY GAGAGVGYGA GAGAGYGAGA GSGAASGAGA GAGAGAGSGA GAGSGAGAGA
3901 GSGAGAGYGA GYGIGVGAGY GAGAGVGYGA GAGAGYGAGA GSGAASGAGA GSGAGAGSGA
3961 GAGSGAGAGS GAGAGSGAGA GSGAGAGYGA GYGAGVGAGY GAGAGVGYGA GAGAGYGAGA
4021 GSGAASGAGA GAGAGAGAGS GAGAGSGAGA GSGAGAGSGA GAGSGAGAGS GAGAGSGAGA
4081 GSGAGAGSGA GAGYGAGVGA GYGAGYGGAG AGYGAGAGSG AASGAGAGSG AGAGSGAGAG
4141 SGAGAGSGAG AGSGAGAGYG AGAGSGAASG AGAGAGAGAG TGSSGFGPYV NGGYSGYEYA
4201 WSSESDFGTG SGAGAGSGAG AGSGAGAGYG AGVGAGYGAG YGAGAGAGYG AGAGSGAASG
4261 AGAGSGAGAG SGAGAGSGAG AGSGAGSGAG AGSGAGAGSG AGAGSGAGAG SGAGAGSGAG
4321 AGYGAGVGAG YGAGYGAGAG AGYGAGAGSG AASGAGAGSG AGAGAGSGAG AGSGAGAGSG
4381 AGAGSGAGAG SGAGAGSGAG SGAGAGSGAG AGYGAGYGAG VGAGYGAGAG VGYGAGAGAG
4441 YGAGAGSGAA SGAGAGSGSG AGSGAGAGSG AGAGSGAGAG AGSGAGAGSG AGAGSGAGAG
4501 YGAGYGAGAG SGAASGAGAG AGAGAGTGSS GFGPYVANGG YSGYEYAWSS ESDFGTGSGA
4561 GAGSGAGAGS GAGAGYGAGV GAGYGAGYGA GAGAGYGAGA GSGAGSGAGA GSGAGAGSGA
4621 GAGSGAGAGS GAGAGSGAGA GSGAGAGSGA GAGYGAGYGA GAGAGYGAGA GVGYGAGAGA
4681 GYGAGAGSGA GSGAGAGSGS GAGAGSGSGA GSGAGAGSGA GAGSGAGAGS GAGAGSGAGA
4741 GSGAGAGSGA GAGYGAGYGI GVGAGYGAGA GVGYGAGAGA GYGAGAGSGA ASGAGAGSGA
4801 GAGSGAGAGS GAGAGSGAGA GSGAGAGSGA GAGSGAGAGS GAGAGSGAGA GYGAGAGVGY
4861 GAGAGSGAAS GAGAGSGAGA GSGAGAGSGA GAGSGAGAGS GAGAGSGAGA GSGAGSGAGA
4921 GSGAGAGYGA GYGAGVGAGY GAGAGYGAGY GVGAGAGYGA GAGSGAGSGA GAGSGAGAGS
4981 GAGAGSGAGA GSGAGAGSGA GSGAGAGYGA GAGAGYGAGA GAGYGAGAGS GAASGAGAGA
5041 GAGSGAGAGS GAGAGSGAGS GAGAGSGAGA GYGAGAGSGA ASGAGAGSGA GAGAGAGAGA
5101 GSGAGAGSGA GAGYGAGAGS GAASGAGAGA GAGTGSSGFG PYVANGGYSR REGYEYAWSS
5161 KSDFETGSGA ASGAGAGAGS GAGAGSGAGA GSGAGAGSGA GAGGSVSYGA GRGYGQGAGS
5221 AASSVSSASS RSYDYSRRNV RKNCGIPRRQ LVVKFRALPC VNC

Data taken from: http://www.ncbi.nlm.nih.gov/

A2 Silk fibroin light chain (*B. mori*)

Number of amino acids: 262

Accession number: P21828

Aminoacid sequence:

1 MKPIFLVLLV ATSAYAAPSV TINQYSDNEI PRDIDDGKAS SVISRRWDYV DDTDKSIAIL
61 NVQEILKDMA SQGDYASQAS AVAQTAGIIA HLSAGIPGDA CAAANVINSY TDGVRSGNFA
121 GFRQSLGPFF GHVGQNLNLI NQLVINPGQL RYSVGPALGC AGGGRIYDFE AAWDAILASS
181 DSSFLNEEYC IVKRLYNSRN SQSNNIAAYI TAHLLPPVAQ VFHQSAGSIT DLLRGVGNGN
241 DATGLVANAQ RYIAQAASQV HV

Data taken from: http://www.ncbi.nlm.nih.gov/

A3 Engineered spider silk eADF4(C16) (*Araneus Diatematus*)

Number of aminoacids: + T7Tag

Aminoacid sequence:

1 GSSAAAAAAA ASGPGGYGPE NQGPSGPGGY GPGGPGSSAA AAAAAASGPG GYGPENQGPS
61 GPGGYGPGGP GSSAAAAAAA ASGPGGYGPE NQGPSGPGGY GPGGPGSSAA AAAAAASGPG
121 GYGPENQGPS GPGGYGPGGP GSSAAAAAAA ASGPGGYGPE NQGPSGPGGY GPGGPGSSAA
181 AAAAAASGPG GYGPENQGPS GPGGYGPGGP GSSAAAAAAA ASGPGGYGPE NQGPSGPGGY
241 GPGGPGSSAA AAAAAASGPG GYGPENQGPS GPGGYGPGGP GSSAAAAAAA ASGPGGYGPE
301 NQGPSGPGGY GPGGPGSSAA AAAAAASGPG GYGPENQGPS GPGGYGPGGP GSSAAAAAAA
361 ASGPGGYGPE NQGPSGPGGY GPGGPGSSAA AAAAAASGPG GYGPENQGPS GPGGYGPGGP
421 GSSAAAAAAA ASGPGGYGPE NQGPSGPGGY GPGGPGSSAA AAAAAASGPG GYGPENQGPS
481 GPGGYGPGGP GSSAAAAAAA ASGPGGYGPE NQGPSGPGGY GPGGPGSSAA AAAAAASGPG
541 GYGPENQGPS GPGGYGPGGP MASMTGGQQM GR

A4 Interaction potentials

$$W_{pp}(r) = W_{elec}(r) + W_{disp}(r) + W_{osmotic}(r) + W_{specific}(r)$$

$$W_{elec}(r) = \frac{(z_2 e)^2 \exp[-\kappa(r - \sigma_p)]}{4\pi\varepsilon_0\varepsilon_r r(1 + \kappa\sigma_p/2)^2}$$

for: $r > (\sigma_p + 2\Delta r)$

$$\kappa^2 = (2e^2 N_a I)/(k_B T \varepsilon_0 \varepsilon_r)$$

$$I = (z_{an}^2 c_{an} + z_{cat}^2 c_{cat})/2$$

$$W_{disp}(r) = -\frac{H}{12}\left[\frac{\sigma_p^2}{r^2} + \frac{\sigma_p^2}{r^2 - \sigma_p^2} + 2\ln\left(1 - \frac{\sigma_p^2}{r^2}\right)\right]$$

for: $r > \sigma_p + 2\Delta r$

$$W_{osmotic}(r) = -\frac{4}{3}\pi\sigma_{ps}^3(\rho_s k_B T)\left[1 - \frac{3r}{4\sigma_{ps}} + \frac{r^3}{16\sigma_{ps}^3}\right]$$

for: $\sigma_{ps} < r < 2\sigma_{ps}$

$W_{osmotic}(r) = 0$ for $r > 2\sigma_{ps}$

$\sigma_{ps} = (\sigma_p + \sigma_{ion})/2$

$\sigma_{ion} = (z_{an}\sigma_{cat} + z_{cat}\sigma_{an})/(z_{cat} + z_{an})$

$W_{specific}(r) = -\varepsilon_{sp}$ for $\sigma_p < r < (\sigma_p + \delta)$

$W_{specific}(r) = 0$ for $r > (\sigma_p + \delta)$

r	the center to center separation
z_2	the valance of the protein
e	the unit of electron charge
$4\pi\,\varepsilon_0$	the dielectric permittivity of free space
σ_p	the unhydrated hard sphere diameter
ε_r	the relative dielectric permittivity of water
Δr	the effective-sphere hydration/stern layer
κ	the inverse of the Debye length
N_a	Avogadro's number
I	the ionic strength
z_{an}, z_{cat}	the anion and cation valences
c_{an}, c_{cat}	the ionic molar concentrations
H	the effective Hamaker constant for protein-protein interaction
ρ_s	the total ionic number density
ε_{sp},δ	Model parameters

Acknowledgement

Herzlichen Dank an:

- Meinen Doktorvater Prof. Dr. Thomas Scheibel für die Unterstützung während meiner Promotion und für die Möglichkeit nach seiner Berufung an die Universität Bayreuth in meinem ersten Promotionsjahr meine Arbeit und Forschung bei verschiedenen Kooperationspartnern in München weiterführen zu können.
- Meinen Zweitbetreuer Prof. Dr. Andreas Bausch, der mich in seinem Labor als externen Mitarbeiter herzlich aufgenommen hat.
- Prof. Dr. Gerhard Winter für die Möglichkeit an seinem Lehrstuhl für Pharmazeutische Technologie der Ludwigs-Maximilians Universität zu arbeiten und dadurch viel über pharmazeutische Forschung zu lernen.
- Prof. Dr. David Kaplan bei dem ich im Herbst 2009 die Möglichkeit erhielt für drei Monate in seiner Gruppe im Department for Biomedical Engineering an der Tufts University in Boston zu arbeiten.
- Das gesamte Fiberlab (Felix Bauer, Claudia Blüm, Johannes Diehl, Lukas Eisoldt, Adrian Gosler, Anja Hagenau, Dr. John Hardy, Markus Heim, David Keerl, Anja Lauterbach, Aldo Leal-Egaña, Eileen Lintz, Susanne Müller, Andreas Schmidt, Kristin Schmidt, Martin Schmidt, Dr. Ute Slotta, Dr. Andrew Smith, Kristina Spiess, Daniela und Michael Suhre, Jasmin Wickinghoff) für die gute Atmosphäre und Zusammenarbeit. Besonderer Dank geht an Markus Heim und John Hardy für ihre Gastfreundschaft und guten Gespräche bei meinen Bayreuth Besuchen.
- Dr. Sebastian Rammensee und Dr. Pablo Fernandez vom Lehrstuhl für Zellbiophysik der Technischen Universität München für die Unterstützung bei den Mechanik Messungen und bei der konfokalen Mikroskopie.
- Dr. Martin Schwab, Markus Hofer und Dr. Julia Myschik vom Lehrstuhl für Pharmazeutische Technologie der Ludwigs-Maximilians Universität München für die fruchtbare Zusammenarbeit und anregenden Diskussionen.

- Dr. Xiao Hu und Dr. Sang Hyuang vom Department for Biomedical Engineering der Tufts University für Ihre Unterstützung während meiner Zeit in Boston.
- Dr. Jabier für die zahlreichen Diskussionen und Einblicke in Zellkulturexperimente.
- Christian Meinle und Dr. Marianne Hanzlik für die Hilfe bei der Raster-elektronenmikroskopie.
- Meinen Mitbewohner Dorian, der mich während des Verfassens meiner schriftlichen Arbeit immer wieder durch seine fröhliche Art auf neue Gedanken brachte.
- Meine Eltern, für Ihre finanzielle und moralische Unterstützung während all der Jahre meiner universitären Ausbildung.
- Meine Freundin Sophie für die wunderbare Zeit die wir zusammen verbringen.